

The influence of crystal-size distributions on dynamic processes in magmatic systems and the rheology of magmas

Dissertation

zur Erlangung des Grades

"Doktor der Naturwissenschaften"

im Promotionsfach Geologie / Mineralogie / Paläontologie

am Fachbereich Chemie, Pharmazie und Geowissenschaften

der Johannes Gutenberg-Universität in Mainz

Johannes Klein

geb. in Mainz

Mainz, Dezember 2018

1. Berichtstatter : -

2. Berichtstatter : -

Tag der mündlichen Prüfung: 03. Mai 2019

Table of Content

TABLE OF CONTENT	V
TABLE OF FIGURES AND TABLES	VII
PREAMBLE	IX
ABSTRACT	1
KURZFASSUNG	2
1. INTRODUCTION	3
1.1. THESIS LAYOUT	7
2. RHEOLOGY	9
2.1. RHEOLOGY OF MAGMAS	10
2.1.1. <i>Chemical composition of melts</i>	11
2.1.2. <i>Dissolved volatiles</i>	12
2.1.3. <i>Magma temperature and pressure</i>	13
2.1.4. <i>Strain-rate dependence</i>	16
2.1.5. <i>Particles</i>	17
2.2. RHEOLOGY OF PARTICLE BEARING SUSPENSIONS - BASIC PRINCIPLES	19
2.3. MAXIMUM PACKING FRACTION ϕ_m	30
2.4. PARTICLE SIZE DISTRIBUTIONS / CRYSTAL SIZE DISTRIBUTIONS	33
2.5. RHEOMETRY	39
2.5.1. <i>Rotational rheometry</i>	40
3. MEASURING PROCEDURE AND VISCOSITY DETERMINATION	46
3.1. MEASUREMENT REQUIREMENTS	46
3.2. SAMPLE PREPARATION	48
3.3. MEASUREMENT OVERVIEW	51
3.4. MEASUREMENT JOB	52
3.5. DATA ANALYSIS	53
4. RHEOLOGICAL EXPERIMENTS - DERIVING A MODEL	54
4.1. RESULTS - SPHERICAL PARTICLES	54
4.1.1. <i>Classifying experimental results</i>	57
4.1.2. <i>Maximum packing fraction ϕ_m</i>	58
4.1.3. <i>The links between CSD, maximum packing fraction and suspension viscosity - a model</i>	61
4.2. INFLUENCE OF PARTICLE SHAPE – TESTING THE MODEL	65
4.2.1. <i>Results of rheometric experiments</i>	67

4.2.2. <i>Model improvements</i>	69
4.2.3. <i>The generalized model</i>	70
4.2.4. <i>A practical application</i>	71
4.3. PROS AND CONS - A SUMMARY.....	73
5. THE EVOLUTION OF CSD'S IN RISING MAGMA AND ITS EFFECT ON MAGMA RHEOLOGY	74
5.1. IDEA AND BACKGROUND.....	74
5.2. EXPERIMENTAL STRATEGY.....	77
5.2.1. <i>Phase Equilibrium Experiments</i>	78
5.2.2. <i>Dynamic Decompression Experiments</i>	79
5.3. TEXTURAL CHARACTERIZATION - CRYSTAL-SIZE DISTRIBUTIONS (CSD)	82
6. METHODOLOGY	87
6.1. PETROLOGICAL EXPERIMENTS – PROCEDURE AND METHODS	87
6.2. SAMPLE PREPARATION.....	91
6.3. ELECTRON MICROPROBE ANALYSES (EMPA).....	91
6.4. IMAGE ANALYSIS	93
6.4.1. <i>ImageJ and Adobe Photoshop</i>	93
6.4.2. <i>CSD corrections</i>	94
7. RESULTS AND DISCUSSION PETROLOGICAL EXPERIMENTS	96
7.1. EQUILIBRIUM EXPERIMENTS	96
7.2. DECOMPRESSION EXPERIMENTS.....	101
7.2.1. <i>Initial pressure 175 MPa</i>	102
7.2.2. <i>Initial pressure 150 MPa</i>	103
7.2.3. <i>Initial pressure 125 MPa</i>	103
7.2.4. <i>Initial pressure 100 MPa</i>	105
7.3 GENERAL REMARKS.....	108
7.4. SOURCES OF ERROR AND ROUTES FOR FUTURE WORK.....	112
8. CONCLUSIONS AND FUTURE WORK	116
BIBLIOGRAPHY	119
ACKNOWLEDGEMENTS	142
APPENDICES	143
CURRICULUM VITAE	144

Table of Figures and Tables

FIGURE 1: H ₂ O BREAKING SiO ₄ CHAINS (FROM GILL, 2010).....	12
FIGURE 2: VISCOSITY IN RELATION TO TEMPERATURE OF VARIOUS MELT TYPES (FROM SPERA, 2000).	14
FIGURE 3: VISCOSITY IN RELATION TO PRESSURE OF VARIOUS MELT TYPES (FROM MUELLER, H.J., 2010).	15
FIGURE 4: DIMENSIONLESS VISCOSITY IN RELATION TO DIMENSIONLESS STRAIN RATE OF VARIOUS MELT TYPES (FROM GONNERMANN & MANGA, 2007).	16
FIGURE 5: EXAMPLE OF AN END MEMBER MODEL OF CALDERA-PRODUCING MAGMATIC SYSTEMS. (FROM CASHMAN & GIORDANO, 2014).	17
FIGURE 6: RELATIVE VISCOSITY IN RELATION TO PARTICLE VOLUME FRACTION – MAXIMUM PACKING FRACTION AND CRYSTAL MUSH (FROM CASHMAN ET AL., 2017).....	18
FIGURE 7: SUMMARY OF TYPICAL RHEOLOGICAL BEHAVIOR (MODIFIED FROM MEZGER, 2006).	19
FIGURE 8: TWO-PLATES MODEL DEFINING RHEOLOGICAL PARAMETERS (MODIFIED FROM MEZGER, 2006). ...	20
FIGURE 9: SCHEMATIC SUMMARY OF DIFFERENT COMMON MODELS OF PARTICLE SUSPENSION RHEOLOGY (MODIFIED FROM MADER ET AL., 2013).	26
FIGURE 10: THE INFLUENCE OF BUBBLES TO A LAMINAR FLOW (FROM LLEWELLIN ET AL. 2002).	29
FIGURE 11: CROSS SECTION OF A CONCENTRIC CYLINDER MEASURING SYSTEM (MODIFIED FROM MEZGER, 2006).	42
FIGURE 12: CROSS SECTION OF A PARALLEL PLATE MEASURING SYSTEM (MODIFIED FROM MEZGER, 2006)...	43
FIGURE 13: CROSS SECTION OF A CONE AND PLATE MEASURING SYSTEMS (MODIFIED FROM MEZGER, 2006). 45	
FIGURE 14: SIEVE COLUMN.....	49
FIGURE 15: VANE SPINDLE MIXING DEVICE.....	50
FIGURE 16: SCHEMATIC SUMMARY OF DIFFERENT PARTICLE DISTRIBUTIONS USED AND ANALYSED IN THIS STUDY.	51
FIGURE 17: MEASUREMENT SETUP USING A PARALLEL-PLATE GEOMETRY	52
FIGURE 18: MEASUREMENT JOB IN RHEOWIN SOFTWARE	53
FIGURE 19: EXPERIMENTAL DATA IN RELATION TO PARTICLE VOLUME FRACTION.	55
FIGURE 20: STATISTICAL DATA IN RELATION TO THE MAXIMUM PACKING FRACTION.	56
FIGURE 21: EXPERIMENTAL DATA FOR RELATIVE VISCOSITY $\eta r, *$ VS. PARTICLE VOLUME FRACTION ϕ OF SUSPENSIONS WITH DIFFERENT PARTICLE MODALITIES.	58
FIGURE 22: EXPERIMENTAL DATA OF THIS STUDY FOR RELATIVE VISCOSITY $\eta r, *$ VS. NORM. PARTICLE VOLUME FRACTION $\phi \phi m$	59
FIGURE 23: MAXIMUM PACKING FRACTION ϕm ESTIMATED BY SETTLING VS. MAXIMUM PACKING FRACTION ϕm ESTIMATED BY RHEOMETRY.	61
FIGURE 24: SCHEMATIC PLOT OF MAXIMUM PACKING FRACTION ϕm VS. POLYDISPERSITY ILLUSTRATING THE APOLLONIAN PACKING.	63
FIGURE 25: MAXIMUM PACKING FRACTION ϕm VS. POLYDISPERSITY Δ (EQ. 2.28) FOLLOWING EQ. (4.3).	64
FIGURE 26: MAXIMUM PACKING FRACTION ϕm VS. POLYDISPERSITY Γ (EQ. 2.29) FOLLOWING EQ. (4.4).....	65
FIGURE 27: SCHEMATIC PLOT OF MAXIMUM PACKING FRACTION ϕm VS. POLYDISPERSITY Γ (EQUATION 2.29) FOLLOWING EQ. (4.4) FOR DISTRIBUTIONS OF ARBITRARY PARTICLE SHAPE WITH ASPECT RATIO $R_p \neq 1$. 66	

FIGURE 28: EXPERIMENTAL DATA OF PARTICLES WITH ARBITRARY SHAPE IN RELATION TO PARTICLE VOLUME FRACTION.	68
FIGURE 29: EXPERIMENTAL DATA OF THIS STUDY AND RE-PARAMETERIZED MODEL FOR MAXIMUM PACKING FRACTION ϕ_m VS. ASPECT RATIO R_p (EQUATION 4.5).....	69
FIGURE 30: EXPERIMENTAL DATA OF THIS STUDY FOR MAXIMUM PACKING FRACTION ϕ_m VS. POLYDISPERSITY Γ (EQUATION 4.4) OF OBLATE (MEAN $R_p \sim 0.09$) AND PROLATE (MEAN $R_p \sim 7$) PARTICLES.	70
FIGURE 31: PRACTICAL APPLICATION STEPS	72
FIGURE 32: (A) SCHEMATIC CROSS-SECTION OF A VOLCANIC CONDUIT SHOWING THE CRYSTALLINITY DEVELOPMENT AT ARBITRARY LOW, MIDDLE, AND UPPER LEVELS IN THE CONDUIT, DEPICTING THE EXPECTED TEXTURAL CHANGES OF SILICIC MAGMA THAT IS UNDERGOING DEGASSING DUE TO DECOMPRESSION.	75
FIGURE 33: PHASE EQUILIBRIA DIAGRAM FOR HYDROTHERMAL EXPERIMENTS ON MINOAN RHYODACITE FROM COTTRELL ET AL., 1999).....	79
FIGURE 34: EXAMPLES OF PROCESSES THAT CAN AFFECT THE SHAPE OF THE CSD.....	84
FIGURE 35: DIFFERENT STAGES OF SAMPLE CONDITIONS DURING PREPARATION.....	88
FIGURE 36: REPRESENTATIVE BACK-SCATTERED ELECTRON IMAGES OF ISOTHERMAL, EXPERIMENTALLY EQUILIBRATED SAMPLES AT DIFFERENT PRESSURES.	100
FIGURE 37: CRYSTAL SIZE DISTRIBUTIONS OF EXPERIMENTALLY EQUILIBRATED SAMPLES	101
FIGURE 38: REPRESENTATIVE BACK-SCATTERED ELECTRON IMAGES OF ISOTHERMAL, EXPERIMENTALLY DECOMPRESSED SAMPLES - INITIAL PRESSURE 125MPA.....	102
FIGURE 39: REPRESENTATIVE BACK-SCATTERED ELECTRON IMAGES OF ISOTHERMAL, EXPERIMENTALLY DECOMPRESSED SAMPLES - INITIAL PRESSURE 150MPA.....	104
FIGURE 40: REPRESENTATIVE BACK-SCATTERED ELECTRON IMAGES OF ISOTHERMAL, EXPERIMENTALLY DECOMPRESSED SAMPLES - INITIAL PRESSURE 125MPA.....	105
FIGURE 41: REPRESENTATIVE BACK-SCATTERED ELECTRON IMAGES OF ISOTHERMAL, EXPERIMENTALLY DECOMPRESSED SAMPLES - INITIAL PRESSURE 100 MPa.	106
FIGURE 42: CRYSTAL SIZE DISTRIBUTIONS OF EXPERIMENTALLY DECOMPRESSED SAMPLES.....	107
FIGURE 43: REPRESENTATIVE BACK-SCATTERED ELECTRON IMAGES OF SKELETAL SHAPED AND ELONGATED PLAGIOCLASE CRYSTALS IN SAMPLE DC3.....	111
FIGURE 44: APPLICATION OF THE AFOREMENTIONED MODEL DERIVED IN THIS THESIS (CHAPTER 4) ON THE SAMPLES OF THE HP/HT-EXPERIMENTS.....	112
TABLE 1: PACKING FRACTION AND COORDINATION NUMBER OF ORDERED PACKINGS OF MONOSIZED SPHERES IN 3D SPACE. (FROM PABST & GREGOROVA, 2013).....	31
TABLE 2: SIEVING FRACTIONS.	49
TABLE 3: OVERVIEW OF PETROLOGICAL EXPERIMENTS - EQUILIBRIUM AND DECOMPRESSION EXPERIMENTS..	90
TABLE 4: RESULTS OF PETROLOGICAL EXPERIMENTS - EQUILIBRIUM AND DECOMPRESSION EXPERIMENTS.....	97

Preamble

Parts of the contents presented in this thesis have been published in the following scientific journals:

Klein, J., Mueller, S. P., & Castro, J. M. (2017). The influence of crystal size distributions on the rheology of magmas: New insights from analog experiments. *Geochemistry, Geophysics, Geosystems*, 18 (11), pp. 4055-4073. (<https://doi.org/10.1002/2017GC007114>).

Klein, J., Mueller, S. P., Helo, C., Schweitzer, S., Gurioli, L., & Castro, J. M. (2018). An expanded model and application of the combined effect of crystal-size distribution and crystal shape on the relative viscosity of magmas. *Journal of Volcanology and Geothermal Research*, 357, pp. 128-133. (<https://doi.org/10.1016/j.jvolgeores.2018.04.018>).

Abstract

The rheology of a magma is recognized as a one of the crucial parameters for the understanding of processes and features throughout a volcanic system. Despite its key role in governing volcanic processes, magma rheology is extremely difficult to constrain in time and space within a natural volcanic system. It is well known from laboratory studies and observations in natural volcanic systems that the amount of crystals suspended in the melt, and the degree to which they interact, are central parameters governing magma rheology. Accounting for, or neglecting the effect of solid particles in volcanological eruption models can change their results by orders of magnitudes and may be a key parameter controlling whether an eruption is explosive or effusive. However, a key question in suspension rheology remains unanswered: How does the size distribution of suspended particles influence the flow?

Crystal-size distributions (CSD) are a widely used tool to describe aspects of a natural sample's crystallization history (e.g., nucleation and growth rates, etc.) in order to examine processes within magma chambers and/or the conduit during magma ascent. Because crystals grow during magma rise, and due to the influence of particle concentration, size distribution and shape on suspension rheology, it is expected that the rheology of ascending magmas will change with time and position within a volcanic conduit.

This thesis investigates systematically the influence of CSD's on the rheology of vesicle free magmatic suspensions by using analogue rotational rheometric experiments with glass particles of different shapes in silicone oil acting as a magma equivalent. With the help of multimodal particle suspensions of well-defined size fractions, the analogue experiments of this study reveal that the polydispersity γ of the suspended particles exerts the largest influence on the maximum packing fraction ϕ_m of the suspension and consequently on its rheological behavior. In this thesis, an empirical model is derived in order to estimate the relative effect of crystal content and CSD's on the viscosity of magma directly from textural image analysis of natural rock samples. This model is applied to and tested by the measurement and analyses of the CSDs in experimentally grown crystal populations from high pressure/high temperature (HP/HT) petrological-experiments of Santorini pumice.

Kurzfassung

Die rheologischen Eigenschaften eines Magmas gelten als einer der entscheidenden Parameter für das Verständnis von Prozessen und Eigenschaften eines vulkanischen Systems. Die Rheologie eines Magmas innerhalb ihres jeweiligen natürlichen vulkanischen Systems bestimmen zu können, ist jedoch äußerst schwierig. Anhand von Laborstudien und Beobachtungen natürlicher vulkanischer Systeme wird vermutet, dass die Menge der in einer Schmelze suspendierten Kristalle und der Grad ihrer Wechselwirkung untereinander zentrale Parameter der Magmarheologie sind. Der Effekt von Partikel in der Schmelze hat enorme Auswirkungen auf vulkanologische Eruptionsmodelle und ist letztlich ein Schlüsselparameter dafür, ob eine Eruption explosiv oder effusiv sein wird. Eine wichtige Frage der Suspensionsrheologie bleibt jedoch trotz allen Fortschritts unbeantwortet: Wie beeinflusst die Größenverteilung der partikel die rheologischen Eigenschaften einer Suspension?

Kristallgrößenverteilungen (CSD) gelten als weit verbreitete Möglichkeit um diverse Aspekte der Kristallisationsgeschichte einer natürlichen Probe (z.B. Keimbildung und Wachstumsraten, etc.) zu beschreiben, um Prozesse innerhalb von Magmakammern und/oder des Schlots während des Magmenaufstiegs zu untersuchen. Da Kristalle während des Aufstiegs des Magmas wachsen und aufgrund des zuvor beschriebenen Effekts der Kristalle auf die Magmenrheologie, ist zu erwarten, dass sich auch die Rheologie der aufsteigenden Magmen mit der Zeit und ihrer Position innerhalb des Vulkanslots ändert.

Die vorliegende Dissertation untersucht systematisch den Effekt von Kristallgrößenverteilungen auf die Rheologie blasenfreier magmatischer Suspensionen mithilfe rheometrischer Rotationsexperimente. Als Magmaäquivalent fungiert im Rahmen dieser Analogexperimente ein Gemisch von Silikonöl mit darin gelösten Glaspartikel. Die Ergebnisse dieser umfassenden Experimentalreihe zeigen, dass die Polydispersität γ der suspendierten Partikel den größten Einfluss auf die maximale Packungsdichte ϕ_m der Suspension und damit auf ihr rheologisches Verhalten ausübt. Kern dieser Arbeit ist folglich ein empirisches Modell, welches es ermöglicht den relativen Einfluss des Kristallgehalts und der Korngrößenverteilung auf die Viskosität von Magma direkt aus der strukturellen Bildanalyse natürlicher Proben abzuschätzen. Dieses Modell wird zudem auf die Analyse der CSDs in experimentell gewachsenen Kristallpopulationen aus Hochdruck- / Hochtemperatur (HP/HT) - Experimenten angewendet und getestet.

1. Introduction

The rheology of a magma is recognized as one of the crucial parameters for the understanding of processes and features throughout a volcanic system – either it be within the magma chamber, in volcanic conduits or during eruptive and post-eruptive depositional processes. It might also be of use interpreting pre-eruptive volcanic unrest and earthquakes, and ultimately predicting volcanic hazards related to magma motion. Despite its key role in governing volcanic processes, magma rheology is extremely difficult to constrain in time and space within a natural volcanic system. The challenge stems from the fact that rheology is dependent upon so many, partly time-dependent variables, such as temperature, pressure, composition, deformation rate, and fraction of suspended particles or bubbles.

Magma is a complex mixture of a liquid, solids and a gaseous phase, and thus, magma rheology depends on the chemical composition of the melt, as well as on the volume fractions and physical characteristics of the two suspended phases – gas bubbles and crystals. It is well-known from laboratory studies, as well as from observations in natural volcanic systems that the amount of crystals suspended in the melt, and the degree to which they interact, are central parameters governing magma rheology. Accounting for, or neglecting the effect of solid particles in igneous petrological and volcanological eruption models can change their results by orders of magnitudes and may be a key parameter controlling whether an eruption is explosive or effusive.

In fact, knowing the flow properties of particle-bearing fluids is vital for understanding not only volcanological phenomena, but also for a variety of many other natural phenomena like landslides, mudflows or avalanches, as well as industrial or technological processes, like biotechnological (e.g Hahn *et al.*, 2015), pharmaceutical and cosmetic (e.g. Gallegos & Franco, 1999), as well as plastics (e.g., Dealy & Wang, 2013), paint (e.g., Strivens, 1999), petroleum and mining industries (e.g., Hasan *et al.*, 2010). Rheology is the study of deformation and flow of material and describes how a substance responds to an applied force. The term *rheology* originates from the Greek: $\rho\epsilon\acute{\iota}$ (rhei) and $\lambda\acute{o}\gamma\omicron\varsigma$ (logos) literally meaning the science of flow. However, this applies not only to the flow behavior of liquids, but also to the deformation of solids, that produced by shear forces cause many materials to flow and can therefore be treated as flowing material (Mezger, 2006). In theory, there are two endmember describing the behavior of a

deforming material: (a) the flow of ideally viscous liquids on the one hand and (b) the deformation of ideally elastic solids on the other. The behavior of most real materials is based on the combination of both a viscous and an elastic portion and therefore, it is called viscoelastic. One major task of rheology is to describe and/or measure exactly this behavior by the relationships between deformations (or rates of deformation) and stresses.

In geosciences, however, during the last four decades significant effort has been addressed to characterize and model the viscosity of silicate melts of various compositions (e.g., Hess & Dingwell, 1996; Giordano *et al.*, 2008; Robert *et al.*, 2014; among others). However, a powerful tool to isolate and systematically investigate different rheological influences are analogue experimental studies. Recent research has considerably improved our understanding of the flow properties of particle-bearing, bubble-free systems (Lejeune & Richet, 1995; Rutter & Neumann, 1995; Deubener & Brückner, 1997; Smith, 1997; Bagdassarov & Dorfman, 1998a, 1998b; Paterson, 2001; Mecklenburgh & Rutter, 2003; Petford, 2003; Lautze & Houghton, 2005; Llewellyn & Manga, 2005; Melnik & Sparks, 2005; Rowland *et al.*, 2005; Rutter *et al.*, 2006; Carricchi *et al.*, 2007; Gonnermann & Manga, 2007; Lavallée *et al.*, 2007; Champallier *et al.*, 2008; Hale & Wadge, 2008; Ishibashi, 2009; de Maissonneuve & Bachmann, 2009; Massol & Jaupart, 2009; Applegarth *et al.*, 2010; Castruccio *et al.*, 2010; Mueller S.P. *et al.*, 2010; Vetere *et al.*, 2010; Cimarelli *et al.*, 2011; Mueller *et al.*, 2011; Vona *et al.*, 2011; Pistone *et al.*, 2012; Del Gaudio *et al.*, 2013; Mader *et al.*, 2013; Del Gaudio, 2014; Moitra & Gonnermann, 2015; Truby *et al.*, 2015), as well as of or bubble-bearing, crystal-free systems (Bagdassarov & Dingwell, 1992, 1993a, 1993b; Lejeune *et al.*, 1999; Llewellyn *et al.*, 2002; Okumura *et al.*, 2006, 2008, 2009, 2010; Rust & Manga, 2002a, 2002b; Stein & Spera, 1992, 2002; Kameda *et al.*, 2008; Caricchi *et al.*, 2011). However, a key question in suspension rheology remains unanswered: How does the size distribution of suspended particles influence the flow?

Whilst considerable progress has been made in understanding the impact of the volume fraction (e.g., Pinkerton & Stevenson, 1992; Caricchi *et al.*, 2007; Mueller S.P. *et al.*, 2010) and shape (Mueller *et al.*, 2011; Mader *et al.*, 2013) of crystals on magma rheology in particular or two-phase mixtures in more general terms, the effect of the **particle size distribution** (PSD) on suspension rheology is still poorly constrained and it remains largely unclear in what way and to what extent a **crystal size distribution** (CSD) affects the rheology of a magma. A highly disperse PSD (i.e., a great variety of different

crystal sizes) leads to a much more efficient packing of crystals in a flowing magma and it is assumed that it is precisely the packing arrangement and the resulting particle interactions that predominantly controls the rheological behavior (e.g., Mader *et al.*, 2013). Despite the impact of PSD on suspension flow, only few studies address its influence on rheology directly (e.g., Olhero & Ferreira, 2004). Theoretical and experimental studies of non-uniform particle distributions are mainly restricted to uni- and bimodal cases, with particles of one and two distinct sizes respectively (e.g., Farris, 1968; Chong *et al.*, 1971; Chang & Powell, 1994; Probst *et al.*, 1994; Luckham & Ukeje, 1999; Wackenhut *et al.*, 2005; Cimarelli *et al.*, 2011; Faroughi & Huber, 2014).

Crystal-size distributions (CSD) are a widely used tool to describe aspects of a natural sample's crystallization history (e.g., nucleation and growth rates, cooling and residence time, qualitative degassing patterns) in order to examine processes within magma chambers and/or the conduit during magma ascent (e.g., Cashman & Marsh, 1988; Marsh, 1998; Moore & Carmichael, 1998; Hammer & Rutherford, 2002; Castro *et al.*, 2003; Mock & Jerram, 2005; Rannou & Caroff, 2010; Riker *et al.*, 2015, among others). Prior to an eruption, magmas undergo complex storage, ascent and decompression histories, which result in equally complex magmatic textures comprising crystals and vesicles in contact with quenched silicate melt (glass). Because crystals grow during magma rise, and due to the profound influence of particle concentration, size distribution, and shape on suspension rheology, it is expected that the rheology of ascending magmas will change with time and position within the volcanic conduit.

The goal of this thesis is to determine how the crystal size distributions in naturally occurring magmatic rocks develops as a function of depth, decompression rate, and volatile content in a magma chamber-volcanic conduit system. Such a project will provide realistic textural maps of a magma-filled volcanic conduit, from which it might be possible to interpret the ascent and eruption histories of volcanoes that have produced magma having clearly undergone pre- and syn-eruptive crystallization (Hammer *et al.*, 2000, 2002; Martel *et al.*, 2000; Castro & Gardner, 2008).

Therefore this thesis investigates systematically the effects of various polydisperse size distributions on the rheology of particle suspensions and link them to natural CSDs. It presents the results of a combination of systematic rheometric experiments using

multimodal particle suspensions of well-defined size fractions as magma-analogue material and high pressure/high temperature (HP/HT) petrological experiments on natural samples as real rock equivalents. Whilst analogue experiments do not capture processes such as crystal breakup and pressure solution, viscous heating effects or shear thinning melt behavior (which are thought to be operative in silicate liquid phases), they have the advantage over experiments with natural magmatic suspensions that they are better characterized with respect to their physical properties and allow more thorough exploration of parameter space - especially since the physical parameters involved can be controlled and isolated to a high degree of accuracy. Petrological HP/HT-experiments of natural volcanic samples on the other hand provide the opportunity to simulate and vary natural processes in a magma chamber and the conduit in order to try and test the results of analogue modeling directly and to compare these findings to natural rocks.

The results of this combined study provide the basis for a comprehensive and unique dataset of rheological parameters for particle bearing suspensions, as a function of particle concentration ϕ and PSD, which is the first of its kind up to date. Starting with simple uni- and bimodal distributions, the complexity (i.e. polydispersity) of the samples' PSD is increased towards tri- and tetramodal distributions. In addition, suspensions with Gaussian distributions with varying variance ('broadness') and skewness ('tailed distributions'; figure 1) are analyzed. The specific rheological parameters investigated are: (a) relative bulk viscosity (η_r), (b) strain rate dependence of viscosity (flow index n), (c) yield strength (τ_0) and (d) the maximum packing fraction ϕ_m of the suspension. The dataset permits validation and improvement of existing rheology models of polydisperse particle suspensions (e.g., Maron & Pierce, 1956; Krieger & Dougherty, 1959; Farris, 1968; Costa *et al.*, 2009) and provides links between the statistical characteristics of a PSD with its maximum packing fraction ϕ_m in order to draw inferences directly on its relative viscosity.

The intention of the petrological HP/HT-experiments is to measure the CSDs in experimentally grown crystal populations in order to test the finding of the analogue experiments on one hand and to gauge when and at what P-T conditions microlite crystallization occurs in a volcanic conduit (to map the conduit) on the other. By using the well-constrained mineral and glass compositional and textural database of Sanorini volcano at hand, this data can be used as starting points for controlled petrological

experiments. In particular, rhyodacitic pumice of the Minoan eruption of Santorini volcano is used as target composition in this thesis (e.g., Cottrell *et al.*, 1999; Druitt *et al.*, 1999). The set of experiments will have two primary goals: (a) to establish the pressure, temperature, and crystal texture relations in magma conduits (*phase equilibrium experiments*), as well as (b) to simulate a range of magma rise scenarios, which will investigate the effects of magma rise speed and total decompression on the ensuing textural and chemical signatures in the eruptive materials (*decompression experiments*).

1.1. Thesis layout

This thesis is mainly divided into two different parts (a) the analogue experiments, and (b) the petrological HP/HT-experiments. Chapter 2 introduces theoretical background and the current state of research in terms of the rheology of magmas and rheology in general, as well as the concept of particle-size distributions and the way this is used in this thesis. It also summarizes the methods of measuring the rheological parameters and presents rheometric setups. The actual experimental methods and techniques used within this thesis are discussed in chapter 3, starting with the measuring procedure in order to determine the viscosity of the sample and the sample preparation that is necessary to do so. This chapter also gives a detailed overview of the analyzed measurements, the measuring routine and how raw data is processed. Chapter 4 contains the main experiments and results of the analogue experiments. It provides the findings of the experimental approach linking PSD, maximum packing fraction and suspension viscosity to a newly developed model. Furthermore, that model as the key finding of this thesis is tested and a practical application for future use is presented and discussed.

Chapter 5 introduces the theoretical background and the ideas behind the petrological experiments used in this thesis. This includes the experimental strategy based on the concepts of phase equilibrium experiments, as well as of dynamic decompression experiments. Furthermore, the theoretical background of crystal-size distributions and the way this is used in volcanology is discussed here. The methodology of these HP/HT-experiments and the corresponding sample preparation is presented in chapter 6 giving an overview of all the measurements and how they were analyzed and processed. Thus, the image analyses and processing steps needed for the use of the model derived in chapter 4 are explained here. Chapter 7 contains the main results of the petrological experiments that

were put in context with the analogue experiments of the first part of this thesis. Limitations and applications, as well as possible strategies for future petrological work are also discussed. Finally, a concluding summary of this thesis and routes for future work in that field of research can be found in chapter 8.

2. Rheology

Rheology is the science of deformation and flow and is a measure of how a substance responds to an applied force. It originates from the Greek: $\rho\epsilon\tilde{\iota}$ (rhei) and $\lambda\acute{o}\gamma\omicron\varsigma$ (logos) literally meaning the science of flow. However, rheological experiments do not merely reveal information about flow behavior of liquids but also about deformation behavior of solids (Mezger, 2006). The connection here is that a large deformation produced by shear causes many materials to flow. All kinds of shear behavior can be viewed as being in between two extremes: flow of ideally viscous liquids on the one hand and deformation of ideally elastic solids on the other. Two illustrative examples for the end members of ideal behavior are low-viscosity mineral oils and rigid steel balls. The behavior of most real materials is based on the combination of both a viscous and an elastic portion and therefore, it is called viscoelastic. One major task of rheology is to describe and/or measure exactly this behavior by the relationships between deformations (strain or strain rates of deformation) and stresses (Mezger, 2006).

Rheology as a science in its own right was not established before the beginning of the 20th century. However, scientists and practical users have long before been interested in the behavior of liquids and solids, although some of their methods have not always been very scientific. This applies for example to Isaac Newton, Blaise Pascal, and Daniel Bernoulli in the 17th and 18th century, or to Thomas Young, Simeon Poisson, Georges Gabriel Stokes or James Clark Maxwell in the 19th to name a small selection (Mezger, 2006). Of special interest are the various attempts to classify all kinds of different rheological behavior, such as the classification of Markus Reiner in 1931 and 1960, and of George W. Scott Blair in 1942 and the introduction of rheology as an interdisciplinary field of research by E.C. Bingham and M. Reiner in 1929 (Mezger, 2006).

The upcoming chapter introduces the basic principles of rheology, its relevance for volcanological research and an overview of the current state of knowledge considering the rheology of particle-bearing suspensions, as well as rheometrical methods used in this thesis.

2.1. Rheology of magmas

As summarized by Mader *et al.* (2013), it is difficult to overstate the importance of an accurate, quantitative description of the rheology of magmas for volcanological research. A magma must possess rheological properties that allow it to be readily transported from the place it originated as a partial melt in the Earth's crust or mantle (Dingwell, 2006). Therefore the rheology of magma is an important parameter throughout a volcanic system. It is extremely important in determining the rates of emplacement of magma and the shapes of igneous bodies and governs transport dynamics in the conduit, rates of physicochemical processes (e.g., degassing, crystallization), as well as processes during and after an eruption (e.g., Papale, 1999; Cashman & Blundy, 2000; Spera, 2000; Sparks & Aspinall, 2004; Lautze & Houghton, 2005; Llewellyn & Manga, 2005; Melnik & Sparks, 2005; Rowland *et al.*, 2005; Dingwell, 2006; Carrichi *et al.*, 2007; Gonnermann & Manga, 2007; Giordano *et al.*, 2008; Hale & Wadge, 2008; de Maissoneuve & Bachmann, 2009; Massol & Jaupart, 2009; Applegarth *et al.*, 2010; among others). It is also a key parameter in modelling igneous petrological and volcanological processes (Pistone *et al.*, 2016) and, during the last decades, a field of intense research in order to characterize and model the viscosity of silicate melts (e.g., Alidibirov & Dingwell, 1996; Hess & Dingwell, 1996; Giordano *et al.*, 2008, among others) or in particular of basaltic (Pinkerton and Norton, 1995; Ryerson *et al.*, 1988; Robert *et al.*, 2014), andesitic (Lejeune & Richet, 1995), rhyolitic (Alidibirov *et al.*, 1997; Murase *et al.*, 1985; Stevenson *et al.*, 1996; Tuffen *et al.*, 2003) and synthetic melts (Brückner & Deubener, 1997). However, magma rheology is extremely difficult to constrain in time and space within a natural volcanic system. Measurements of viscosity have been made in the laboratory at both atmospheric and higher pressures on a variety of liquids formed by melting common igneous rocks. In addition, viscosities have been calculated from the actual measured flow rates of lava issuing from active volcanoes. Magma rheology is therefore a controlling input to all models of magmatic flow and hence our ability to predict volcanic hazards or interpret the volcanic record.

A magma is basically a mixture of three phases: a viscous silicate melt, crystals, and a volatile phase and its viscosity can span more than 15 orders of magnitude ($10^{-1} - 10^{14}$ Pa s; Figure 2), primarily in response to variations in temperature, melt composition and the proportions of suspended solids and/or exsolved fluid phases (Dingwell, 1996; Spera,

2000; Giordano *et al.*, 2004a,b; Giordano *et al.*, 2008). The rheology of silicate melts has been well-studied for a wide range of melt compositions and conditions (e.g., Hess & Dingwell, 1996; Giordano *et al.*, 2006; Neuville, 2006; Poe *et al.*, 2006; Vetere *et al.*, 2006; Hui & Zhang, 2007; Giordano *et al.*, 2008, 2009; Whittington *et al.*, 2009; Vetere *et al.*, 2014). Silicate melts can be treated as Newtonian liquids provided the strain-rate remains below a level defined by the structural relaxation timescale of the fluid λ_r (Mader, 2013). The structural relaxation timescale is thought to describe the timescale on which the material's internal microstructure can re-organize to accommodate strain and identifies the transition between relaxed, ductile flow and unrelaxed, brittle fracture (Mader, 2013). Gonnermann and Manga (2007) identify six parameters that affect the rheological behavior of a magma: (a) the chemical composition of the melt, (b) the volatile-dependent viscosity of the melt phase, (c) the magma temperature, (d) pressure, (e) the volume fraction and size of gas bubbles, (f) the volume fraction and shape of crystals, and (g) the rate of magma deformation. As a result, the rheology of magmas is extremely variable, with viscosities ranging over many orders of magnitude, often within a single volcanic eruption. The correlation between melt composition, temperature and melt viscosity has been investigated in numerous experimental studies, e.g., Shaw (1972), Webb & Dingwell (1990a; 1990b), Hess & Dingwell (1996), Giordano & Dingwell (2003). The viscosity models established in these studies, are now widely used in geological flow models and gave rise to a considerably enhanced understanding of the fluid dynamics behind magmatic and volcanological processes.

2.1.1. Chemical composition of melts

Strong interatomic bonds within a network of silicon and oxygen atoms are the main cause for the 'viscosity' of a volcanic melt. Therefore, the total amount of Silica and Oxygen in the melt, as well as the amount of other network forming components such as Al, Fe³⁺ or P⁵⁺ is a key factor in determining the viscosity (Spera, 2000; Gill, 2010). The structure of silicate melts is a disordered, three-dimensional network of interconnected SiO₄ tetrahedra and the degree of polymerization of these tetrahedra via bridging oxygen atoms determines the intrinsic viscosity of silicate melts, which can vary over orders of magnitude with chemical composition or volatile content (Giordano & Dingwell, 2003).

The rearrangement of the average molecular structure of a silicate melt is known as structural relaxation and is due to a continuous process of polymerization and depolymerization within the melt. It involves breaking and remaking of Si-O bonds, in other words a self-diffusive motion of atoms (Giordano & Dingwell, 2003). While the local structure is continually rearranging, the average structure of a melt is constant with time, akin to a dynamic equilibrium and is in part responsible for the viscous character of silicate melts (Moynihan, 1996). Following Mysen *et al.* (1982; 1984) and Mysen *et al.* (2005) the relation of non-bridging oxygens per tetrahedron (NBO/T) gives the degree of the polymerization. If NBO/T = 0 the melt is completely polymerized and the pure silicic melt has a high viscosity, while NBO/T = 4 represents a completely depolymerized melt with isolated SiO₄ tetrahedra resulting in a lower viscosity (Giordano & Dingwell, 2003).

2.1.2. Dissolved volatiles

The dominant volatile species in most magmas is H₂O. It dissociates into molecular water and hydroxyls when it dissolves and disrupts the bridging oxygens of the polymerized silicate network and therefore decrease the viscosity of the melt (Figure 1; Silver *et al.*, 1990; Best & Christiansen, 2001; Giordano & Dingwell, 2003; Gill, 2010). Such components are called network modifiers. While that behaviour is also known for other volatile components (CO₂, Cl, Br, I, S) and cations (Li⁺, K⁺, Na⁺, Ca²⁺, Mg²⁺), they appear to be less important in terms of directly influencing viscosity compared to the effect of H₂O (e.g., Dingwell *et al.*, 1998; Spera, 2000; Bourgue & Richet, 2001; Zimova and Webb, 2006).

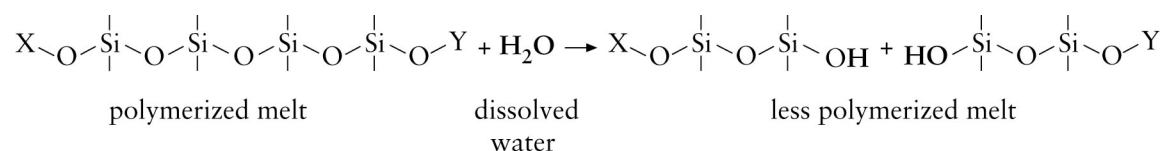


Figure 1: H₂O breaking SiO₄ chains (from Gill, 2010)

For rhyolitic melts, Hess & Dingwell (1996) developed a widely used empirical viscosity model. Viscosity varies by several orders of magnitude for typical water contents and temperatures observed in rhyolitic magmas (e.g., the addition of 3 wt.% H₂O lowers the viscosity of rhyolite melt up to three orders of magnitude; Spera, 2000). Similar

dependencies are observed for other melt compositions (Russell *et al.* 2002), but with comparative small effects on the viscosity of depolymerized (mafic and ultramafic) liquids because fewer bridging oxygen (BO) exist in in those melts (Spera, 2000; Giordano & Dingwell, 2003).

2.1.3. Magma temperature and pressure

Since higher temperatures are supposed to facilitate the depolymerization of melts, its viscosity strongly depends on temperature and decreases with higher temperatures (Figure 2). This dependency can be described by several models. Following Spera (2000), the simplest is the so-called Arrhenian model for a melt of fixed composition:

$$\eta = \eta_0 * \exp\left(\frac{E_A}{R*T}\right) \quad (2.1)$$

where η_0 is the asymptotic viscosity as $T \rightarrow \infty$, E_A is the activation energy for viscous flow, and R is the universal gas constant. For melts this means, that there is a linear relation between $\log \eta$ and $\frac{1}{T}$. However, the Arrhenian model is a rather simplistic approach, although very useful as a first estimate of a temperature-viscosity relationship.

Most silicate melts do not follow the Arrhenian temperature-viscosity relationship (Giordano & Dingwell, 2003; among others). This is especially true for fragile liquids (e.g., melts containing a high proportion of NBO). An empirical relationship for predicting the temperature dependence of viscosity data in fragile non-Arrhenian melts at 1 bar pressure is the so-called Tammann-Vogel-Fulcher (TVF) expression:

$$\eta = \eta_0 * \exp\left(\frac{B}{T-T_0}\right) \quad (2.2)$$

where B and T_0 are functions of composition but not of temperature (Giordano & Dingwell, 2003). In fact, T_0 is close to but usually somewhat less than T_g , the glass transition temperature (Spera, 2000). TVF model therefore shows that the variation in melt viscosity with reciprocal temperature decreases as temperature increases and is not a constant (E_A) as in the Arrhenian model (Spera, 2000). In fact, recent research extended the

TVF model making it a far more robust model (e.g., Giordano & Dingwell, 2003; Hui & Zhang, 2007).

Giordano *et al.* (2008) have calibrated an empirical model that gives melt viscosity as a function of composition and temperature based on the TVF formulation. This empirical model also provides estimates of the glass transition temperature and melt fragility as a function of melt composition at low pressure. However, pressure effects are not considered in the present form of this model. For less precise work, the Arrhenian model still finds application because it is so simple to implement, although extrapolating beyond the bounds of the experimental measurements is risky at best (Giordano *et al.*, 2008; among others).

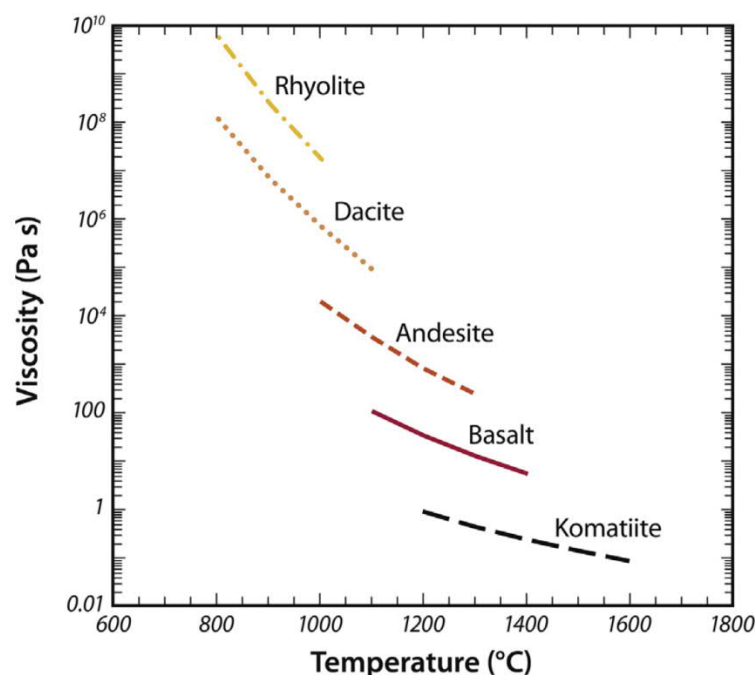


Figure 2: Viscosity in relation to temperature of various melt types (from Spera, 2000).

Apart from temperature, there is also a distinct effect of pressure on viscosity. As a general rule viscosity of fluids increases with elevated pressures. However, silicate melts often show a different trend and have lower viscosity at higher pressures (Figure 3; Mueller, H.J. *et al.*, 2010). It is thought that pressure increases the solubility of volatiles and therefore increases the depolymerization of melts. A measure of the pressure dependence of viscosity is the activation volume V_A . It is usually a small fraction of the molar volume of the melt and changes sign, from negative to positive, as the fraction of NBO increases and in the case of polymerized melts pressure increases (Spera, 2000). A

typical value for V_A for a network tetrahedral melt such as $\text{NaAl} - \text{Si}_3\text{O}_8$ at low pressure is around $-6 \text{ cm}^3/\text{mol}$, whereas for more depolymerized melt (e.g., $\text{CaMgSi}_2\text{O}_8$) V_A is around $3 \text{ cm}^3/\text{mol}$. Melts with a negative value of V_A show a decrease in viscosity as pressure increases, while the opposite is true for melts with positive V_A (Spera, 2000). Fully polymerized network melts, for which essentially all the oxygen is bridging oxygen (BO) typically possess intermediate range order defined by the formation of n-membered rings ($n = 4 - 10$) of tetrahedra at low pressure. As pressure increases, the ring structure collapses and the “anomalous” effect of viscosity ($-V_A$) diminishes to a point that free-volume effects dominate and viscosity increases with pressure ($+V_A$). Elevated pressure also drives oxygen into higher (five and six fold) coordination with Si and Al and such changes in the network structure also have been linked to the change from anomalous to normal pressure dependence of viscosity (Mueller, H.J. *et al.*, 2010).

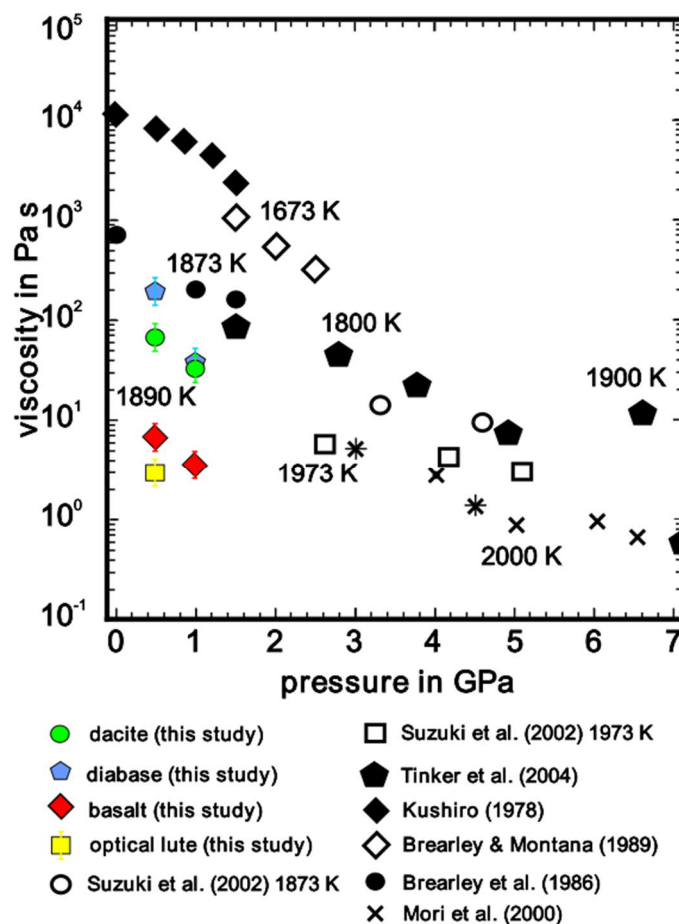
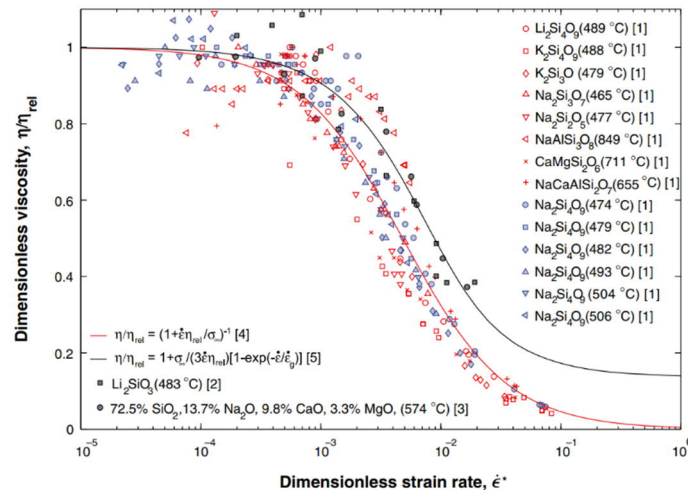


Figure 3: Viscosity in relation to pressure of various melt types (from Mueller, H.J., 2010).

2.1.4. Strain-rate dependence

As a consequence of structural relaxation (Moynihan *et al.*, 1996), silicate melts respond to applied forces with viscous deformation (Gonnermann & Manga, 2007). This is characterized by the flow relaxation rate $\dot{\epsilon}_r$ (Webb & Dingwell, 1990a; 1990b; Yue & Brückner, 1994; Moynihan *et al.*, 1996). At small deformation (strain) rates ($\dot{\gamma} \ll \dot{\epsilon}_r$) the melt is in a fully “relaxed” state, corresponding to Newtonian flow. At $\dot{\gamma} \sim \dot{\epsilon}_r$ the flow becomes shear-thinning, with a strain-rate-dependent (SRD) viscosity defined as η / η_{rel} , where η_{rel} is the Newtonian (relaxed) melt viscosity and η is the measured viscosity. Finally, at high deformation (strain) rates ($\dot{\gamma} \gg \dot{\epsilon}_r$) the induced relative motions of structural units are no longer compensated by random reordering of bridging oxygens, resulting in structural (brittle) failure of the melt (Gonnermann & Manga, 2007). SRD viscosities of silicate melts of a wide range of compositions and temperatures appear to have a similar dependence on the dimensionless strain rate, $\dot{\epsilon}^* = \dot{\gamma} \tau_s$ (Figure 4), where $\tau_s = \eta_{rel} / G$ is the structural relaxation time with a shear modulus $G \sim 10^{10}$ Pa (Webb & Dingwell, 1990a,b; Yue & Brückner, 1994; Simmons, 1998). Measured viscosities are well represented by the SRD equation (Simmons, 1998)

$$\frac{\eta}{\eta_{rel}} = (1 + \eta_{rel} \dot{\epsilon} / \dot{\epsilon}_r)^{-1} \quad (2.3)$$



- [1] Webb & Dingwell (1990)
 [2] Deubener & Brückner (1997)
 [3] Thies (2002)
 [4] Simmons *et al.* (1982)
 [5] Brückner & Yue (1994)

Figure 4: Dimensionless viscosity in relation to dimensionless strain rate of various melt types (from Gonnermann & Manga, 2007).

Here $\sigma_{\infty} \propto \eta_{rel}^{0.24}$ is the maximum shear (cohesive) strength that can be supported by the melt (Simmons, 1998). In the SRD equation it is assumed that viscous heating (shear heating) during viscosity measurements is negligible (Gonnermann & Manga, 2007). However, Yue & Brückner (1994) derive an alternative formulation that includes a correction for viscous heating.

2.1.5. Particles

Due to decompression and cooling, crystals nucleate and grow in the ascending magma (Hammer *et al.*, 1999; Hammer & Rutherford 2002; Couch *et al.*, 2003a). As a result the addition of crystals to a melt changes the chemical composition and the content of dissolved volatiles in the melt phase, but also affects the overall rheology of the magma and introduces non-Newtonian effects (Gonnermann & Manga, 2007). This is thought to be due to interaction of the suspended particles itself and/or deflection of the sheared flow field. Depending on particle shape and particle geometry, fluids can contain particles up to a certain limit when the suspension reaches its densest possible packing. This maximum packing fraction ϕ_m represents the volume fraction, at which particles can no longer flow past each other and the suspension becomes jammed, i.e. the viscosity goes, theoretically, to infinity. A more detailed overview on particle suspension rheology can be found in the upcoming chapters 2.2. and 2.3.

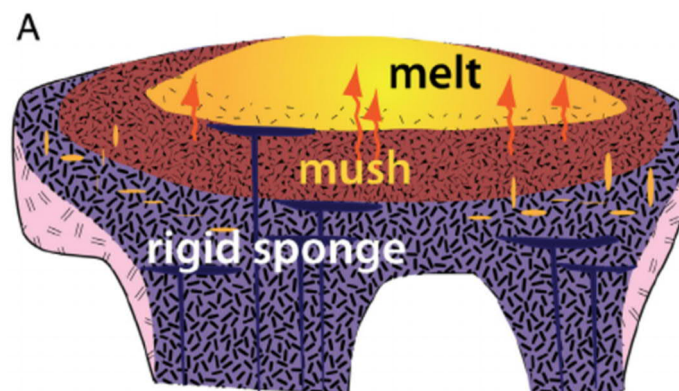


Figure 5: Example of an end member model of caldera-producing magmatic systems. (from Cashman & Giordano, 2014).

Recent research of individual (intermediate–silicic) magmatic systems have shown that magma storage regions are composed primarily of crystalline mush (Figure 5; e.g., Hildreth, 2004; Hildreth & Wilson, 2007; Lipman, 2007; Bachmann & Bergantz, 2008; Reid, 2008; Bachmann, 2010; Deering *et al.*, 2011; Walker *et al.*, 2013). In that context, following Cashman *et al.* (2017) the term “mush” refers to any system of crystals and melt in which the crystals form a continuous framework through which melt is distributed (Fig. 6). Thus, mushes are by definition at or above the solidus temperature and are synonymous with partially molten rock (Cashman & Giordano, 2014).

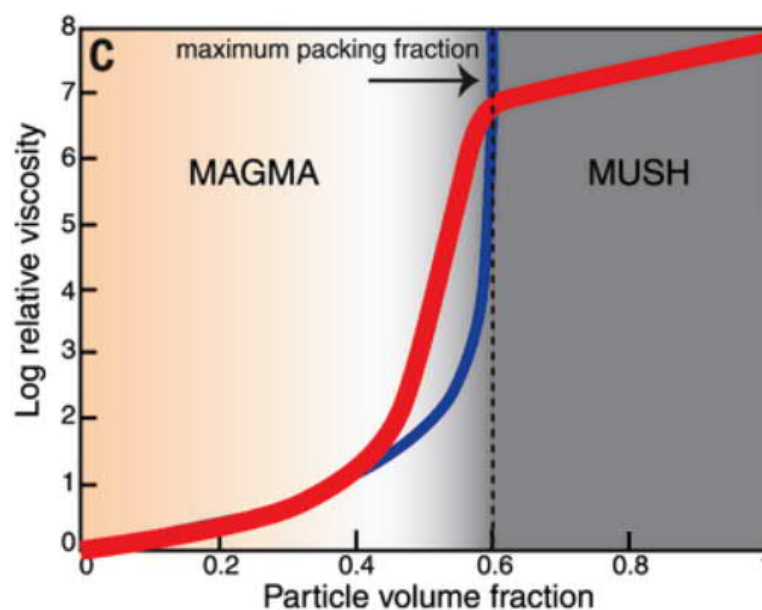


Figure 6: Relative viscosity in relation to particle volume fraction – maximum packing fraction and crystal mush (from Cashman *et al.*, 2017)

Because the rheology of those mushes is controlled by deformation of the crystalline framework, these mushes in their entirety are not eruptible (Cashman *et al.*, 2017). Most of these mush zones end up forming silicic plutons (Lipman, 1984; Bachmann *et al.*, 2007; Hildreth & Wilson, 2007; Lipman, 2007), although some erupt as crystal-rich ignimbrites (Lipman *et al.*, 1997; Lindsay *et al.*, 2001; Bachmann *et al.*, 2002; Maughan *et al.*, 2002). Mush fragments can be erupted as crystal clots (glomerocrysts), cumulate nodules, or restite (Cashman *et al.*, 2017). As discussed by Bachmann and Bergantz (2008) extraction of the interstitial melt may occur when mush zones contain 50-60 vol. % crystals so that chamber-wide convection currents are hindered by the formation of a quasi-rigid crystalline skeleton. The rheological transition from liquid to solid behavior occurs at ~50-60 vol. % crystals (Figure 6; Marsh, 1981; Brophy, 1991; Vigneresse *et al.*,

1996; Petford, 2003). However, the permeability is still high enough that melt can be efficiently extracted (McKenzie, 1985; Wickham, 1987; Bachmann & Bergantz, 2004). A mush-dominated view of igneous systems has great explanatory power, but requires new conceptual models for addressing questions related to both magma evolution and the behavior of volcanic systems (Cashman *et al.*, 2017).

2.2. Rheology of particle bearing suspensions - basic principles

The rheology of a suspension is generally characterized as a fluid in which the addition of particles increases the viscosity nonlinearly (Lavallee *et al.*, 2007). In order to describe the deformation or flow of matter quantitatively it is necessary to establish how the deforming stress, the shear stress τ , is related to the rate of deformation, the shear strain-rate $\dot{\gamma}$ in the first place. A constitutive relation is given by the equation $\tau_{ij} = f(\dot{\gamma}_{ij})$ where τ_{ij} and $\dot{\gamma}_{ij}$ are tensors that give a three-dimensional description of stress and strain-rate (Mader *et al.*, 2013). For most flows of practical interest that are used to measure or investigate rheology, the rectilinear nature of the flow and the symmetry of the tensors allows the equation to be reduced to the one-dimensional form $\tau = f(\dot{\gamma})$. As a result, in the simplest case the rate of deformation $\dot{\gamma}$ of a material is proportional to its imposed stress τ and its constitutive equation for most flow conditions of interest is given by:

$$\tau = \mu \dot{\gamma} \quad (2.4)$$

where μ is the Newtonian viscosity, which is independent of strain rate and has the unit Pa s. By convention, stress is plotted against strain-rate to produce a so-called flow curve (Figure 7); in the Newtonian case a straight line through the origin with a slope of μ .

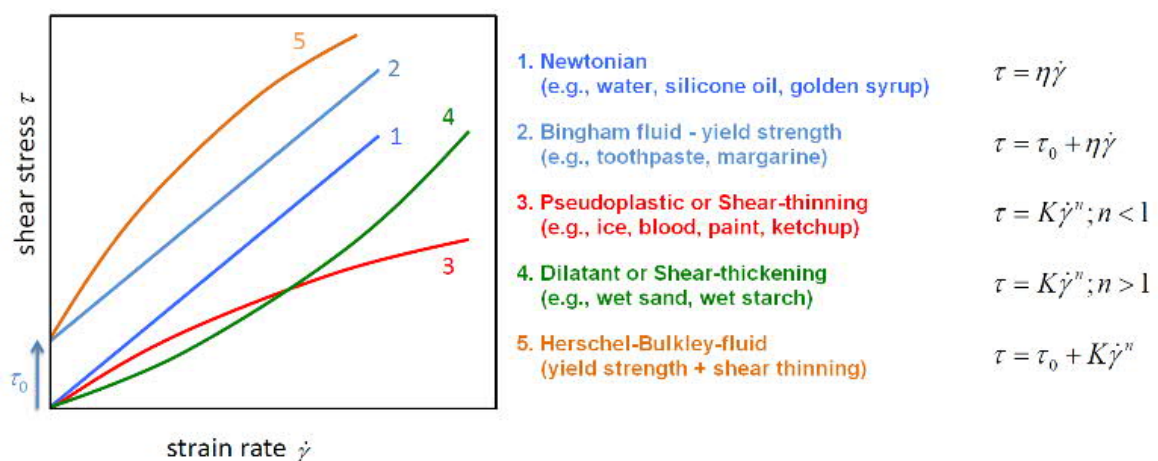


Figure 7: Summary of typical rheological behavior (modified from Mezger, 2006).

To define the fundamental rheological parameters used in equation (2.4), a widely used model is the so-called two-plates model (figure 8). While the upper plate with area A is set in motion by the shear force F with a resulting velocity v , the lower plate is stationary ($v = 0$). Due to this shear stress τ the sample between both plates is sheared and will flow in the gap h . It is assumed that the sample adheres to both plates and does not slide or slip along them and that the flow in between the plates is laminar and shows no turbulences (i. e. vortices). Shear stress τ then is defined as the force F per area A and has the unit Pa:

$$\tau = \frac{F}{A} \quad (2.5)$$

The shear rate $\dot{\gamma}$ is defined as the deformation (shear) or velocity v per plate distance h and has the unit s^{-1} :

$$\dot{\gamma} = \frac{v}{h} \quad (2.6)$$

For laminar flow conditions the difference in velocity between neighboring layers shows the same value ($dv = \text{const.}$) since the velocity $v(h)$ between the moving upper plate and the immovable lower plate decreases linearly. Because all layers are assumed to have the same thickness ($dh = \text{const.}$), the shear rate $\dot{\gamma}$ shows a constant value throughout the whole shear gap and is independent of the position of the flowing layer.

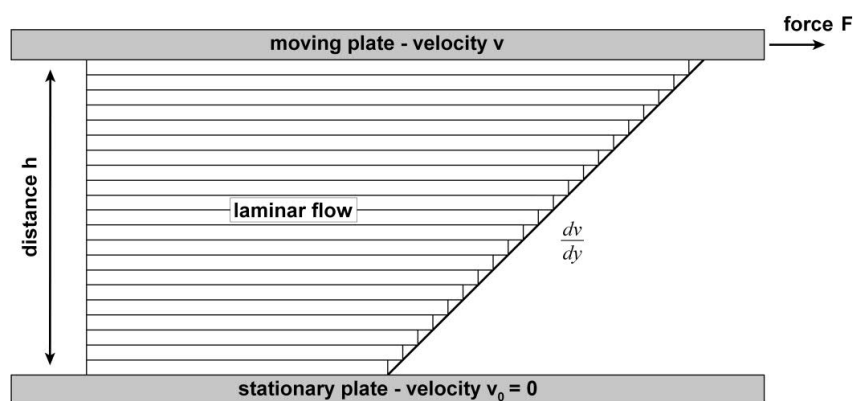


Figure 8: Two-plates model defining rheological parameters (modified from Mezger, 2006).

However, the addition of another phase to a Newtonian liquid, either a liquid to form an emulsion (e.g., Frankel & Acrivos, 1970), gaseous to form a bubble suspension (e.g., Llewellyn *et al.*, 2002), or solid as considered here, complicates matters considerably. Mostly it increases the bulk viscosity of the system possibly by several orders of magnitude, and may additionally introduce various so-called *non-Newtonian* effects such as shear thinning (e.g., Zarraga *et al.*, 2000), shear thickening (e.g., Sierou *et al.*, 2002; Fernandez *et al.*, 2013), yield strength and viscoelasticity (Mueller S.P. *et al.*, 2010). These changes in rheology can have dramatic effects on the eruptive behaviour of a volcanic system: an increase in viscosity accompanying the growth of crystals can cause, for example, a shift from effusive flow to a plugged system – and eventually lead to an explosive eruption (e.g., Melnik & Sparks, 2005). In experimental rheometry, however, it is common to describe the rheology of a fluid in terms of an apparent viscosity η_{app} measured at a particular stress or strain rate. While for a Newtonian fluid $\eta \equiv \mu$, for a non-Newtonian fluid the apparent viscosity is a function of strain rate. Consequently a single measurement of η at a given strain rate $\dot{\gamma}$ gives a rather poor indication of the overall rheological behaviour. Furthermore, the apparent viscosity of a suspension η_s is often normalized by the viscosity of the pure suspending liquid μ_0 (for a Newtonian liquid) and reported as the relative apparent viscosity ($\eta_r = \frac{\eta_s}{\mu_0}$).

In fact, many fluids exhibit non-Newtonian rheology (Mader *et al.*, 2013). It is not possible to define a single, strain-rate-independent viscosity for such non-linear flow curves. As discussed by Mader *et al.* (2013), the source of the non-Newtonian rheology seen in many single phase fluids is supposed to be associated with the arrangement of the molecules and the nature of the bonds between them (i.e., polymers are usually non-Newtonian, as is the process of creep, which is the very slow flow of crystalline solids such as ice or rock). In magma non-Newtonian rheology typically arises from the presence of a dispersed phase of either crystals or bubbles. Such multiphase suspensions are commonplace in nature and in industry and display all manner of non-Newtonian behavior.

Non-Newtonian behavior cannot be described by a simple linear correlation, so the three-parameter Herschel-Bulkley model is often used as a constitutive equation:

$$\tau = \tau_0 + K \dot{\gamma}^n \quad (2.7)$$

where the consistency K is cognate with viscosity, the flow index n defines the degree of non-Newtonian behaviour ($n < 1$ for shear thinning behaviour; $n > 1$ for shear thickening behaviour), and τ_0 is the yield strength (Herschel & Bulkley, 1926). For a Newtonian suspension, where $n = 1$ and $\tau_0 = 0$, the consistency K equals viscosity η and has the dimensions of dynamic viscosity: Pa s. In case $n \neq 1$ the fluids are called power law fluids and K has non-integer dimensions: Pa s ^{n} . As shown by Castruccio *et al.* (2010), Mueller S.P. *et al.* (2010), Del Gaudio *et al.* (2013) and Truby *et al.* (2015) among others, this model fits the flow curves of crystal bearing magmas adequately good. Figure 7 summarizes the flow curves of different rheological behavior related to different materials.

In rheometry, shear forces are applied to non-Newtonian fluids in order to investigate their properties. As mentioned before, in experimental rheometry it is common to describe the rheology of a fluid in terms of an apparent viscosity η measured at a particular stress or strain rate. While for a Newtonian fluid η equals μ , for a non-Newtonian fluid, apparent viscosity is a function of strain rate, and a single measurement of η at a given strain rate gives a rather poor indication of the exact rheological parameters. Furthermore, the apparent viscosity of a suspension η_s is often normalized by the viscosity of the pure suspending liquid μ_0 (for a Newtonian liquid) and reported as the relative apparent viscosity

$$\eta_r = \frac{\eta_s}{\mu_0} \quad (2.8)$$

- by analogy a relative consistency can therefore be defined as

$$K_r = \frac{K_s}{\mu_0} \quad (2.9).$$

K has non-integer dimensions: Pa s ^{n} . This fractional unit involves certain limitations and is not amenable to non-dimensionalization when $n \neq 1$ as discussed by Mueller *et al.* (2011) and Mader *et al.* (2013). Truby *et al.* (2015) addressed this problem by introducing a characteristic timescale t_c of a shear-thinning suspension against which the strain-rate can be non-dimensionalized, giving

$$\eta_p = \eta_*(t_c \dot{\gamma})^{n-1} \quad (2.10)$$

where η_p is the apparent viscosity and η_* is a ‘reference viscosity’ of the suspension (i.e. the apparent viscosity at strain-rate $\dot{\gamma} = 1/t_c$ (Truby *et al.*, 2015). Following this, a relative reference viscosity $\eta_{r,*}$ can be defined. Conveniently, t_c is close to or equals 1 s for most conditions of interest, so numerically, the values of K and $\eta_{r,*}$ are often similar or even identical (Truby *et al.*, 2015), so that equation (2.1) can be expressed as:

$$\tau = \tau_0 + \eta_{r,*} \dot{\gamma}^n \quad (2.11)$$

As discussed by Mueller S.P. *et al.* (2010), the rheology of a suspension of solid particles is mainly influenced by two different sets of parameters: (a) the properties of the fluid flow field, particularly the deformation rate $\dot{\gamma}$, and (b) the (intrinsic) properties of the suspension, such as the particles’ volume fraction ϕ (defined as the ratio of volume occupied by particles on total volume of suspension), the shape of the particles, and their size distribution. Servais *et al.* (2002) extend that list to properties like the maximum packing volume fraction ϕ_m , particle density, surface roughness, adsorbed agents on the particle surface, interparticle forces, aggregation and wetting properties of the suspended particles in the continuous phase. Numerous theoretical, experimental and semi-empirical studies exist on the dependency of suspension rheology on particle volume fraction ϕ . More detailed reviews can be found in Pabst (2004), Stickel & Powell (2005) or Mader *et al.* (2013).

Many of the models developed therein build upon the fundamental work by Einstein (1906, corrected 1911), in which he proposes – based on purely theoretical considerations – a linear relationship between the relative viscosity η_r of an ideally dilute suspension and ϕ .

$$\eta_r = 1 + B\phi \quad (2.12)$$

where the constant B is referred to as the so called ‘Einstein coefficient’ or ‘intrinsic viscosity’ with a theoretical value $B = 2.5$ for spheres (Figure 9). However, extensive experimental effort have not only found $1.5 \lesssim B \lesssim 5$ (cf. Happel, 1957; Brenner, 1970; Jeffrey & Acrivos, 1976; Pabst *et al.*, 2006), but also that Einstein's theory is only valid for $\phi \lesssim 0,01$ (Thomas, 1965) or $\phi \lesssim 0,02$ (Rutgers, 1962a; 1962b), which therefore defines the

limit of the dilute regime. Several researchers have attempted to extend the equation to cover semi-dilute suspensions by considering the coefficients of higher order terms in ϕ such as

$$\eta_r = 1 + B\phi + B_1\phi^2 + \dots \quad (2.13)$$

with $B = 2.5$ and $7.35 \lesssim B_1 \lesssim 14.1$ derived from consideration of particle–particle interactions (Figure 9; Guth & Gold, 1938; Vand, 1948; Manley & Mason, 1955; Mendoza & Santamaria-Holek, 2009). Lower values of B_1 have been found when Brownian motion (Saitô, 1950; Batchelor, 1977) and inertia (de Bruijn, 1942) are important.

However, polynomial relationships in (2.12) and (2.13) typically describe experimental data poorly when $\phi > 0.25$ and get worse as particle volume fraction increases (Mueller S.P. *et al.*, 2010). This is due to the fact, that both equations predict a finite value of viscosity as $\phi \rightarrow 1$, which is unphysical since there seems to be a densest possible packing for monodisperse spherical particles is $\phi_m \approx 0.74$, at which particle concentration the viscosity must be infinite (Torquato *et al.*, 2000). Because of the importance of the maximum packing fraction ϕ_m for suspension rheology and its widely use in a variety of models as an empirically-determined parameter, it will be discussed further down below (see chapter 2.3).

Using the fundamental work by Einstein as a starting point, many studies as those of Roscoe (1952; 1967), Maron & Pierce (1956), Krieger & Dougherty (1959), Gay *et al.* (1969), Dabak & Yucel (1986), Liu (2000) or Costa (2005) and Costa *et al.* (2009) covered and discussed the relationship of the effective viscosity η and the particle volume fraction ϕ , i.e., $\eta_r = \eta(\phi)$. Most of them not only stated a power law increase of η_r with ϕ , but also at least one parameter accounting for the ‘intrinsic’ properties of the suspension (i.e. the contribution of the particle load to the bulk viscosity). Roscoe (1952) extended Einstein’s limited model to higher concentrations of spheres and introduced the concept of a critical or maximum packing fraction ϕ_m at which incompressible solid particles reached their maximum concentration and would prevent the flow:

$$\eta_r = \left(1 - \frac{\phi}{\phi_m}\right)^{-2.5} \quad (2.14)$$

This so-called Einstein-Roscoe formulation has been widely used for volcanological and petrological applications (Figure 9). For example, Shaw *et al.* (1968) used it to explain the changes in viscosity due to crystal content of basalts, Marsh (1981) applied the equation for the calculation of viscosities of magmas, using a value of 0.6 for ϕ_m and Pinkerton & Stevenson (1992) used the equation for lavas with low crystals contents, while other studies used the equation for numerical modelling of magma dynamics (e.g., Huppert *et al.*, 1988; Papale *et al.*, 1998).

Krieger & Dougherty (1959) proposed a semi-empirical generalized form of (2.14) and considered the contribution of successive packets of suspension to the total particle volume fraction and to the suspension viscosity (termed the ‘functional equation’ approach by Pabst 2004) deriving the following relationship:

$$\eta_r = \left(1 - \frac{\phi}{\phi_m}\right)^{-B\phi_m} \quad (2.15)$$

where B is a constant and called the “Einstein coefficient” (Figure 9; Costa, 2005; Mueller S.P. *et al.*, 2010). This relationship is a popular choice for fitting to experimental data, in which case B and ϕ_m are considered to be fitting parameters (Jeffrey & Acrivos, 1976; Pabst, 2004; Pabst, *et al.* 2006; Mueller S.P. *et al.*, 2010; 2011). Based on the Ree–Eyring flow equations (Ree & Eyring, 1955a; 1955b) a simpler version of (2.9), with the same functional form was derived by Maron & Pierce (1956) and also independently by Quemada (1978):

$$\eta_r = \left(1 - \frac{\phi}{\phi_m}\right)^{-2} \quad (2.16)$$

This relationship has found widespread application and is used for data fitting when only one fitting parameter is desired. Note that binomial expansion of equations (2.14), (2.15) and (2.16) recovers the polynomial given in equation (2.13).

Although converging the Einstein relationship (2.12) for low concentrations and asymptote to infinite viscosity when ϕ approaches ϕ_m , by its mere nature the Einstein-Roscoe, Maron-Pierce and Krieger-Dougherty equations do not take into account the onset of non-Newtonian effects such as yield strength and strain rate-dependent viscosity, which

becomes significant at high crystal concentrations (Rutgers, 1962a; Hofmann, 1974; Pinkerton & Norton, 1995; Costa *et al.*, 2009; Mader *et al.*, 2013). In addition, the effects of polymodal size distributions of particles are not considered. A comprehensive summary of different types of non-Newtonian effects observed in concentrated suspensions of force-free spheres is given for example by Jeffrey & Acrivos (1976), Stickel & Powell (2005) or Castruccio *et al.* (2010).

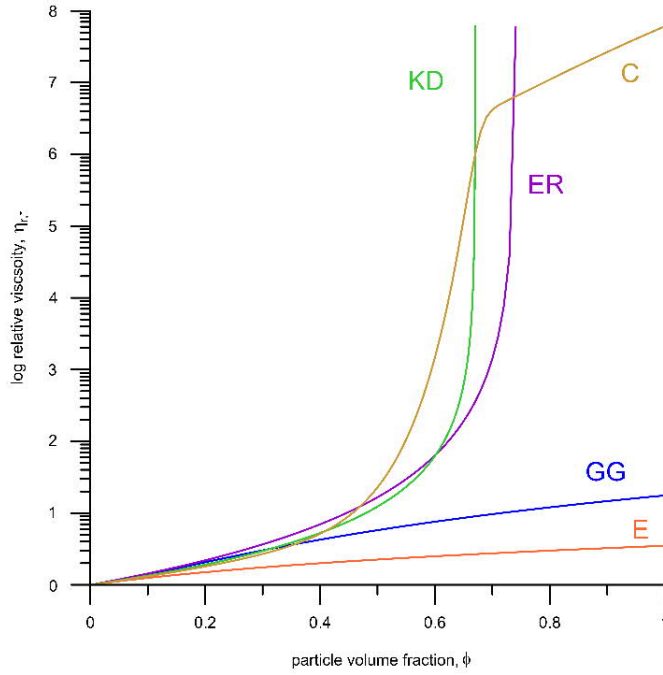


Figure 9: Schematic summary of different common models of particle suspension rheology (modified from Mader *et al.*, 2013).

It is known that even completely solid materials ($\phi = 1$) can deform plastically, albeit slowly, so that a model like $\eta_r = \eta(\phi)$ should not have a singularity at $\frac{\phi}{\phi_m} = 1$ and become infinitive but give finite values of η_r for $\phi_m \leq \phi \leq 1$ (Mader *et al.*, 2013). An attempt to encapsulate viscosity across the full range $0 \leq \phi \leq 1$ and to include the effect of crystal geometrical characteristics (i.e. crystal shape), has been presented by Costa (2005) and modified in Costa *et al.* (2009) (Figure 9). This model provides a set of empirical equations describing the relative viscosity of crystal-bearing magmas as function of crystal volume fraction and strain-rate:

$$\eta_r(\phi_*, \alpha, \delta, \xi) = \frac{\left(1 - \frac{\phi}{\phi_*}\right)^\delta}{\left[1 - F\left(\frac{\phi}{\phi_*}, \gamma\right)\right]^{B\phi_*}} \quad (2.17)$$

with

$$F = (1 - \xi) \operatorname{erf} \left[\frac{\sqrt{\pi}}{2(1-\xi)} \frac{\phi}{\phi_*} \left(1 + \frac{\phi^\alpha}{\phi_m^\alpha} \right) \right] \quad (2.18)$$

In this approach by Costa *et al.* (2009), the maximum packing fraction is replaced by the critical particle volume fraction ϕ_* at which particle-particle interactions start to dominate and the viscosity becomes very large. The rate of growth of viscosity is controlled by α as $\phi \rightarrow \phi_*$ and by δ as $\phi \rightarrow 1$ in the region of $\phi > \phi_*$. The value of viscosity attained at $\phi = \phi_*$ is controlled by ξ . For $\phi < \phi_*$ on the other hand (2.17) reduces to the Krieger–Dougherty equation (2.15) and as $\phi \rightarrow 0$ to the Einstein equation (2.21). However, as discussed by Mader *et al.* (2013) that model requires 4 parameters (5, if one includes the Einstein coefficient B) to be fitted experimentally (ϕ_* , α , δ , ξ) and so far there is no physical theory that relates the parameters to observable physical characteristics of the system.

Owing to the fact that magmas are three-phase systems (consisting of gas bubbles, solid crystals and silicate melt) as discussed before, there is also the need to consider bubble-bearing systems prior to building rheological models of such a three-phase system. Several studies focused on the physical properties of crystal-bearing, bubble-free systems (Lejeune & Richet, 1995; Deubener & Brückner, 1997; Smith, 1997; Bagdassarov & Dorfman, 1998a, 1998b; Paterson, 2001; Petford, 2003; Mecklenburgh & Rutter, 2003; Rutter & Neumann, 1995; Rutter *et al.*, 2006; Lavallée *et al.*, 2007, 2008; Caricchi *et al.*, 2007, 2008; Champallier *et al.*, 2008; Cordonnier *et al.*, 2009, 2012; Kohlstedt & Holtzman, 2009; Mueller S.P. *et al.*, 2010, 2011; Cimarelli *et al.*, 2011; Vona *et al.*, 2011; Forien *et al.*, 2011; Del Gaudio, 2014; Moitra & Gonnermann, 2015) or bubble-bearing, crystal-free systems (Bagdassarov & Dingwell, 1992, 1993a, 1993b; Lejeune *et al.*, 1999; Llewellyn *et al.*, 2002; Okumura *et al.*, 2006, 2008, 2009, 2010; Rust & Manga, 2002a, 2002b; Stein & Spera, 1992, 2002; Kameda *et al.*, 2008; Caricchi *et al.*, 2011).

While the most sophisticated model for two-phase magmatic systems of crystal-bearing suspensions up to now is given by the aforementioned model of Costa *et al.* (2009), the most sophisticated model for two-phase magmatic systems of bubble-bearing suspensions however, is given by Llewellyn *et al.* (2002). In bubble-melt mixtures, viscosity can be either, an increasing or decreasing function of the volume fraction of the low-viscosity phase ϕ depending on the rate at which the mixture is sheared (Spera, 2000).

At low rates of shear $\dot{\gamma}$, bubbles act as non-deformable inclusions and η_r increases with increasing ϕ similar to when solids (e.g., crystals) are added to melt. In distinction, at high shear rate, viscous stresses cause the bubbles to deform and the mixture viscosity decreases with increasing bubble fraction. If the flow is ‘steady’, the bubbles reach an equilibrium deformation, which is described by the bubble capillary number

$$Ca = \frac{\eta \dot{\gamma} r_b}{\sigma} \quad (2.19)$$

where η is the viscosity of the fluid, r_b represents the bubble radius, and σ the melt-vapor interfacial tension. If, however, the flow is ‘unsteady’, the bubbles may deform and relax such as the shape of the bubbles is not in equilibrium, which is described by the dynamic capillary number:

$$Cd = \lambda \frac{\dot{\gamma}}{\dot{\gamma}} \quad (2.20)$$

which gives the ratio of the bubble relaxation time λ to the timescale over which the strain rate changes appreciably.

Following Rust and Manga (2002a; 2002b) and Stein and Spera (2002), the capillary number can be thought of as the ratio of viscous tractions acting on the boundaries of a bubble that distort it from a spherical shape relative to interfacial surface forces that tends to preserve its spherical shape. Small values of Ca correspond to conditions where surface tension dominates and bubbles retain their spherical shapes. As a consequence, a relative viscosity relation of the form $\eta_r = f(\phi, Ca)$ can be expected such that for small capillary number (roughly $Ca < 1$), η_r is an increasing function of ϕ . In contrast, for regimes with $Ca > 1$, the relative viscosity decreases with increasing bubble content.

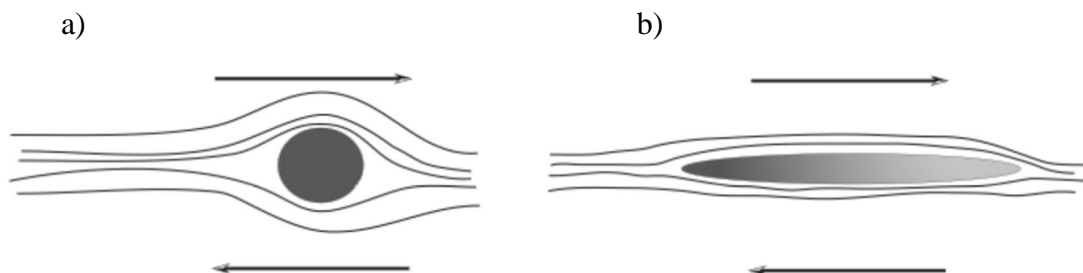


Figure 10: The influence of bubbles to a laminar flow (from Llewellyn et al. 2002). (a) high $Cd \gg 1$ (slow relaxation) and (b) small $Cd \ll 1$ (rapid relaxation)

Thus, when $Cd \ll 1$, bubble relaxation is rapid compared to the timescale of appreciable change in strain rate, hence the flow is approximately steady and the viscosity of the two-phase mixture can either increase or decrease with ϕ depending on the bubble shape as in the case of steady-flow conditions (Llewellyn *et al.*, 2002). By contrast, when $Cd \gg 1$, the bubbles cannot relax fast enough to reach their equilibrium deformation. They deform with the flow to a greater extent so bubbles flow past bubbles and, therefore, flow-line distortion, is reduced (Figure 10). Since natural systems span the range from $Ca < 1$ to $Ca \gg 1$, it is important to consider the dynamic regime when considering the effect of bubbles on the viscosity of magma (Spera, 2000; Llewellyn *et al.*, 2002).

As discussed by Pistone *et al.* (2016), to date, only a few rheological models account for the simultaneous presence of particles and bubbles. By using the so-called effective medium theory, in which one phase (either crystals or bubbles) is treated as a continuous medium that suspends the other, Harris and Allen (2008) adopted the treatment for the viscosity of a three-phase mixture to describe the rheology of multiphase basaltic lava flows following the approach of Phan-Thien and Pham (1997). If one phase is much smaller than the other in relative size, that phase is treated as an effective medium. When crystals are much smaller than bubbles, the three-phase mixture becomes the proxy of a bubble-bearing suspension; when crystals are much larger than bubbles, the three-phase mixture becomes the proxy of a crystal-bearing suspension. When both phases display similar size, the resulting multiphase mixture viscosity is intermediate between the two above described. Thus, the three-phase mixture is reduced to a two-phase system in the rheological model cases (Pistone *et al.*, 2016).

By using this effective medium approach, Truby *et al.* (2015) developed a three-phase rheology model on two-phase constitutive equations treating the bubble suspension as the continuous medium in which the particles are suspended. This approach carries the implicit assumption that the bubbles are small compared to the particles (similarly to the case when bubbles are smaller than crystals, as reported in the approach by Harris & Allen, 2008). In the form

$$\eta_{r,*} = (1 - \phi_b)^{-1} \left(1 - \frac{\phi_p}{\phi_m}\right)^{-2} \quad (2.21)$$

they validate the model against experimental data for three-phase suspensions of bubbles and spherical particles in the low-capillarity regime (in which flow is steady and bubbles remain spherical/rigid during deformation) and applied it to basaltic systems characterized by low melt viscosity ($\sim 10^5$ Pa s).

However, as mentioned by Pistone *et al.* (2016), despite the potential of their model to be applied to a wide range of crystallinity (~ 50 vol.%) and bubble content (> 30 vol.%), this three-phase rheological model does not include the dynamics of mutual interactions between crystals and gas bubbles occurring during deformation. Moreover, due to the application of the effective medium theory, in their two-phase type model, bubbles are not deformable in a low-viscosity suspension. Therefore, neither the model of Harris and Allen (2008), nor the model of Truby *et al.* (2015) might be directly applied to describe the rheology of high-viscosity systems containing gas-pressurised bubbles or to quantify the rheology of high-viscosity systems deforming in unsteady flow conditions, which are characteristic for the ascent of highly viscous magmas (e.g., Caricchi *et al.*, 2011).

2.3. Maximum packing fraction ϕ_m

As discussed in Mader *et al.* (2013) most expressions intended to model data in the (semi-) concentrated regime explicitly include this parameter ϕ_m and treat it as an empirically-determined parameter defined by the volume fraction at which the viscosity is expected to become infinite. In the form

$$\eta_r = f\left(\frac{\phi}{\phi_m}\right) \quad (2.22)$$

it is simply a direct scalar measure of suspension microstructure (Stickel & Powell, 2005). In suspension rheology literature it is widely accepted that ϕ_m (sometimes also ϕ_{max} , ϕ_c , or ϕ_{crit}) is an adequate proxy for the particle microstructure of a suspension, encapsulates most rheologically relevant microstructural information of any given particles suspension and therefore might possibly be a key factor to describe the viscosity of a suspension (cf. Liu & Masliyah, 1996; Servais *et al.*, 2002; Pabst, 2004). When the solid fraction reaches ϕ_m , a rheological transition occurs from a regime where the rheology is basically determined by the liquid phase to a regime where the effect of crystals is predominant and

the viscosity values are much higher (Costa, 2005). Experiments presented by Costa *et al.* (2009) linking crystallizing magma to partially melted rocks suggest that relative viscosity levels out again at very high crystal volume fraction.

However, the maximum packing fraction is also an important parameter for all kinds of packing problems. Literally, ϕ_m describes the densest possible packing for a given particle geometry and size distribution, but it can also, in a rheological sense represent the volume fraction, at which particles can no longer flow past each other and the suspension becomes jammed, i.e. the viscosity goes to infinity. Thus, there exist ambiguities in the exact definition of ϕ_m , mainly depending on how it is measured. For monodisperse spheres a geometrically perfectly ordered face-centred cubic (fcc) close packing is the most densest packing possible and yields $\phi_m = 0.74$ (Torquato *et al.*, 2000). That corresponds also to hexagonal closest packing (hcp) and its stacking variants, all with a coordination number of 12 (i.e. a chosen particle has 12 nearest neighbors in direct point contact; Torquato *et al.*, 2000). More realistic scenarios feature randomly organized, disordered packings, with lower values $\phi_m \approx 0.63 - 0.65$ (e.g., Bernal & Mason, 1960; Rintoul & Torquato 1996; 1997; and others). This is mostly referred to as the random close packing ϕ_{rcp} and is typically defined as a collection of particles packed into the densest possible amorphous configuration, although more rigorous definitions are available (Torquato *et al.*, 2000). However, Torquato *et al.* (2000) also showed that there is no constitutive definition of what is a random closed packing.

Packing type	Packing fraction	Coordination number
Closest packing(fcc / hcp)	0.7405	12
Tetragonal-sphenoidal	0.708	10
Body-centered cubic	0.680	8
Orthorhombic	0.605	8
Simple cubic	0.524	6
Diamond	0.340	4

Table 1: Packing fraction and coordination number of ordered packings of monosized spheres in 3D space. (from Pabst & Gregorova, 2013).

A simple cubic packing, has a $\phi_m \approx 0.52$ and a coordination number of 6 (Table 1). However, it is not known whether stable packings of monosized spheres with lower packing fraction and coordination number exist in 3D space (diamond packing with a packing fraction of 0.34 and a coordination number of 4 is unstable; Pabst & Gregorova, 2013). Higher packing fractions can be achieved by polydisperse particle systems and nonspherical (e.g., polyhedral or anisometric) particles, but following Kansal *et al.* (2002), ϕ_m of a suspension with spheres of very diverse sizes cannot be greater than $\cong 0.93$ ($\phi_m \cong 0.87$ for a polydisperse random sphere packing).

Generally, values of ϕ_m determined from rheological flow experiments (i.e., by extrapolation of the suspension viscosity towards infinity) are lower than the estimated values for static geometrical maximum packing and supposed to be slightly higher than randomly packed particles: $\phi_m \approx 0.67 - 0.68$ (Rutgers, 1962a; Kitano *et al.*, 1981; Evans & Gibson, 1986; Pabst *et al.*, 2006; Castruccio *et al.*, 2010; Cimorelli *et al.*, 2011; Mueller S.P. *et al.*, 2010, 2011). With increasing particle anisotropy (i.e., increasing particle aspect ratio), ϕ_m tends to decrease (e.g., Saar *et al.*, 2001; Mueller S.P. *et al.*, 2010; 2011), while a high degree of polydispersity increases ϕ_m , and hence substantially influence the rheological properties of a suspension. A hypothetical end-member example of this effect is a suspension of spheres with uniform diameter, in which the spaces between the spheres is successively filled by a set of smaller spheres. This way, one could – theoretically – approach a space filling of close to 100 %, i.e. $\phi_m = 1$ (the so-called *Appollonian packing*). Theoretically, in such a material, granular flow might be possible even at extremely high particle concentrations, and common suspension rheology models would drastically overestimate their viscosity.

Due to its use as an adequate proxy for the particle microstructure and as a possible key factor to describe the viscosity of a suspension, it might be helpful to link the maximum packing fraction directly to the apparent viscosity of polydisperse suspensions, i.e. to predict the viscosity of a particle bearing suspension directly by knowing the maximum packing fraction of its particles. To date, however, no first principles theory is available to predict the effects of polydispersity on the maximum packing fraction except in certain limiting cases (Dames *et al.*, 2001; Servais *et al.*, 2002; Le Meins *et al.*, 2002; Olhero & Ferreira, 2004; Brouwers, 2010; Hahn *et al.*, 2015; Mwasame *et al.*, 2016). Thus, there is no constitutive definition or characteristic estimation of either ϕ_m and ϕ_{rcp} in

terms of their rheological impact and what it actually means for a particle-bearing suspension to reach ϕ_m as discussed for example by Torquato *et al.* (2000). For a further review referring jammed hard-particle packings, Torquato & Stillinger (2010) can be recommended.

2.4. Particle Size Distributions / Crystal Size Distributions

Despite their explicit relevance for suspension flow, few studies address the influence of particle size distribution (PSD) on rheology directly and the effect of the crystal size distribution (CSD) on the rheology of magma is still poorly constrained. Crystal size is the most commonly quantified textural parameter in igneous rocks (Rannou & Carroff, 2010). Consequently, analyses of crystal-size distributions are widely used tools to examine processes within magma chambers and/or the conduit during magma ascent in volcanology (e.g., Marsh, 1981; Cashman & Marsh, 1988, Marsh, 1988a; 1988b; Marsh, 1998; Moore & Carmicheal, 1998; Hammer *et al.*, 1999; Hammer *et al.*, 2000; Martel *et al.*, 2000; Hammer *et al.*, 2002; Hammer & Rutherford, 2002; Mastin, 2002; Wallace *et al.*, 2002; Castro *et al.*, 2003; Mock & Jerram, 2005; Armienti, 2008; Castro & Gardner, 2008; Pichavent *et al.*, 2009; Metrich *et al.*, 2010; Rannou & Caroff, 2010; Gurioli *et al.*, 2014; Riker *et al.*, 2015, among others). A more detailed summary and discussion concerning the relevance of CSD's to volcanology can be found in chapter 5.

Aspects of a natural sample's crystallization history (e.g., nucleation and growth rates, cooling and residence time, qualitative degassing patterns) can be extracted from the form of a crystal size distribution (Cashman & Marsh, 1988). Following Pupier *et al.* (2008), in general terms CSD theory considers the cumulative distribution of crystal size $N(L)$, defined by the number of crystals by unit volume whose size is smaller than L . Thus, the population density $n(L)$ is defined as the number of crystals per unit volume and per size interval ΔL (i.e. for sizes in the range L to $L + \Delta L$). $n(L)$ and $N(L)$ are related through the relation

$$N(L) = \int_0^L n(L) dL \quad (2.23)$$

As a consequence, a CSD is a plot of the natural logarithm of the population density ($\ln(n)$; n =number of crystals per unit volume per unit length) versus the crystal size, measured as either the length or breadth of the crystal in two or three dimensions. The

basis for plotting a CSD is the standard histogram, and methods to convert a histogram to a CSD are demonstrated by Higgins (2006a; 2006b). CSD data typically fall onto straight or curved lines in CSD space and the slopes and y-intercepts of these lines can be used to distinguish different crystal populations within the rock and the time evolution of the crystal population (e.g., Hammer *et al.*, 1999, Higgins & Roberge, 2007).

Many magmas have polymodal size-distributions of crystals, which could affect rheology as a function of crystal content because small crystals may be able to pass through gaps between larger crystals. Therefore it is straightforward that there is a relation between the particle size distribution of a suspension and its shape and the maximum packing fraction of the given particles (e.g., McBirney & Murase, 1984), and therefore the PSD has a huge effect on the rheology. Nonetheless, extensive literature on theoretical and experimental studies of non-uniform particle distributions are mainly constricted to the bimodal case and in many cases to spherical particles only (e.g., Thomas, 1965; Farris, 1968; Lee, 1970; Chong *et al.*, 1971; Bierwagen & Saunders, 1974; Hoffman, 1974; Berryman, 1983; Zheng *et al.*, 1990; Hoffman, 1992; Chang & Powell, 1994; Probst *et al.*, 1994; Zhou *et al.*, 1995; Gondret & Petit, 1997; D'Haene & Mewis, 1994; Yu *et al.*, 1997; Luckham & Ukeje, 1999; He & Ekere, 2001; LeMeins *et al.*, 2002; Darias *et al.*, 2002; Liu & Ha, 2002; Wackenhut *et al.*, 2005; Brouwers, 2006; 2013; Morgan & Jerram, 2006; Cimarelli *et al.*, 2011; Baranau & Tallarek, 2014; Faroughi & Huber, 2014; Shewan & Stokes, 2015), or discuss the optimal blend ratio of different particle size fraction to lower the viscosity in order to optimize industrial processes (e.g., Farris, 1968; Wildemuth & Williams, 1984; 1985; Dames *et al.*, 2001; Subbanna & Kapur., 2002; Servais, 2002; Buranasrisak & Narasingha, 2012; Hahn *et al.*, 2015). In a review, Metzner (1985) concludes that the distribution of particle sizes has little effect on suspension viscosity when $\phi < 0.2$, while at high particle concentration levels the effects are of enormous magnitude, and extraordinarily high solids concentrations can be achieved by using multimodal distributions of particle size. However, the conclusion of Metzner (1985) that available experimental results are probably too limited to produce definitive design equations, is still valid and more precised by Servais (2002): a method to calculate the packing fraction for a continuous particle size distribution is still required.

However, none of these individual models allow a satisfactory application to natural volcanic rocks, where the concentrations, shapes and size distributions of the particles are

variable due to changing, temperature, shear rate, oxygen fugacity, etc. (e.g., Arzilli & Carroll, 2013; Kolzenburg *et al.*, 2016; Vetere *et al.*, 2010; among others). Since it is not possible to estimate effective viscosities in the field, there is the need of an integrated model accounting for volume fraction, aspect ratio and CSD by combining and partly extending existing empirical models of for example Mader *et al.* (2013) and Maron and Pierce (1956).

Basis for many analytical investigations is the study of Farris (1968). In a purely theoretical treatment, he proposed an effective medium model for the rheology of bimodal suspensions, in which the coarser particle size-class is treated as being suspended in a fluid consisting of the pure liquid and all finer particle size-classes (the ‘effective medium’). He defines so-called stiffening factors $H_f = \frac{\eta_f}{\mu}$ and $H_s = \frac{\eta_s}{\eta_f}$, where η_f is the viscosity of the liquid including fine particles, η_s the viscosity of the bulk viscosity of the liquid and both fine and coarse particles, and μ the liquid viscosity. The relative viscosity of the bimodal suspension is hence given by $\eta_r = H_s H_f$. By extension, this equation can be, theoretically, also applied for n particle sizes: $\eta_r = H_1 H_2 H_3 \cdots H_n = \prod_{i=1}^n H_i$, where H for the i -th size class is given by $H_i = \eta_i / \eta_{i-1}$; $\eta_0 = \mu$. As shown by Servais *et al.* (2002), excellent agreement between theoretical and experimental viscosity for up to trimodal suspensions has been reported for colloidal and non-colloidal polymethyl methacrylate (PMMA) beads in silicone oil, polystyrene spheres in silicone oil (Barnes *et al.*, 1989; Larson, 1999), glass beads and fibres in ceramic composites (Milewski, 1973) and coal in water (Funk & Dinger, 1993). However, Mwasame *et al.* (2016) extended this approach by assuming that each smaller particle size class contributes to the suspension viscosity through a weighting function in two ways: by altering the background viscosity, as well as by increasing the contribution of the larger particles to the suspension viscosity.

From a statistical point of view each size distribution is described by several parameters which according to Blott & Pye (2001) fall into four principal groups: those measuring (a) the average size, (b) the spread of the sizes around the average (standard deviation), (c) the symmetry or preferential spread (skewness) to one side of the average, and (d) the degree of concentration of the grains relative to the average (kurtosis). In fact, all of those values together characterize a distribution and it is not enough to consider only one value to fully describe a distribution. The reduction to a single statistical parameter

would be the key to link PSD with the maximum packing fraction in the first place to make assumptions on the relative viscosity of a suspension by just considering the particles dissolved in the fluid. As discussed in Blott & Pye (2001; 2012) the statistical characteristics of distributions can be obtained either by mathematical or graphical methods. While the classical approach of these graphical methods is based on the idea of plotting frequency data as a cumulative frequency curve, extracting prescribed values from the curve (percentiles) and entering these into established formulae (e.g., Trask, 1932; Krumbein, 1938; Otto, 1939; Inman, 1952; Folk & Ward, 1957 or McCammon, 1962), the mathematical ‘method of moments’ (Krumbein & Pettijohn, 1938; Friedman & Johnson, 1982) on the other hand is the most accurate way since it employs the entire sample population. Originally developed for sedimentological purposes the software Gradistat (Blott & Pye, 2001) provides automated calculation of the statistical characteristics of a given distribution either way. On the other hand those calculations can be checked using image analysis.

Linked to particle size distributions and also widely discussed in a variety of studies are the characteristics and effects of polydispersity on PSDs (Pusey, 1987; Lubachevsky & Stillinger, 1990; Schaertl & Sillescu, 1994; Phan *et al.*, 1998; Schöpe *et al.*, 2007; Farr & Groot, 2009; Kurita & Weeks, 2011; Kurita *et al.*, 2012; Pond *et al.*, 2011; Poon *et al.*, 2012; Desmond & Weeks, 2013; Kurita, 2015; Shewan & Stokes, 2015; Gu *et al.*, 2016). Though mostly evaluated by numerical models it is widely accepted, that an increasing polydispersity increases the maximum packing fraction (cf. Schaertl & Sillescu, 1994; Kansal *et al.*, 2002). Physically, this is straightforward since with increasing polydispersity the particles pack to higher volume fractions because the smaller particles pack more efficiently by either layering against larger particles or by fitting into the voids created between neighbouring larger particles (cf. Desmond & Weeks, 2013 and references therein). Polydispersity δ is defined as the standard deviation of a probability distribution normalised by its mean - in terms of mathematical statistics the coefficient of variation or in other words a dimensionless measure of the degree of variation in a distribution (cf. Liddle, 2014).

According to Phan *et al.* (1998) the polydispersity of a size distribution can be calculated using equation

$$\delta^* = \frac{\sqrt{r^2 - \bar{r}^2}}{\bar{r}}. \quad (2.24)$$

where r is particle radius and overbars indicate an average. It must be taken into account that most of these studies and numerical models are limited to bi-disperse or rather simple particle distributions like log-normal distributions (Farr & Groot, 2009). So far there is no comprehending model describing polydisperse suspensions.

However, Phan *et al.* (1998) present an empirical model to evaluate the effect of polydispersity δ on the maximum packing fraction with

$$\phi_{max} = \phi_{max}^0 \left[1 - \frac{3}{2} \delta^* + \frac{15}{4} \delta^{*2} \right] \quad (2.25)$$

where

$$\phi_{max}^0 = 4 \pi \overline{r^3} / 3 v_0 \quad (2.26).$$

As a matter of fact, they expect their model to overestimate the effect of polydispersity due to the simplicity of their model. Desmond & Weeks (2013) on the other hand take a step forward and widen the above mentioned model to statistical characteristics of distributions with random close packing of spheres. In a purely theoretical approach they found that skewness and polydispersity can have a significant effect on the packing density, whereas the kurtosis has almost no clear effect. In the end they come up with an empiric model to describe the above mentioned relation:

$$\phi_{rcp} = \phi_{rcp}^* + c_1 \delta + c_2 S \delta^2 \quad (2.27)$$

where $\phi_{rcp}^* = 0,634$ is the packing fraction for a monodisperse packing of spheres, c_1 and c_2 are empirical constants and δ the polydispersity of the distribution. The polydispersity in that case is defined by:

$$\delta = \frac{\sqrt{\langle r^2 \rangle - \langle r \rangle^2}}{\langle r \rangle} \quad (2.28)$$

where σ is the standard deviation, r is particle radius, $\langle r \rangle$ is the mean and overbars indicate an average. In their study, they also present an empirical model to evaluate the effect of polydispersity δ on the maximum packing fraction, which is extended by Desmond and Weeks (2013) to statistical characteristics of distributions with random close packing of

spheres. They showed that skewness and polydispersity have a significant effect on the packing density, whereas kurtosis has almost no effect.

The definition of polydispersity δ following equation (2.28) neglects the influence of the shape of a given distribution and only quantifies of the degree of variation in that distribution. To take the shape of the distribution into account, Wadsworth *et al.* (2017) adopted a parameter derived by Torquato (2013) as a measure for the polydispersity based on the specific surface area of the particles. For monodisperse spheres with sphere number density ρ , sphere volume V , the volume fraction ϕ and sphere radius r , the specific surface area s_m is as follows:

$$s_m = \frac{3 \rho V \phi}{r} \quad (2.29)$$

The specific surface area of a system of polydisperse spheres s_p with a distribution of radii and for which $\langle r^2 \rangle$ and $\langle r^3 \rangle$ are the second and third moments of the distribution respectively, is as follows:

$$s_p = 3 \rho V \phi \frac{\langle r^2 \rangle}{\langle r^3 \rangle} \quad (2.30)$$

The parameter γ represents the ratio of the specific surface of a polydisperse system s_p to that of a monodisperse system s_m at the same volume fraction with radius r , so that an increasing degree of polydispersity decreases the surface area ratio γ at the same time, while $\gamma = 1$ represents the monodisperse limit (Torquato, 2013):

$$\gamma = \frac{s_p}{s_m} = \frac{r \langle r \rangle}{\langle r^3 \rangle} \equiv \frac{\langle r \rangle \langle r^2 \rangle}{\langle r^3 \rangle} \quad (2.31)$$

where $\langle r^i \rangle$ is the i -th moment of a given size distribution. Following Chianese and Kramer (2012), the i -th moment of a size distribution is defined as

$$m_n = \int_0^\infty r^i n(L) dr \quad (2.32)$$

By using these moments, the shape of a distribution is represented and polydispersity γ should be a more robust parameter than δ alone.

2.5. Rheometry

The measuring technology and experimental techniques used to determine rheological properties, to measure deformation and flow behavior of a great variety of matters and to explain it, are known as *rheometry* while the actual experimental devices are defined as *rheometers*. In contrast to that, measuring systems used for viscosity measurements are specified as *viscometers* (Mezger, 2006). In the most simple case this applies to the flow of a material on a horizontal, inclined or vertical plane, in a channel or bowl, as well as in flow cups. Even in devices showing rising, sinking, falling or rolling elements it is possible to investigate rheological behaviour. Most of those empirical methods are used in everyday life without actually knowing it and were in use before rheometrical tests were done on a scientific basis (Mezger, 2006). There are innumerable devices, set-ups or geometries for a variety of different applications and in most cases there are even international standard procedures for a given method (International Standards Organisation ISO, American Society for Testing and Materials ASTM, German Industry Standards DIN, etc.). A summary of a wide range of rheometers can be found for example in Umstätter (1954), Ubbelohde (1965) or Mezger (2006) amongst many others.

Following Willenbacher and Georgieva (2013) there are two distinctively different types of rheometers that can be categorized by the flow type in which material properties are investigated: (a) (simple-) shear and (b) extensional flow. Shear rheometers can be divided into (i) rotational or alternatively oscillatory rheometers, in which the shear is generated between a fixed and a moving solid surface, (ii) while the shear in pressure driven rheometers (e.g., pipe or capillary rheometers) is generated by a pressure difference over the channel through which the material flows. Extensional rheometers measure the rheology of a fluid among others by capillary breakup, uniaxial extension/compression or sheet stretching. However, due to difficulties to generate homogeneous extensional flow especially for liquids with low viscosity, development of extensional devices has proceeded much slower than for shear rheometers. The most successful commercially available instrument is the capillary breakup extensional rheometer (CaBER). The thinning and breakup of fluid filament controlled by the balance between surface tension and viscoelastic force provides valuable information about materials rheological properties in an elongational flow (Willenbacher and Georgieva, 2013, Mezger, 2006).

Since the experimental study of this thesis is based on rotational rheometry, the following section focuses on the different geometries of rotational rheometers and its advantages and disadvantages, as well as on necessary requirements on the respective experiments. If not cited otherwise, this section is based on Schramm (2004), Mezger (2006) and Willenbacher and Georgieva (2013).

2.5.1. Rotational rheometry

Rotational instruments have the advantage that the rheological properties of materials can be characterized in a steady simple shear flow with a homogeneous regime of deformation. In order to determine the full range of rheological parameters of the suspension this can be done one-directionally in a steady or transient manner, or in sinusoidal oscillations. To measure the flow properties of a fluid there are two different modes:

- a controlled shear stress mode (CS) imposing constant torque, and
- a controlled shear rate mode (CR) characterized by constant shear rate.

During a measurement using the controlled shear stress mode (CS), the shear stress τ - or technically spoken the torque M - is set and controlled, while the resulting rotational speed n - or shear rate $\dot{\gamma}$ - is measured in order to be able to calculate the viscosity. This method seems to be the most appropriate measuring mode since in nature any motion of a fluid is a reaction to an applied force. It is also the classical method to determine yield stresses of a dispersion, paste or gel. However, depending on the purpose of a measurement it can be useful to measure the viscosity of a fluid at a defined flow velocity in order to simulate certain processes for example. This applies to the controlled shear rate mode, where the rotational speed n - or shear rate $\dot{\gamma}$ - is set and controlled, while the resulting torque M - or shear stress τ - is measured. Furthermore, modern rotational rheometers are capable to impose harmonic oscillations for measuring the viscoelastic material properties. The function of stress vs. strain rate, the so-called *flow curve*, is indicative of the rheological behavior of a fluid and represents the basis for the calculation of the rheological parameters (e.g., Figure 7).

In modern rotational rheometry, three types of measuring systems are commonly used: concentric cylinder, cone-and-plate and parallel-plate (Figure 11-13).

2.5.1.1. Concentric Cylinder Measuring System (Couette / Searle)

A cylinder measuring system consists of an outer cylinder (cup) and an inner cylinder (bob). The term *concentric* indicates that both cylinder-shaped components are showing the same rotation axis if mounted in measuring position. There are two modes of operation depending on whether the cup or the bob is rotating. The Couette set-up corresponds to a rotating cup and a stationary bob (Couette, 1890), while in the Searle method the bob is set in motion and the cup is fixed (Searle, 1912). This latter one is the more widely used concentric cylinder measuring system. Considering the flow of a sample enclosed in the gap between the cup with radius R_a and a rotating bob with radius R_i at an angular velocity ω , the shear rate $\dot{\gamma}$ is given by:

$$\dot{\gamma} = 2 \omega \frac{r_a^2}{r_a^2 - r_i^2} \quad (2.33),$$

while shear stress τ in the sample, is given by:

$$\tau = \frac{M_d}{2 \pi r_i^2 L} \quad (2.34),$$

where M_d is the torque measured on the bob and L the effective immersed length of the bob.

A crucial parameter of either the Couette or the Searle set-up is the gap between the two concentric cylinders. As long as the measuring system is showing a relatively narrow gap so that the sample confined in the gap experiences a constant shear rate, it can be compared to the aforementioned Two-Plates-Model to define the rheological parameters. The larger the gap, however, the less favorable are the conditions for the definition of the rheological parameters due to secondary flow effects (flow instabilities and turbulent flow of low-viscosity liquids), transient behavior (time-dependent effects) and inhomogeneous deformation behavior induced by a large gap. Wider gap viscometers are preferable for suspensions with relatively large particles, but the inaccuracy involved due shear rate changes across the gap should be taken into account. In order to limit the shear gap dimension, ISO standard 3219 defines the ratio of the radius of the outer cylinder to that of the inner cylinder for a narrow gap size as follows:

$$\delta_{cc} = \frac{r_a}{r_i} = 1.0847 \quad (2.35).$$

However, a great advantage of concentric cylinder systems is the fact that it is possible to measure the rheological parameters over a relatively large area along the length L of the bob, so that the annular gap remains filled even in the case of samples showing the Weissenberg or “rod-climbing”-effect. The shape of the bob also minimizes possible end effects, which are actually likely to occur as a result of the different shearing conditions in the liquid covering the ends of the cylinders. Therefore the ratio of the length L to the gap between cylinders is maintained greater than 100 and the shape of the bottom of the bob is designed as a cone with an angle α , which is chosen so that the shear rate in the bottom match the one in the narrow gap between the concentric cylinders ($\alpha \sim 120^\circ$).

Concentric cylinder systems are especially suitable for low-viscous liquids, since they cannot flow off the shear gap. In addition, a cover or a solvent trap can easily prevent sample evaporation and the temperature of a sample can be easily controlled due to the large contact area. Apart from the standardized concentric cylinder measuring system, there are innumerable varieties of different set-ups either with different gap sizes, bob shapes or even with a double-gap geometry.

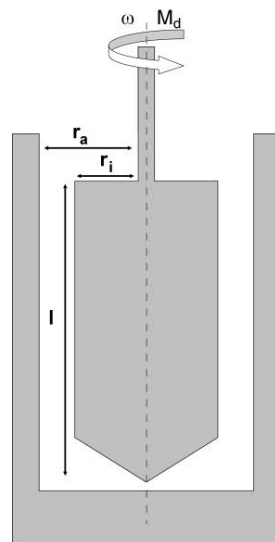


Figure 11: Cross section of a concentric cylinder measuring system (modified from Mezger, 2006).

2.5.1.2. Parallel-Plate Measuring system

The parallel plate geometry is characterized by a confined sample in the gap H between two flat, coaxial parallel plates. The sample is sheared by the rotation of one of the plates

(mostly the upper plate) at angular velocity ω . As a consequence, the circumferential velocity v of the sheared sample depends on the distance between the plates h and distance r from the rotational axis:

$$v(r, h) = \omega r \frac{h}{H} \quad (2.36),$$

and thus:

$$\dot{\gamma}(r) = \frac{r \omega}{H} \quad (2.37).$$

The shear rate $\dot{\gamma}$ at a constant ω is not constant within the entire shear gap. It is dependent on the distance r from the rotational axis and increases linearly from zero at the center of the plate ($r = 0$) to maximum at the outer rim of the plate ($r = R_p$). Since this is a serious disadvantage from a rheological point of view, the specification of the shear rate $\dot{\gamma}$ is usually related to the maximum shear rate value at the rim of the plate. By changing the gap height H and the angular velocity ω , shear rate can be varied in a wide range.

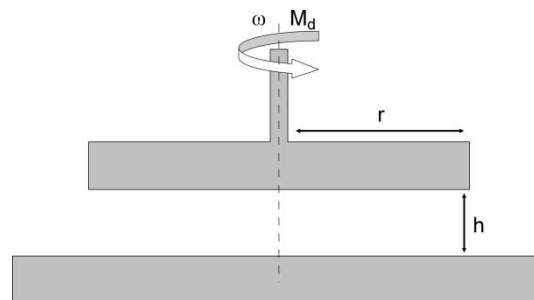


Figure 12: Cross section of a parallel plate measuring system (modified from Mezger, 2006).

The shear stress τ is a function of the shear rate $\dot{\gamma}$, which is not constant within the gap. Thus, to relate the shear stress to the total torque an expression for the dependence is necessary. In the case of Newtonian liquid the shear stress depends linearly on the shear rate and can be expressed as follows:

$$\tau(r) = \frac{2 M_d}{\pi r_p^3} \quad (2.38).$$

Parallel-plate measuring systems provide measurements of rather small amounts of a given sample and it is also possible to analyze suspensions with relative large particles by using

large gap heights. This depends on the characteristics of the liquid, as it should be avoided to create secondary flow effects, turbulences or flow instabilities, creep and migration off the gap. On the other hand, operating at small gaps viscosity can be obtained at relatively high shear rates, even though internal friction and therefore heating effects must be considered. Small gaps also allow for reduction of errors due to edge effects and secondary flows. As a rule of thumb, the gap size should be at least 5 times larger than the largest of the particles. Otherwise frictional forces would falsify the test result (Mezger, 2006).

2.5.1.3. Cone and Plate Measuring system

The dependence of the shear rate $\dot{\gamma}$ on radius and on gap dimension is not relevant when using a cone and plate measuring system. That system is characterized by a relatively flat circular cone and a stationary plate, while the conical area is defined by the cone radius R and the cone angle α . By convention the angle should not be greater than $\alpha = 1^\circ$ and in no case greater than $\alpha = 4^\circ$. The apex of the cone is usually cut off to avoid any friction between the rotating cone and the lower plate. The gap h is increasing with the distance r from the rotation axis and reaches its maximum value at the edge of the cone:

$$h(r) = r \tan \alpha \quad (2.39),$$

while the circumferential velocity v is also increasing with increasing the distance r :

$$v(r) = \omega r \quad (2.40),$$

Hence the shear rate is constant within the entire gap and does not depend on the radius r :

$$\dot{\gamma}(r) = \frac{\omega}{\tan \alpha} \approx \frac{\omega}{\alpha} \quad (2.41).$$

The shear stress measured by the torque M_d on the cone is given by:

$$\tau = \frac{3 M_d}{2 \pi R_p^3} \quad (2.42),$$

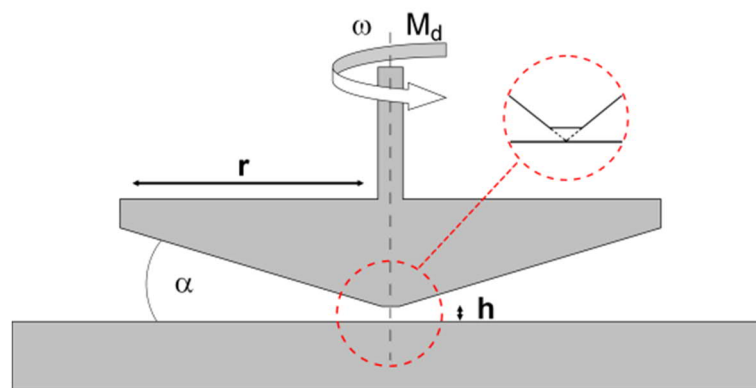


Figure 13: Cross section of a cone and plate measuring systems (modified from Mezger, 2006).

A great advantage of the cone-and-plate geometry is that the shear rate remains constant and thus provides homogenous shear conditions in the entire shear gap. The geometry can also analyze small sample quantities and heating is rather quick. Limited maximum particle size of the investigated sample, difficulties with avoiding solvent evaporation and temperature gradients in the sample, however, are typical disadvantages of the cone-and-plate measuring system. As a rule of thumb, the maximum particle size should not be greater than 20% of the gap size. Otherwise frictional forces would falsify the test result. Despite of the many disadvantages, the constant shear conditions within the gap is the reason why cone-and-plate systems should be the preferred measuring set-up unless conditions like particle size dictate otherwise.

3. Measuring Procedure and viscosity determination

One of the strengths of analogue experiments over those on natural material is that the physical parameters involved can be controlled to a high degree of accuracy. Therefore, meticulous sample preparation with a precise knowledge of the liquid viscosity and the character of the particle content is quintessential.

The actual rheometric experiments for this thesis were performed on a ThermoScientific Haake MARS III rotational rheometer equipped with a P35 Ti parallel-plate sensor geometry running controlled shear stress tests. The plate diameter of that geometry is 35mm, while the fixed gap between the two measurement plates was chosen to be at 1.25mm. Rheological measurements were performed on synthesised sets of suspensions of glass particles immersed in a strictly Newtonian silicone oil. This chapter describes and summarizes the systematic experimental effort and techniques in terms of sample preparation and the actual measurement routine used throughout this thesis.

3.1. Measurement requirements

From a mathematical point of view the deformation of a fluid due to shear leads to complicated differential equations that can only be solved under the assumption of boundary conditions (Schramm, 2004). It is extremely important to consider these limiting parameters affecting a measurement for precise and comprehensive rheological measurements. This applies both on parameters characterizing the measured sample, as well as on technical parameters controlling the experimental set up. Assuming that the rheometer itself is calibrated and works within normal parameters, the main sources for errors are related to the interaction of the measured suspension with the measuring geometry and the suspension itself.

For that reason it must be assured, that the carrier liquid used in this study does not transform or alter during a measurement. The liquid used in this study is the silicone oil ELBESIL B30000 (viscosity ~ 30 Pa s at 25°C , density ~ 970 kgm^{-3} at 25°C). This non-aqueous, viscous liquid was chosen to prevent electroviscous effects and dehydration and to minimize particle settling during the actual measurements. The rheology of the pure silicone oil was determined for each sample batch and found to be strictly Newtonian over

the range of stress and strain rates investigated in this work. Although viscosity of a given melt can span several orders of magnitude according to its temperature, the viscosity of the silicone oil is within the range expected for low viscosity magmas at subliquidus temperature (McBirney & Murase, 1984; Spera, 2000; Giordano & Dingwell, 2003; Giordano *et al.*, 2008). Since the viscosity of liquids is strongly dependent on temperature, it is also very important to control the temperature of the sample during a measurement. All experiments were performed at 20°C, which was kept constant throughout the entire analysis and controlled during each run by the use of a so-called Peltier heat pump module.

By the mere nature of this study it must also be assured to analyse homogeneous two-phase samples (i.e., liquid plus particles). For experiments on those suspensions, it is important to produce virtually bubble-free samples, as a gas phase adds a plethora of additional non-Newtonian complexities to the rheological behaviour. Adding particles to the liquid and using parallel-plate sensor geometry requires careful gap setting. There is a strong dependency between gap size and the size of the biggest particle, so that it was chosen to be at 1.25mm - according to a rule of thumb by Mezger (2006) five times bigger than the largest particle (in our case 250µm). If particles are too big for a given gap size, they would directly touch the surfaces of the measuring system resulting in frictional resistance, which falsifies the measurement.

The density contrast between silicone oil and the particles and therefore possible settling effects must also be considered. From Stokes' law, we can compute that the time required for an isolated particle in a dilute suspension to fall or rise in the gap between the two plates is about half an hour for the largest particle; for a concentrated suspension, it is much longer because settling and creaming are hindered. Taking the total runtimes for our rheometric experiments in account settling effects can be considered as negligible, since the measurement duration was much shorter for each sample (the mean experiment duration was about 15 minutes). However, the difference between the density of crystals and that of oil B30000 is comparable with that reported in parallel-plate experiments by Mueller S.P. *et al.* (2010), Cimarelli *et al.* (2011), Del Gaudio *et al.* (2013) or Del Gaudio (2014), where sinking effects were also excluded.

Furthermore the possibility of wall slip effects at the measurement plates as discussed for example by Yilmazer & Kalyon (1989), Buscall *et al.* (1993), Barnes (1995)

or Buscall (2010) must be considered, especially since our measurement geometry does not comprise rough surfaces,. However, similarly to the study of Mueller S.P. *et al.* (2010) at low to intermediate particle concentrations there is no significant difference between samples measured with and without roughened sensor surfaces and showed no indication of wall slip. Only for suspensions with the highest particle concentration slip seems to play a considerable role. Since the modelling results presented in this thesis are mainly based on low to intermediate particle concentration samples, it is assumed that wall slip plays, if at all, only a minor role.

Another effect that might affect rheological measurements especially those with samples of non-spherical particles are transient effects during the flow initiation. Suspensions of non-spherical particles must be sheared to large total strain before repeatable rheometric results can be obtained (Hinch & Leal 1973; Okagawa *et al.* 1973; Ivanov *et al.* 1982; Powell 1991), because particles are, initially, randomly oriented and equilibrium orientation distributions are established only after a period of shearing. Before that equilibrium is achieved, transient oscillations in apparent viscosity are observed (Mueller S.P. *et al.*, 2010). Therefore the samples are treated with a pre-shear treatment before the actual measurement (see chapter 3.4).

3.2. Sample preparation

The most important task of this study was to develop techniques to synthesize systematic and reproducible bubble-free particle suspension samples with a well-characterized PSD. This includes not only the acquisition and testing of suitable particles and carrier liquids, but also methods to homogenize the particle load in the sample.

For this project, three different types of particles were used: spherical glass beads (Ballotini by Eisenwerk Würth; density $\sim 2447 \text{ kg m}^{-3}$), prolate glass fibres (LANXESS; density $\sim 2560 \text{ kg m}^{-3}$), as well as oblate glass flakes (Kremer Pigmente; density $\sim 2520 \text{ kg m}^{-3}$). Following previous studies of Mueller S.P. *et al.* (2010) and Truby *et al.* (2015), particle sizes were chosen so that they are not subject to Brownian motion (high Peclet number), are strongly coupled to the flow (low Stokes number) and that inertial effects can be neglected (low particle Reynolds number). In particular, this means that the particles

used in this study were in a size range between 32 μm and 250 μm . This was warranted by meticulous sieving.

Using a column of sieves with a wire mesh cloth (the top sieve with the largest mesh size, while each lower sieve has smaller openings than the one above; Figure 14), particles were sieved manually to get 14 different size fractions (Table 2). Particle-size distribution in one particular size fraction is assumed to be Gaussian. A sieving cycle consisted of 15 minutes of sieving and was repeated five times. Care must be taken when sieving fibres. Due to their arbitrary shape the sieving procedure was limited to 10 minutes and consisted only of horizontal and tapping movements in order to prevent larger particles in fractions of smaller ones.

For the following synthesis of particle-bearing suspensions, particle volume fraction was controlled by carefully adding a known mass of particular, pre-calculated particle size fractions to a known mass of up to 30 ml of silicone oil (ELBESIL B30000). By this means samples of similar initial particle volume fractions ϕ_p in the range of $0.05 \leq \phi_p \leq 0,55$ (errors in particle volume fraction are $\pm 1\%$) with varying modality (uni-, bi- tri- and tetramodality), as well as polymodal batches of specific defined skewness and variance were prepared. Exact values of the given distributions are reported in the appendix.



Figure 14: Sieve column.

< 32 μm
32 – 38 μm
38 – 45 μm
45 – 53 μm
53 – 63 μm
63 – 75 μm
75 – 90 μm
90 – 106 μm
106 – 125 μm
125– 150 μm
150 – 180 μm
180 – 212 μm
212 – 250 μm
> 250 μm

Table 2: Sieving fractions.

In order to keep the suspensions free of bubbles, each sample was centrifugalized for 30 minutes at 2500 rpm at room temperature (compare to Mueller S.P. *et al.* 2010) prior to careful re-homogenization by a custom-built motor-driven mixing device with a vane spindle before each measurement (Figure 15). To control the exact sizes and the relative proportions of the samples' particle load, in addition to weighing, the PSD were measured by image analysis. For this purpose, the RADIUS particle-size measurement technique is used (Seelos & Sirocko, 2005). Originally developed for the particle analyses of sediment thin sections, this tool provides a comparatively fast analysis of 2-D particle-size distributions of digital images of a given sample by calculating statistical parameters of the distribution like mean, mode, sorting, variance or skewness. An example is shown in Figure 16.



Figure 15: Vane spindle mixing device.

3.3. Measurement overview

The rheometric experiments of this thesis covered a broad parameter space in terms of particle size distributions. In order to derive and develop a valid (semi-)empirical model, the first approach for rheometric experiments was limited to samples with spherical particles. In total, this study consists of 274 experimental batches of varying modality (uni-, bi- tri- and tetramodality), as well as polymodal batches of specific defined skewness and variance for suspensions with spherical glass beads (e.g., Figure 16). Based on the data set of those experiments, further analyses of both 25 unimodal and 24 suspensions with varying polydispersity consisting of either glass flakes (oblate) or glass fibres (prolate) were carried out. Samples feature similar initial particle volume fractions ϕ_p in the range of $0.05 \leq \phi_p \leq 0.4$ (errors in particle volume fraction are $\pm 1\%$). Suspensions with particles of arbitrary shape are in a range of aspect ratios $0.035 \leq r_p \leq 35$ (i.e., the range most relevant to magmatic suspensions).

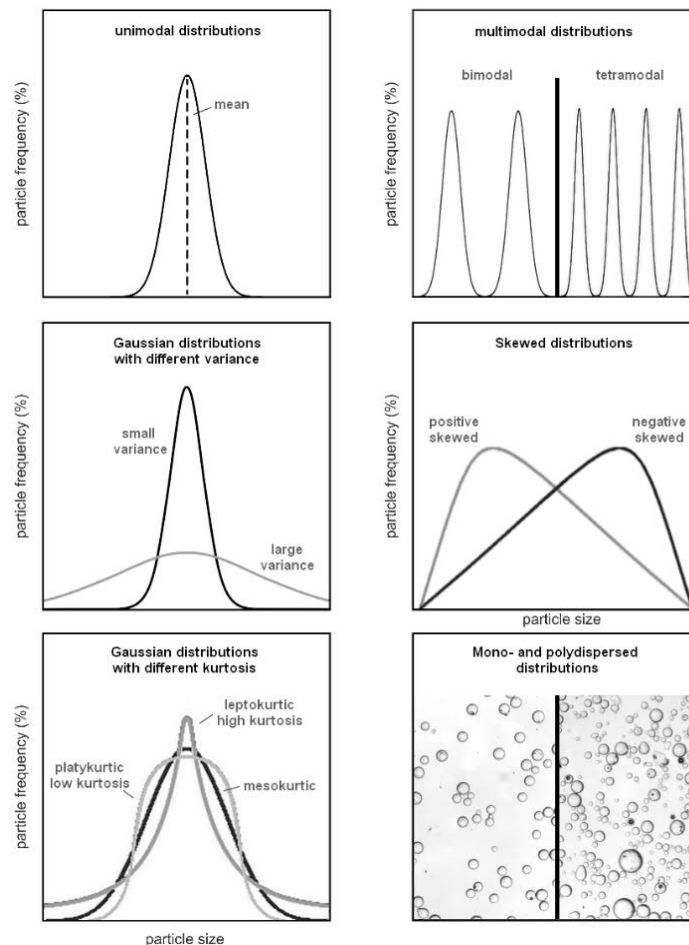


Figure 16: Schematic summary of different particle distributions used and analysed in this study.

3.4. Measurement job

The measurement routine using the software Rheowin consisted of four essential parts. After filling the rheometer with the sample, the correct gap size has to be set in the first place. That is done by reaching a trim position that is 0.1mm greater than the pre-set gap size of 1.25mm in order to guarantee the optimal filling of the parallel-plate measuring geometry. In case of excess suspension that amount has to be removed before the geometry is allowed to reach the final gap size (Figure 17). To take care of equilibrium starting conditions for each test, prior to the start of the measurement the sample was exposed to a heating phase in which the sample was allowed to thermally equilibrate for 120 seconds. All experiments were performed at 20°C. The heating phase is followed by a continuous 0–300–0 Pa controlled stress ramp as a pre-shear treatment. As shown by Mueller S.P. *et al.* (2010) or Cimarelli *et al.* (2011) this is needed to eliminate transient effects during the flow initiation.



Figure 17: Measurement setup using a parallel-plate geometry

The actual flow curve determination consisted of a 25-step ‘up ramp’ of incrementally increasing shear stress τ up to a maximum value of 500 Pa, followed by a 25-step ‘down ramp’ to investigate a possible onset of non-Newtonian behavior (Figure 18). At each stress step, the rheometer recorded the corresponding strain-rate $\dot{\gamma}$ once it had reached equilibrium flow conditions. The precision of the stress and strain-rate measurements is estimated at $\pm 2\%$. Experimental reproducibility is tested by repeating

measurements of equally prepared samples obtaining reproducible results within 2%. On average, one measurement took about 15 to 20 minutes.

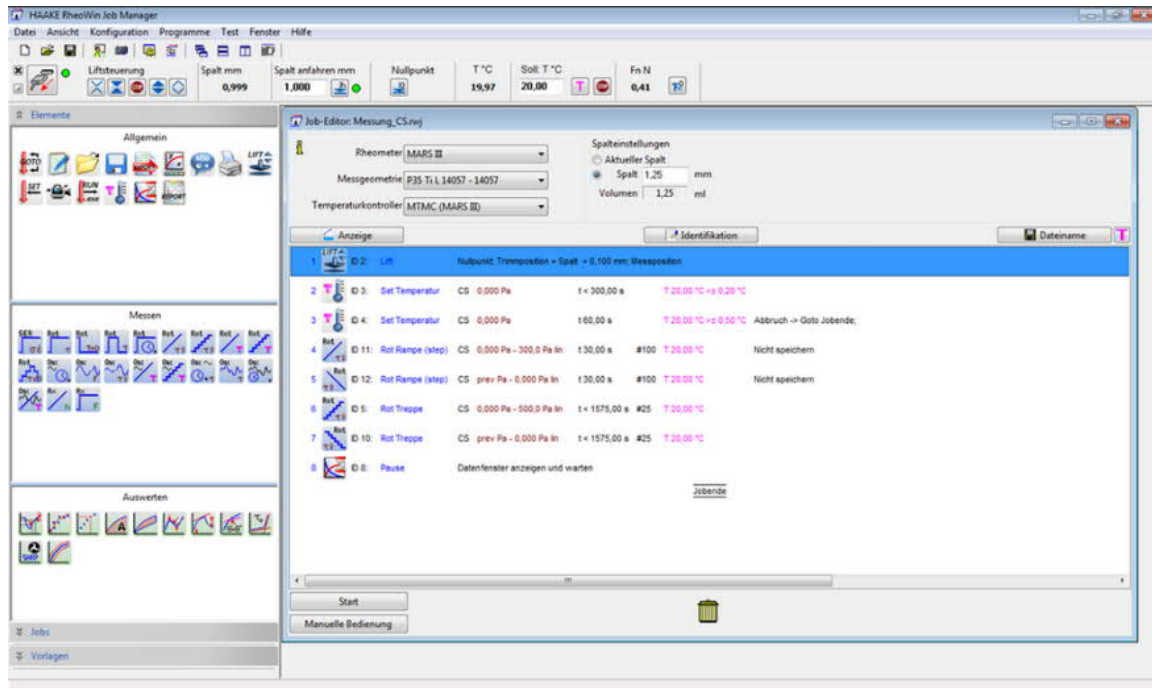


Figure 18: Measurement job in RHEOWIN software

3.5. Data Analysis

Our rheometric experiments yield raw flow curves of applied shear stress τ against resultant shear strain-rate $\dot{\gamma}$. Like other studies (Castuccio *et al.*, 2010; Mueller S.P. *et al.*, 2010; Cimarelli *et al.*, 2011; Truby *et al.* 2015) this thesis determines the yield stress τ_0 , consistency K and flow index n for each sample by fitting the Herschel-Bulkley model (equation 2.6) to each measured flow curve obtaining reasonably good fits ($R^2 = 0,975 - 0,999$). Maximum packing fraction ϕ_{max} of each sample is determined by fitting the model of Maron and Pierce (equation 2.14) to each $\eta_r(\phi)$ of a given particle size fraction obtaining as well reasonably good fits ($R^2 = 0,985 - 0,999$). Statistical values for each distribution were calculated using the software GRADISTAT (Blott & Pye, 2001). Polydispersity was calculated by using equation (2.26) (Desmond & Weeks, 2013; Phan *et al.*, 1998) as well as equation (2.29) (Torquato, 2013; Wadsworth *et al.*, 2017). These values were also checked by image analysis using the software RADIUS (Seelos & Sirocko, 2005).

4. Rheological experiments - Deriving a model

This chapter summarizes the results of the systematic experimental approach leading to the derivation of a (semi-)empirical model trying to describe the effect of PSDs on the rheology of suspensions. Following the preparation steps presented in *chapter 3*, the first approach for the rheometric experiments of this thesis was to analyse samples with spherical particles, prior to the introduction of possible effects related to the shape of the respective particles. The subsequent sections follow this approach, so that the study of analogue samples firstly focuses on suspensions containing spherical particles in order to derive a (semi-)empirical model before potential relationships between PSD's and the rheological parameters of its respective suspensions are tested with the use of particles with arbitrary shapes and finally natural samples.

4.1. Results - spherical particles

The experimental data for relative viscosity $\eta_{r,*}$ and flow index n (equation 2.9) for the synthesized polymodal distributions (uni-, bi- tri- and tetramodal) are presented in figure 19. Results for relative reference viscosity $\eta_{r,*}$ and flow index n of distributions with varying skewness and variance are in the same figure (appendix). While the first mentioned figures plot $\eta_{r,*}(\phi)$, the latter ones displays $n(\phi)$. Since yield stress for all samples is found to be either small or negative (which is unphysical) but within 2σ error of zero, it is generally neglected. Maximum strain rates achieved were approximately 0.03–0.05 s⁻¹ for concentrated samples, and up to 16 s⁻¹ for very dilute suspensions.

The experiments of polymodal particle suspensions show results that are qualitatively consistent with those from previous studies limited to uni- and bimodal distributions (Mueller S.P. *et al.*, 2010; Cimorelli *et al.*, 2011; Del Gaudio *et al.* 2013; Del Gaudio 2014; Truby *et al.*, 2015). For example, the viscosity shows a nonlinear increase in relative consistency with increasing particle volume fraction (figure 3a), and the onset of a shear thinning behavior (decrease of flow index n) at $\phi > 0,3$ (figure 3c). This observation applies as well to suspensions with particle distributions with varying skewness and variance (figures 19a and 19c).

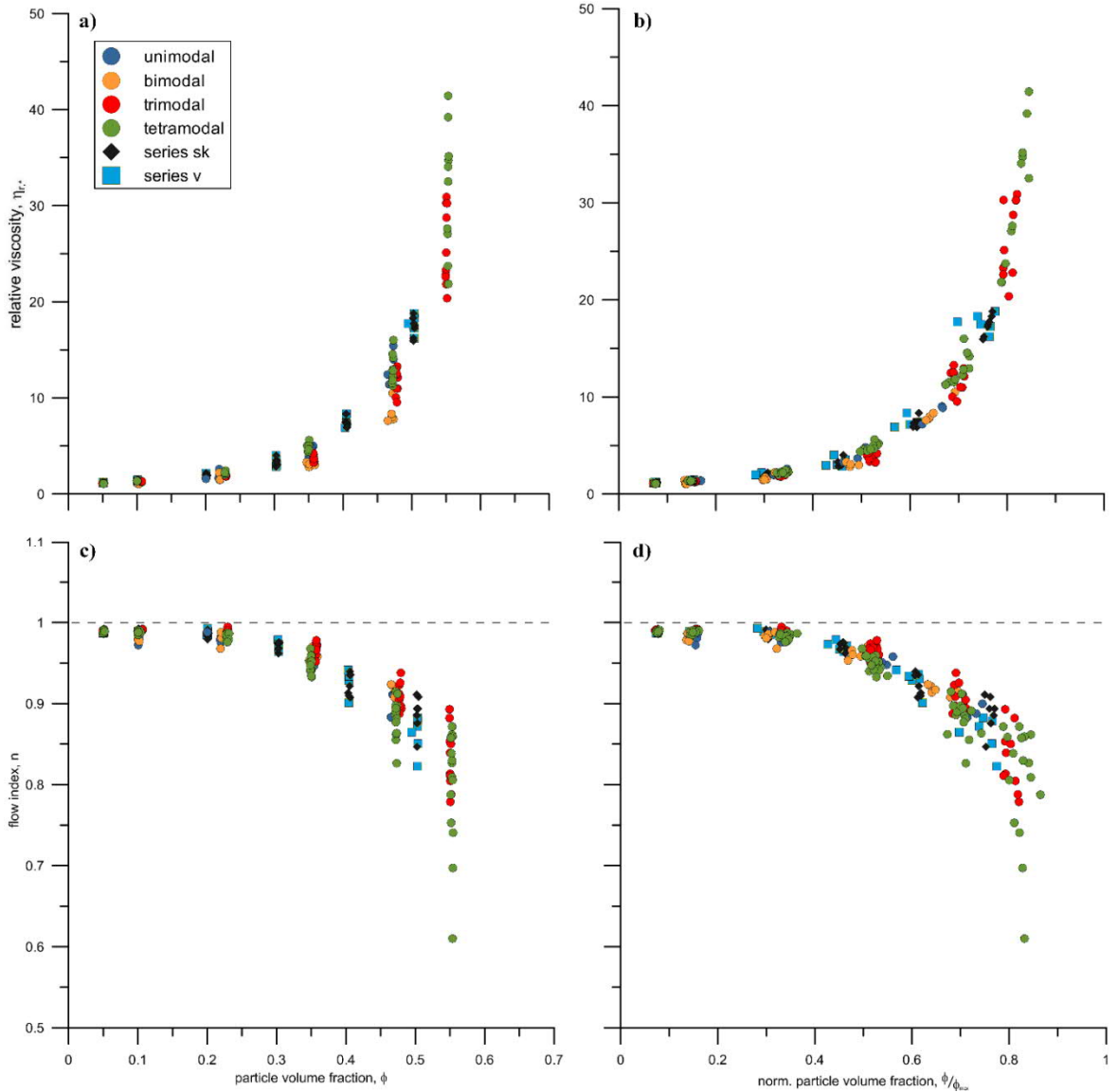


Figure 19: Experimental data in relation to particle volume fraction. a) relative viscosity $\eta_{r,*}$ vs. particle volume fraction ϕ , (b) relative viscosity $\eta_{r,*}$ vs. norm. particle volume fraction $\frac{\phi}{\phi_m}$, (c) flow index n vs. particle volume fraction ϕ and (d) flow index n vs. norm. particle volume fraction $\frac{\phi}{\phi_m}$ for the synthesized polymodal distributions- error bars smaller than symbols.

A size dependency of our samples is indicated by figure 20a, where the mean of the particles used in this study is shown in relation to ϕ_m , which is negatively correlated to the particle size. When relating ϕ_m to variance (the degree of modality of a given distribution), a higher variance leads to a higher ϕ_m of the suspension as it is shown in figure 20b. In figure 20c, a correlation between ϕ_m and skewness of a distribution is evident. The less skewed a distribution ($Sk = 0$), the higher ϕ_{max} , whereas more skewed distributions (either

positive or negative) feature slightly lower values of ϕ_m . There is, however, no direct relation between kurtosis and ϕ_m as can be seen in figure 20d.

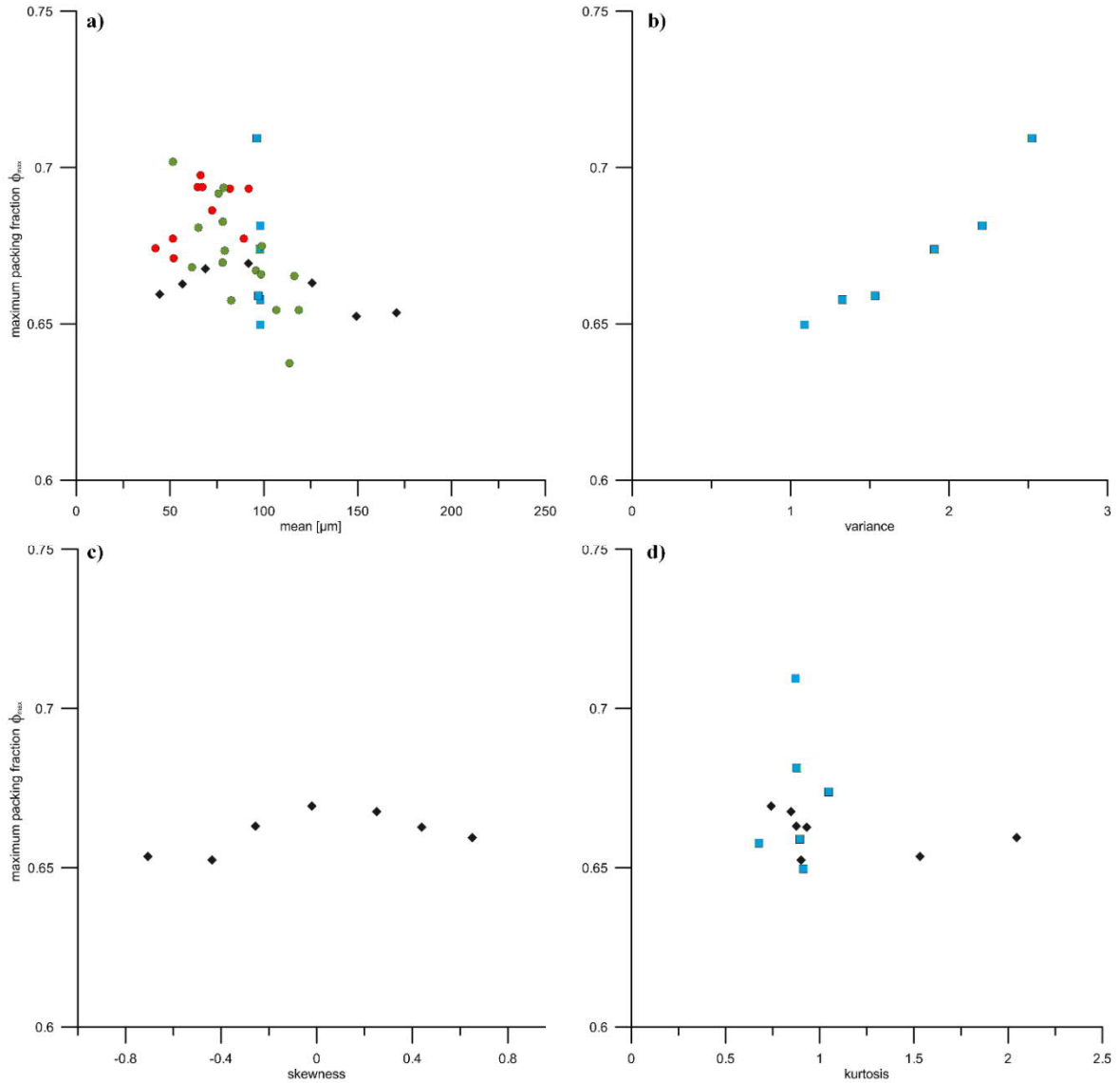


Figure 20: Statistical data in relation to the maximum packing fraction. (a) ϕ_m vs. mean, (b) ϕ_m vs. variance (standard deviation), (c) ϕ_m vs. skewness and (d) ϕ_m vs. kurtosis - error bars smaller than symbols. Same symbols as in figure 19.

4.1.1. Classifying experimental results

Based on intensive literature research, the systematic experiments with controlled tri- and tetramodal particle content as well as with controlled variance and skewness are the first of their kind. Being qualitatively consistent with previous rheological studies on particle-bearing suspensions (Castruccio *et al.*, 2010; Mueller S.P. *et al.*, 2010; Mader *et al.*, 2011; Del Gaudio *et al.*, 2013 or Truby *et al.*, 2015; among others), the results of the experiments presented in figure 19 illustrate a nonlinear increase in relative viscosity $\eta_{r,*}$ with increasing particle volume fraction. This is due to the fact, that the analogue approach of the experimental procedure used in our study limits the suspensions to the dilute and semi-dilute flow regime in which the aforementioned models in *chapter 2* show only minor differences. Divergences become much more important as the particle fraction of the analyzed suspension approaches ϕ_m , which in the case of our study can be neglected, since it is almost impossible to perform analogue experiments at $\frac{\phi}{\phi_m} > 0.8$ within a reasonable and controllable range of error.

In addition the onset of a non-Newtonian behavior in form of shear thinning - shown by a decrease of flow index n - at $\phi > 0.3$ can be noticed. Shear thinning is believed to be due to different processes including shear heating, particle rotation along the flow direction, and cluster reduction (Quemada, 1978; Chang & Powell, 1993; among others). Following Deubelbeiss *et al.*, (2011), due to the low values of viscosity of the fluid and suspensions and shear rate reached in the experiments shear heating as a main cause of shear-thinning can be excluded. Likely more relevant effects are particle rotation and particle interaction (Mueller *et al.*, 2011; Del Gaudio *et al.*, 2013). Furthermore, neglecting yield stress of the measured suspensions is justified and consistent with the experimental results of Mueller *et al.* (2010), who found that yield stress is generally close to zero for $\frac{\phi}{\phi_m} < 0.8$.

The experimental study also shows, qualitatively, the effect of polymodality on particle size distributions. An increasing modality increases the maximum packing fraction, which is consistent with results from numerical modelling studies (Pusey, 1987; Schaertl & Sillescu, 1994; Phan *et al.*, 1998; Kansal *et al.*, 2002; Farr & Groot, 2009;

Desmond & Weeks, 2013; Shewan & Stokes, 2015). As can be seen in figure 21 our experiments of multimodal particle suspensions feature this particular effect: the higher the modality or the amount of different particle sizes in a suspension gets, the higher the maximum packing fraction. A conclusion that can be drawn from this is that suspensions with a higher modality have effectively a lower viscosity at the same particle volume concentration than suspensions with a lower modality. This becomes particularly relevant when looking for optimized particle-load to viscosity ratios.

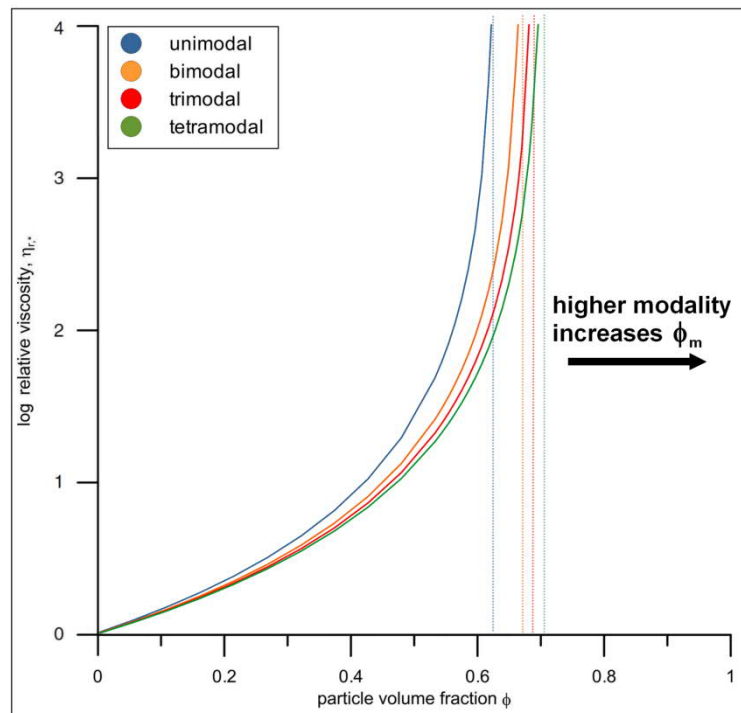


Figure 21: Experimental data for relative viscosity $\eta_{r,*}$ vs. particle volume fraction ϕ of suspensions with different particle modalities. Dashed lines indicate maximum packing fraction ϕ_m that increases with increases modality.

4.1.2. Maximum packing fraction ϕ_m

A striking result of the experimental series is linked to the value of maximum packing fraction of particle-bearing suspensions. Considering figure 22, where the relative viscosity of the experimental suspensions of spherical particles with different size distributions and the results of Mueller S.P. *et al.* (2010) of particles with arbitrary shape is plotted in relation to $\frac{\phi}{\phi_m}$, it can be seen, that most of the data fall onto one single trend, regardless of

whatever particle shape (Mueller S.P. *et al.*, 2010) or particle size distribution (this study) the suspension contains. This suggests that the parameter ϕ_m encapsulates most rheologically relevant microstructural information of any given particles suspension.

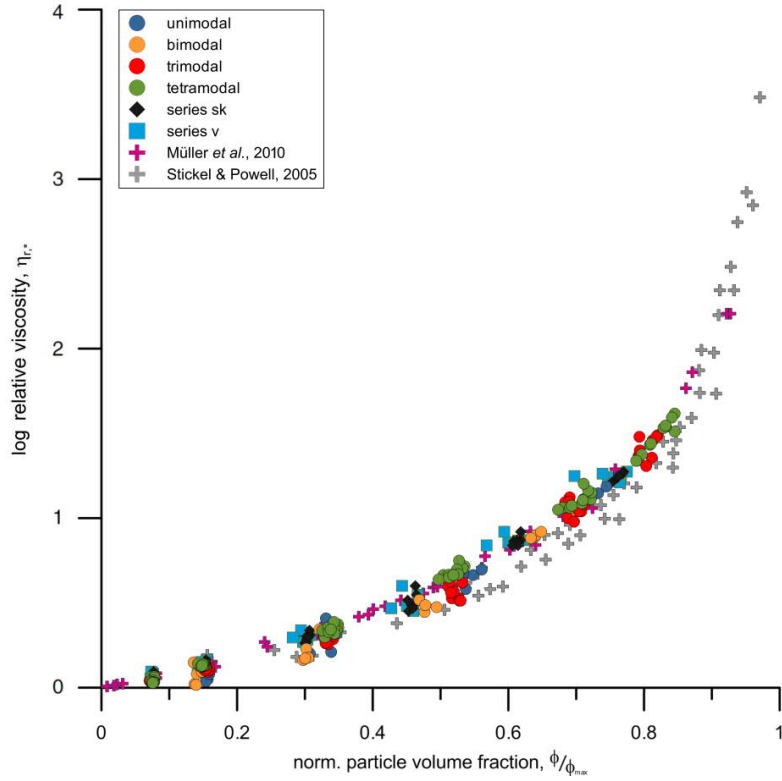


Figure 22: Experimental data of this study for relative viscosity $\eta_{r,*}$ vs. norm. particle volume fraction $\frac{\phi}{\phi_m}$, with reference to data of particles with arbitrary shape from Mueller S.P. *et al.* (2010); reference data from Stickel & Powell (2005) includes data from Chang & Powell (1994), Chong *et al.*, (1971) - error bars smaller than symbols

As outlined in section 2.3., there exist ambiguities in the exact definition of ϕ_m , mainly depending on how it is measured. Therefore, given its importance in suspension rheology, this lack of clarity has to be addressed. Most models in rheology containing a value of maximum packing fraction treat it as an empirically determined and adjustable parameter. In the form

$$\eta_r = f\left(\frac{\phi}{\phi_m}\right) \quad (4.1)$$

it is simply a direct scalar measure of suspension microstructure (Stickel & Powell, 2005). From an ideal geometrical point of view, ϕ_m describes the densest possible packing for a given particle geometry and size distribution and can therefore be defined as $\phi_{m,geom}$,

while more realistic scenarios feature randomly organized packings, with lower values that are referred to as random close packing $\phi_{m,rcp}$. (Torquato *et al.*, 2000). Values of ϕ_m determined from rheological flow experiments (e.g., by extrapolation of $\eta \rightarrow \infty$ in equation 2.5) are generally lower than the values for static geometrical maximum packing and may be referred to as a rheologically determined $\phi_{m,rheol}$.

In rheological terms, the importance of flow needs to be taken into account, so that ϕ_m represents the volume fraction, at which particles can no longer flow past each other and the suspension becomes jammed, i.e. the viscosity tends towards infinity. Therefore one might argue whether it makes sense to distinguish between a theoretical derived ϕ_m and a rheological ϕ_m . Especially given the fact, that up to the present there is no constitutive definition or characteristic estimation of either ϕ_m and ϕ_{rcp} in terms of their rheological impact and what it actually means for a particle-bearing suspension to reach ϕ_m as discussed for example by Torquato *et al.* (2000). For a further review referring jammed hard-particle packings, Torquato & Stillinger (2010) can be recommended.

It could be assumed that differences between $\phi_{m,rcp}$ and $\phi_{m,rheol}$ are due to the effect of shear during the rheometric measurements, which forces the particles to pack more efficient than by static settling in the centrifuge. Comparison of ϕ_m -values determined by simple settling experiments (representing $\phi_{m,rcp}$) with the ϕ_m -values derived from fitting the rheological data to equation (2.4; representing $\phi_{m,rheol}$; figure 23) allows the general statement:

$$\phi_{m,rcp} < \phi_{m,rheol} < \phi_{m,geom} \quad (4.2)$$

Those settling experiments consisted of a small series of experiments with different batches of glass bead mixtures filled to a given amount of silicone oil. The particles were let sink randomly into the oil until the maximum packing $\phi_{m,rcp}$ was reached and the excess amount of particles could be removed. By weighing the resulting mixtures it is possible to calculate the exact value of $\phi_{m,rcp}$.

Consequently, I propose to distinguish clearly between a theoretical, geometrically derived $\phi_{m,geom}$ and a rheological $\phi_{m,rheol}$ and strictly use the value $\phi_{m,rheol}$ when

considering rheological problems, since small changes of the value of ϕ_m might result in a dramatic change of the viscosity.

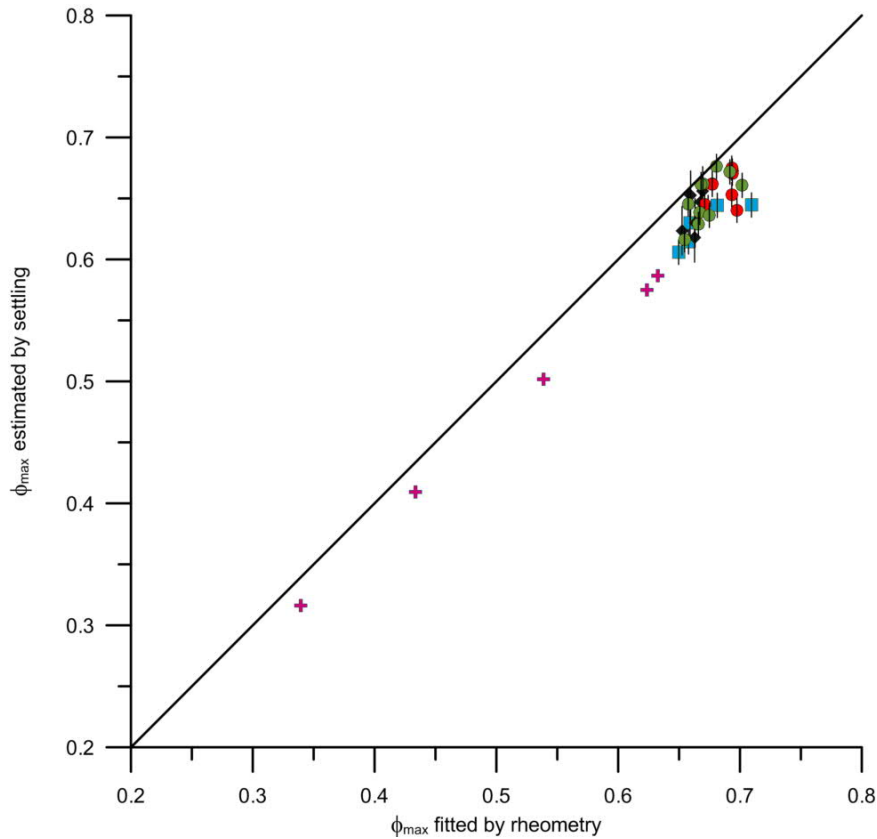


Figure 23: Maximum packing fraction ϕ_m estimated by settling vs. maximum packing fraction ϕ_m estimated by rheometry. Same symbols as in figure 22.

4.1.3. The links between CSD, maximum packing fraction and suspension viscosity - a model

The nature of the parameter ϕ_m as the overarching expression of textural and rheological properties of a suspension makes it ideally suited to act as a link between the statistical characteristics of a suspension's particle size distribution and its viscosity. In order to find that 'missing link' between the maximum packing fraction and the viscosity of polymodal distributions, this thesis focused on the statistical parameters (e.g., skewness, variance) of different particle size distributions by analyzing analogue samples with varying pre-determined characteristics.

significance as the first parameter describing a distribution (Figure 20a). More information describing a distribution is provided by its variance. Figure 20b shows, that there is a strong correlation between variance and ϕ_m , which is sensible since a higher variance implies a higher number of different particle sizes (and therefore a higher dispersity), which results in a more efficient packing and therefore a higher ϕ_m .

Considering the skewness of the distributions, figure 20c shows that the more skewed a distribution is (either positively or negatively skewed), the lower ϕ_m gets - or in other words the less skewed, the higher ϕ_m . This is quite intriguing since it could be expected from earlier studies (e.g., Desmond & Weeks, 2013), that more positively skewed distributions (more smaller particles) result in a higher ϕ_m . Kurtosis, however, shows no significant relationship with ϕ_m and might therefore be neglected (figure 20d). In summary, these experiments clearly show a major influence on ϕ_m of variance and skewness, while particle size plays a subordinate role. Nonetheless, neither variance nor skewness can fully describe a distribution of particles in a suspension and therefore underline the need for another parameter (e.g., polydispersity; see section 2.4).

The results of the rheometric experiments appear to contradict Desmond & Weeks (2013), who focus on the effect of polydispersity δ and find in a numerical analysis of sphere packings with different particle size distributions, that packing density can increase significantly with increasing skewness especially for distributions with large polydispersity δ (equation 2.26). Even given the fact that the analyzed analogue distributions feature only a small range of polydispersity δ compared to those of Desmond & Weeks (2013), the results suggest that the packing density ϕ_m cannot be increased significantly with increasing skewness. This implies that the value of polydispersity δ itself has much more influence on ϕ_m than variance or skewness alone.

From a theoretical point of view, the maximum packing value of a suspension with monomodal spheres and therefore a polydispersity = 0, is characterised by $\phi_m \approx 0.63 - 0.65$ (e.g., Bernal & Mason, 1960; Rintoul & Torquato 1996; 1997; and others) assuming that the particles are randomly organized in disordered packings (see section 2.3). Increasing the polydispersity and therefore filling the voids in between larger particles, increases ϕ_m at the same time. Consequently, a polydispersity with very high values, might

drive ϕ_m of a suspension to reach up to a theoretical maximum value of $\phi_m = 1$, which is known as the *Apollonian packing*. Figure 24 shows a schematic plot based on that theoretical approach: a non-linear relation between ϕ_m and polydispersity that approaches $\phi_m = 1$ asymptotically with increasing polydispersity.

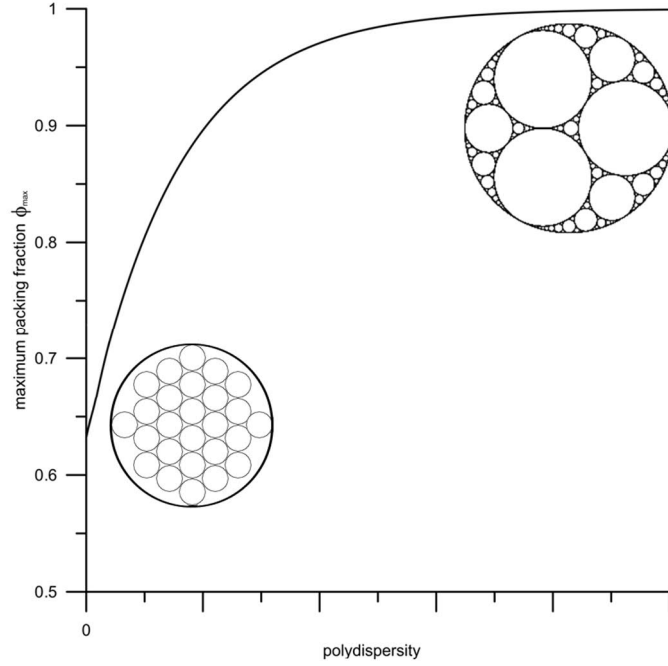


Figure 24: Schematic plot of maximum packing fraction ϕ_m vs. polydispersity illustrating the *Apollonian packing*.

Based on this theoretical approach it is possible to develop a (semi-)empirical model by fitting the experimental data according to following equation (figure 25):

$$\phi_m = 1 - \left((1 - \phi_{m,0}) e^{(-\delta * \phi_{m,0})} \right) \quad (4.3)$$

where $\phi_{m,0}$ is the maximum packing fraction for a monomodal size distribution of spheres with variance = 0 and skewness = 0 - in our study $\phi_{m,0} = 0.6496$, which is in good agreement with previously reported values for monomodal particle distributions (e.g., Rintoul & Torquato, 1996; among others). Although the dataset covers only a small portion of polydispersity and ϕ_m and, accordingly, display only a limited correlation, this parameterization fulfills the theoretical requirements expected from a δ - ϕ_m relationship.

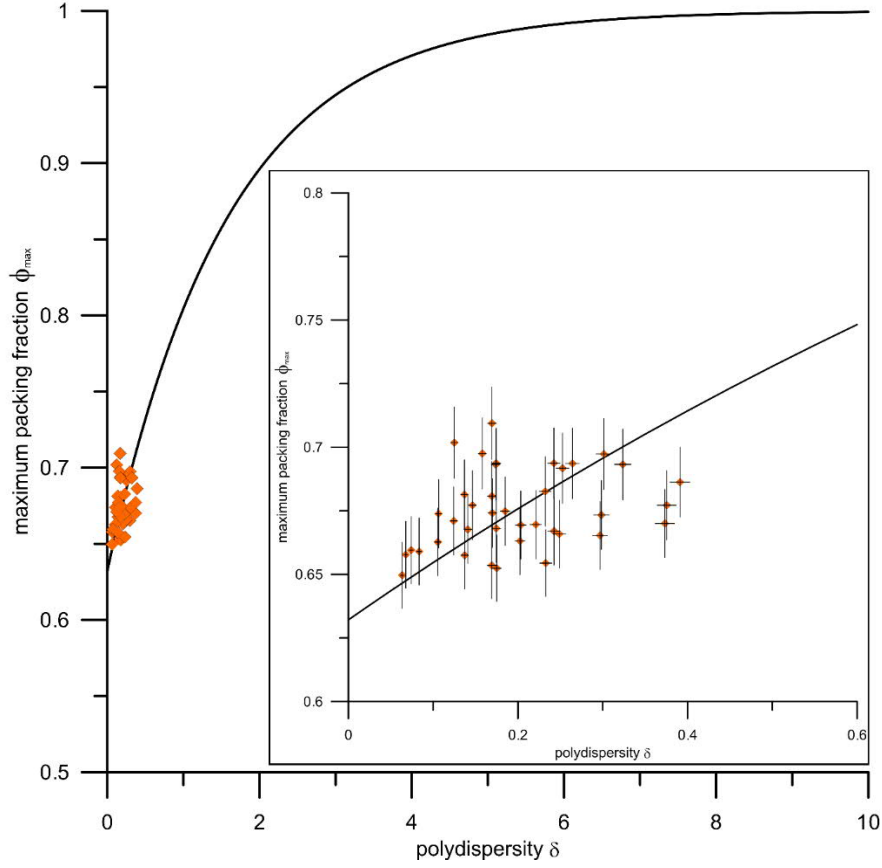


Figure 25: Maximum packing fraction ϕ_m vs. polydispersity δ (eq. 2.28) following eq. (4.3).

As mentioned in section 2.4, Desmond & Weeks's (2013) definition of polydispersity does not include much information about the shape of a distribution. We here adopt the definition of polydispersity γ of Wadsworth *et al.* (2017, eq. 2.29) and parameterize our experimental data results to following equation:

$$\phi_m = 1 - \left((1 - \phi_{m,0}) \gamma^a \right) \quad (4.4)$$

where $a = 0.173$ is an empirical constant (see figure 26). By using the moments of a distribution, an increasing degree of polydispersity decreases γ . While $\gamma = 1$ represents the monodisperse limit (a monomodal distribution with particles of the same size), an increasing polymodality and therefore decreasing parameter γ leads the maximum packing fraction ϕ_m to converge to 1. The theoretical requirements discussed before, however, are still fulfilled. As an example, imagine two particle-bearing suspensions A and B with an identical particle volume fractions ($\phi = 0.6$) and a monomodal maximum packing fraction

$\phi_{m,0} = 0.64$ (spherical particles), but with different size distributions and, accordingly diverging polydispersity values of $\gamma_A = 0.8$ and $\gamma_B = 0.4$. According to equation (4.4), values for maximum packing fraction of those suspensions are $\phi_{m,A} = 0.654$ and $\phi_{m,B} = 0.693$. Inserting these values into the Maron-Pierce model (equation 2.4), the obtained relative viscosities are $\eta_{r*,A} = 148.53$ and $\eta_{r*,B} = 55.76$, respectively. This illustrates that - particularly at concentrated suspensions - a varying PSD can have a considerable effect on suspension rheology.

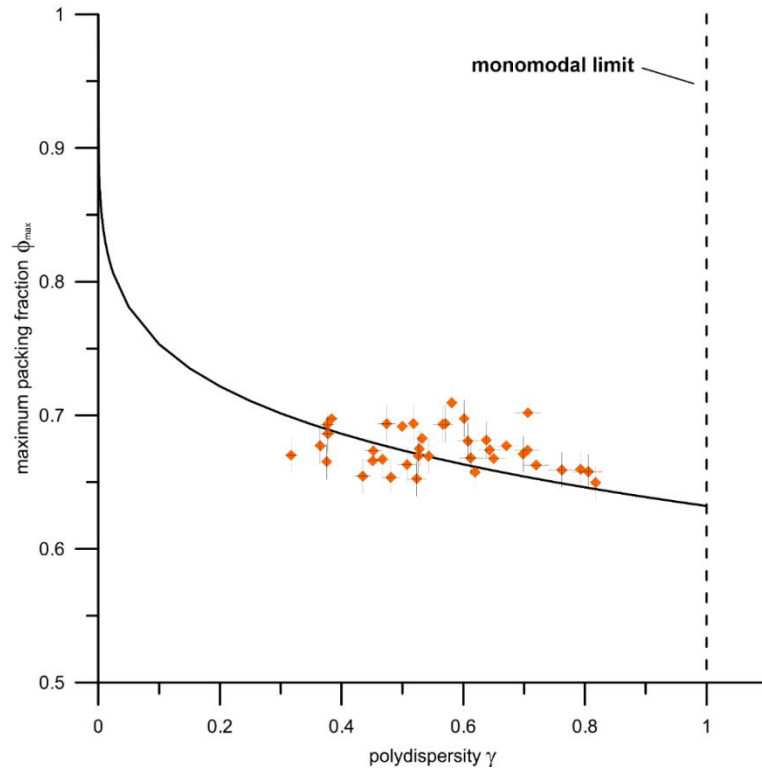


Figure 26: Maximum packing fraction ϕ_m vs. polydispersity γ (eq. 2.29) following eq. (4.4).

4.2. Influence of particle shape – testing the model

Owing to the fact that the maximum packing fraction ϕ_m is the dominant parameter controlling the rheological behaviour of a suspension, the semi-empirical model (Figure 26; equation 4.4) offers the possibility to directly link the statistical parameters of a particle-bearing suspension with a given size distribution to its rheological behavior. However, the model is based on experiments with spherical particles. Prior to rheometric experiments with particles of arbitrary shape in order to quantify its effect on that model, it is necessary to consider if the model comprises any information of particle shape.

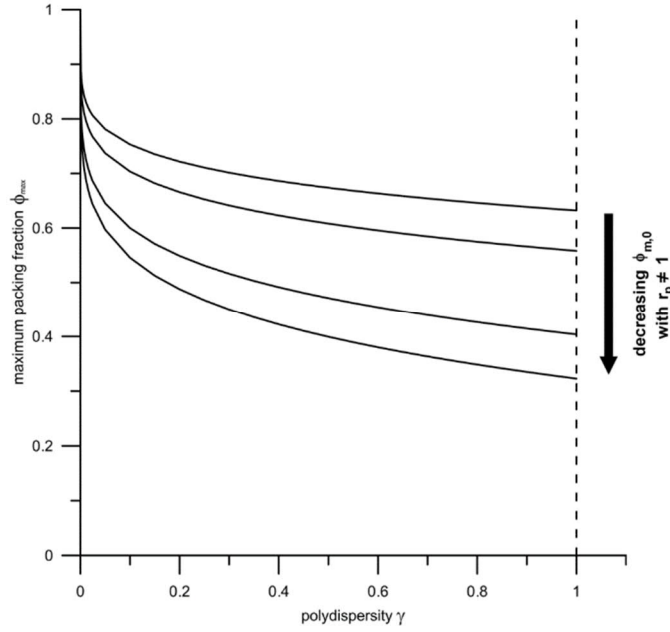


Figure 27: Schematic plot of maximum packing fraction ϕ_m vs. polydispersity γ (equation 2.29) following eq. (4.4) for distributions of arbitrary particle shape with aspect ratio $r_p \neq 1$.

The only parameter of equation (4.4) that might be affected by the shape of particles is $\phi_{m,0}$. Particle shape exerts a strong control on the maximum packing fraction as shown experimentally (e.g., Milewski, 1973; Parkhouse & Kelly, 1995; Rahli *et al.*, 1999), geometrically (Evans & Gibson, 1986), and numerically (e.g., Donev *et al.*, 2004; *et al.*, 2004; Williams & Philipse, 2003). The effect of particle shape on the relative viscosity can thus conveniently be evaluated through its effect on the maximum packing fraction. Based on high-resolution rheometry data, Mueller *et al.* (2011) proposed an empirical relationship between maximum packing fraction and the aspect ratio r_p of suspended particles:

$$\phi_m = \phi_{m1} \exp \left[-\frac{(\log_{10} r_p)^2}{2 b^2} \right] \quad (4.5)$$

where ϕ_{m1} is the maximum packing fraction for particles with $r_p = 1$, and b is a fitting parameter ($b = 1.08$). The aspect ratio r_p is defined as $r_p = \frac{l_a}{l_b}$, where l_a is the particle's axis of rotational symmetry and l_b is its maximum diameter perpendicular to that axis (assuming that non-spherical particles can be approximated as prolate/oblate spheroids or cylinders; Mueller S.P. *et al.*, 2010). Following equation 4.5, for particles having an aspect ratio $r_p \neq 1$, ϕ_m of related particle size distributions decreases drastically, so that those

distributions also have a lower $\phi_{m,0}$ (figure 27). This would add information of particle shape into the model without infringing the theoretical requirements and the general outcome of the model. Rheometric experiments on suspensions with arbitrary particle shape will test that theoretical idea.

4.2.1. Results of rheometric experiments

The experimental results for relative viscosity $\eta_{r,*}$ and flow index n (equation 2.9) for the synthesized uni- and polymodal distributions of prolate and oblate particles are presented in figure 28. Similar to the experiments with spheres the figures plot $\eta_{r,*}(\phi)$, as well as $n(\phi)$. Yield stress is also neglected for all samples, since it is found to be either small or negative (which is unphysical) but within 2σ error of zero. Likewise, maximum strain rates achieved were approximately $0.03\text{--}0.05\text{ s}^{-1}$ for concentrated samples, and up to 16 s^{-1} for very dilute suspensions.

The results presented in figure 28 follow the similar behavior that can be seen in the experiments of spherical particles in figure 19: a nonlinear increase in relative viscosity $\eta_{r,*}$ with increasing particle volume fraction. Again that is qualitatively consistent with previous rheological studies on particle-bearing suspensions (Castruccio *et al.*, 2010; Del Gaudio *et al.*, 2013; among others) and also the onset of a non-Newtonian behavior can be noticed. However, shear thinning indicated by decrease of flow index n seems to set in much earlier at $\phi > 0.1$ than for spherical particles. Since effects like particle rotation and particle interaction are thought to be the main cause for shear thinning (Mueller *et al.*, 2011), that might be expected. In summary, this set of rheometric experiments provides a solid and reliable dataset to test the model derived in section 4.1.3 for its capability to predict the maximum packing fraction of polydisperse suspensions with non-spherical particles ($r_p \neq 1$).

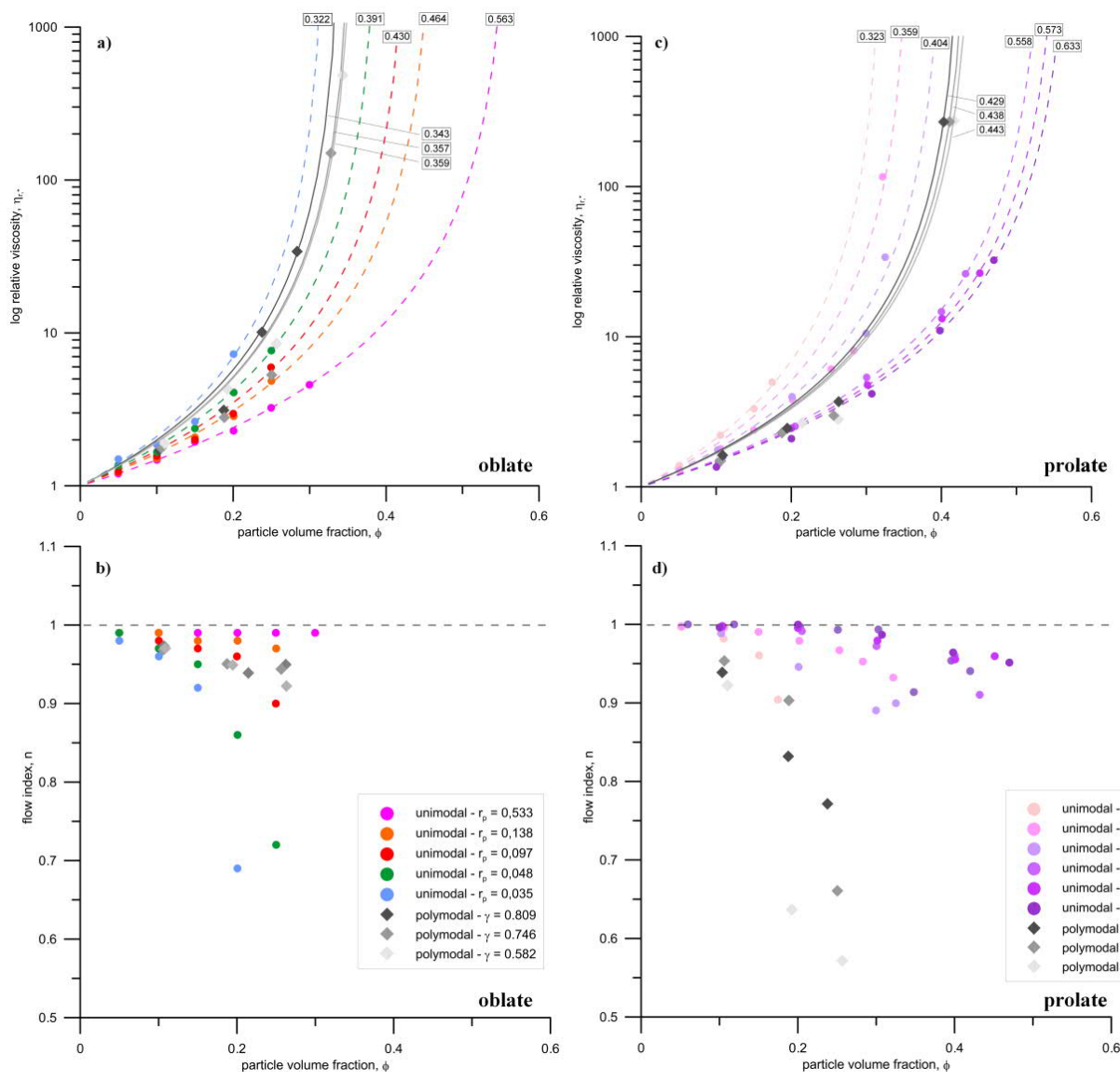


Figure 28: Experimental data of particles with arbitrary shape in relation to particle volume fraction.

4.2.2. Model improvements

Since the only parameter of equation (4.4) that might be affected by the shape of particles is $\phi_{m,0}$, as discussed in section 4.2, it seems reasonable to make use of the relationship between aspect ratio of particles and ϕ_m established by Mueller *et al.* (2011) and modified in Mader *et al.* (2013). Illustrated in Figure 29, that model predicts that if particles having an aspect ratio $r_p \neq 1$, ϕ_m of related particle size distributions decreases drastically. However, this model is largely based on particles with aspect ratio $r_p > 1$. Based on a set of complementary rheometric experiments of new oblate ($r_p < 1$) particle-bearing suspensions, their relation (equation 4.5) is extended and re-parametrized to provide a more robust fit (Figure 29). The complete set of experimental data can be found in the appendix.

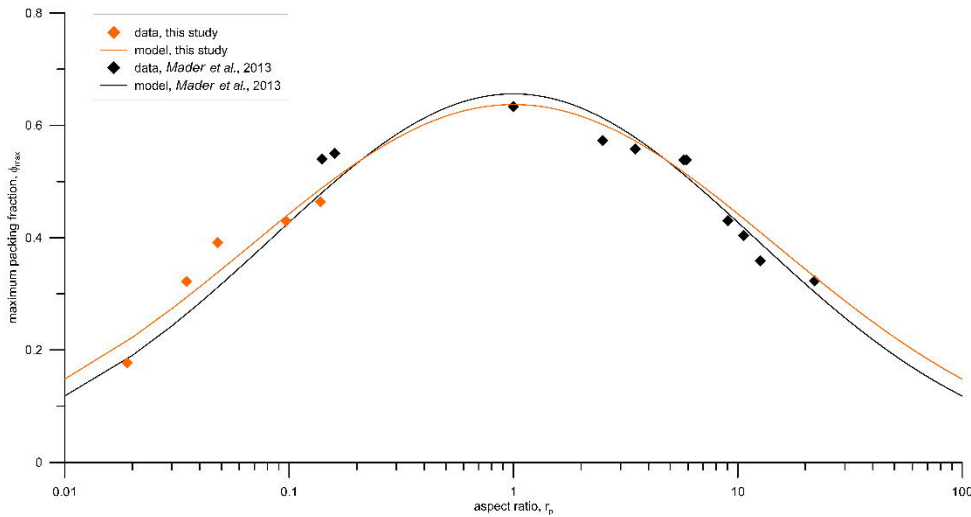


Figure 29: Experimental data of this study and re-parameterized model for maximum packing fraction ϕ_m vs. aspect ratio r_p (equation 4.5)

The re-parametrization of equation (4.5) yields minor changes to the fitting parameters. While in Mader *et al.* (2013) these values were given as $\phi_{m1} = 0.656$ and $b = 1.08$, for the data of this thesis the best fit is achieved for $\phi_{m1} = 0.637$ and $b = 1.171$. Figure 30 shows the results for prolate and oblate particle suspensions with varying polydispersity γ . In order to test the applicability of equation (4.4) for non-spherical particles, sets of polydisperse suspensions with mean aspect ratios of ~ 7 and ~ 0.09 were used. With the corresponding $\phi_{m,0}$ values calculated from equation (4.5) and Mader *et al.*

2013, the new data substantiate that equation (4.4) is a robust tool to estimate ϕ_m also for polydisperse distribution of prolate and oblate particles (Figure 30). For $r_p \neq 1$, the maximum packing fraction ϕ_m of the suspension systematically decreases, while maintaining the general relation between polydispersity γ and ϕ_m .

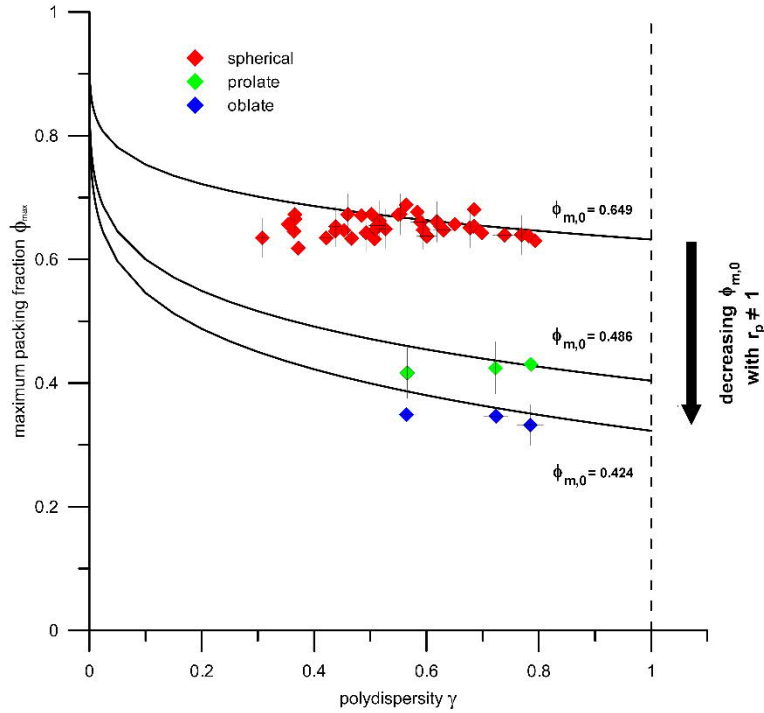


Figure 30: Experimental data of this study for maximum packing fraction ϕ_m vs. polydispersity γ (equation 4.4) of oblate (mean $r_p \sim 0.09$) and prolate (mean $r_p \sim 7$) particles.

4.2.3. The generalized model

Reasonably predicting the relative viscosity of natural crystal-bearing magma requires the consideration of crystal volume fraction, shape and size distribution. By combining the aforementioned models, a comprehensive model accounting for these key textural variables might be provided. As shown before, the only parameter in equation (4.4) that is directly affected by the shape of crystals is the maximum packing fraction of a monomodal suspension, $\phi_{m,0}$. By substituting the shape-specific parameter ϕ_m derived from equation (4.5) for $\phi_{m,0}$, it is possible to use equation (4.4) to quantify a theoretical ϕ_m for polydisperse suspensions with non-spherical particles. Implemented into the Maron-Pierce model, equation (2.14) can then be extended and expressed as:

$$\eta_{r,*} = \left(1 - \phi \left[1 - \left(\left(1 - \left\{ \phi_{m1} \exp \left[-\frac{(\log_{10} r_p)^2}{2 b^2} \right] \right\} \right) \gamma^a \right) \right]^{-1} \right)^{-2} \quad (4.6)$$

This expression takes into full account the volume fraction or crystallinity ϕ , the mean aspect ratio r_p of the crystals, and the polydispersity γ , when predicting the relative viscosity of a particle-bearing liquid. For natural magmas, these parameters can be readily obtained through image analysis with well-established techniques and software of rock samples (e.g., Hammer & Rutherford, 2002; Higgins, 2000; among others). Hence, equation (4.6) provides, for the first time, a means to estimate relative magma viscosity purely based on a comprehensive textural description of a section sample.

4.2.4. A practical application

As a last step the polydispersity model should be applied to natural volcanic rocks in order to test the empirical findings and draw inferences on plausible relative viscosity from rock texture. Therefore data available in DynVolc database (2017) was utilized. This database integrates physical observations of dynamic volcanic processes and spans the full range of explosive and effusive activity types. For each eruptive style, the database tabulates field, textural (i.e., vesicle and crystal size distributions) and chemical analyses of samples, and where available associated geophysical measurements.

Figure 31 shows the example of five different volcanic systems: (1) Mauna Ulu (Robert *et al.*, 2014), (2) Mt. Etna (Harris *et al.*, 2011), (3) Stromboli (Pistolesi *et al.*, 2011; Gurioli *et al.*, 2014), (4) Villarica (Gurioli *et al.*, 2008) and (5) Mt. Dore (Latutrie *et al.*, 2017). This selection spans compositions from mafic to intermediate magmas and encapsulates various eruption styles, thereby resulting in different crystallinities and crystal phases. Using 2D binary BSE images of given rock samples (Figure 31a), it is possible to gather textural data of those rocks in order to estimate the variables needed for the calculation of relative viscosity $\eta_{r,*}$. While polydispersity γ can be calculated following equation (2.29) using the equivalent diameter of the crystals, the relation between major and minor axis of the crystals determine a 2D average value of aspect ratio r_p of the particular rock samples. Due to the nature of the log-Gaussian function of equation (4.5),

the information of 2D aspect ratios r_p also contain 3D information. 2D-3D size and shape conversions of image analyses, however, are still quite essential aspects of CSD analyses and still in debate (e.g., Jerram *et al.*, 2009; Jerram & Higgins, 2007; Morgan & Jerram, 2006; Sahagian & Proussevitch, 1998; among others). The histogram of one sample from Villarica volcano (Gurioli *et al.*, 2008) is shown as an example in figure 31b.

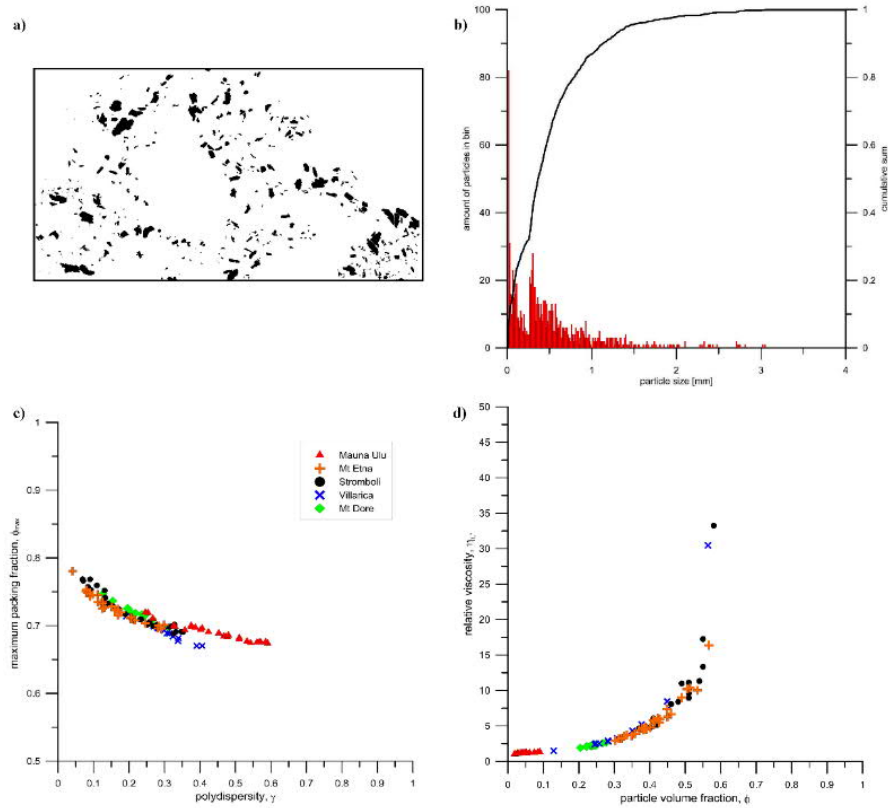


Figure 31: Practical application steps

This aforementioned textural data allows application of equation (4.4) on the data to calculate ϕ_m of each particular sample (Figure 31c), before actually estimating the relative viscosity $\eta_{r,*}$ with the Maron-Pierce model (equation 2.14; Figure 31d). A user-friendly spreadsheet that calculates the relative viscosity $\eta_{r,*}$ following these steps, summarized in equation (4.6), can be found in the appendix. The present example (figure 31) illustrates that the basaltic lava samples from Mauna Ulu are characterized by a relatively high polydispersity value γ ($0.2 < \gamma < 0.6$), which, in addition to a relatively low crystallinity, results in the lowest predicted relative viscosity $\eta_{r,*}$ (< 2.5). By contrast, the trachyandesitic samples from Stromboli showing lower polydispersity values γ ($0.05 < \gamma < 0.35$), which results a much more disperse CSD and consequently, a relatively high $\eta_{r,*}$ (up to 35).

4.3. Pros and cons - a summary

Despite the promising results, this model only focuses on the relative effect of crystal-size distributions on the rheology of magmas systems and the occurrence of vesicles in natural rocks is not taken into account. As such, we envision that the predicted μ values could be applicable to vesicle-free domains of magmatic flow in either conduit margins or dense sections of active lava flows. As direct viscosity measurements on active lavas are exceedingly difficult if not impossible (only few studies have succeeded to measure the viscosity in-situ using either penetrometers or rotational viscometers; Einarsson, 1949, 1966; Gauthier, 1973; Panov *et al.*, 1988; Pinkerton & Norton, 1995; Pinkerton & Sparks, 1978), our application provides a new and robust way to establish baseline data on magma rheology from samples of specific flow regimes in active or extinct volcanic systems. Future variants of the current model may incorporate the complex effects of bubbles on magma rheology (Manga *et al.*, 1998). It can be anticipated that vesicles and their size distributions might not only affect the value of polydispersity but also the physical properties of the magma (e.g., Manga *et al.*, 1998; Truby *et al.*, 2015; among others). Apart from that, a crucial parameter in the model is the aspect ratio r_p . The model relies on the assumption, that a meaningful average crystal aspect ratio r_p of the given rock sample can be constrained. Further research on the effect of a large range of particle aspect ratio on the rheology of suspensions – also in 3D - is needed.

5. The evolution of CSD's in rising magma and its effect on magma rheology

Because crystals grow during magma rise, and due to the profound influence of particle concentration, size distribution, and shape on suspension rheology, it is expected that the rheology of ascending magmas will change with time and position within the volcanic conduit (Figure 32). In order to temporally and spatially constrain magmatic textural development in the volcanic conduit, experiments on rhyodacitic melt compositions collected from Santorini (Greece) are performed, using an approach that simulates the rise of magma at various rates. The goal of these experiments is to determine how the crystal size distributions in naturally occurring magmatic rocks develops as a function of depth, decompression rate, and volatile content in a magma chamber-volcanic conduit system. In an ideal case, it would be possible to interpret the ascent and eruption histories of volcanoes that have produced magma having clearly undergone pre- and syn-eruptive crystallization from realistic textural maps of a magma-filled volcanic conduit (Hammer *et al.*, 2000, 2002; Martel *et al.*, 2000; Castro & Gardner, 2008). The upcoming chapter covers the second part of this study and outlines the methods and findings of the petrological experiments conducted for this thesis.

5.1. Idea and background

It is a well-accepted theory that the ascent of magma in the conduit alongside the mass eruption rate (Wilson, 1980) controls the style of volcanic eruptions to a large extent. According to Riker *et al.* (2015), the reasons for this are thought to be kinetic timescales of decompression-driven vesiculation and crystallization that strongly influence the ease of gas escape from viscous melts (Cashman *et al.*, 2004; Rust & Cashman, 2011). While vesiculation is the dominant process operating on very short timescales (seconds to minutes; Gardner *et al.*, 1999; Mourtada-Bonnefoi & Laporte, 1999), crystallization in response to degassing become increasingly important at longer timescales ($t > \text{hours}$; Hammer & Rutherford, 2002; Couch *et al.*, 2003a; Martel & Schmidt, 2003). Induced by decompression, the supersaturation of dissolved volatiles such as H_2O , CO_2 and others leads to the nucleation and growth of bubbles (Sparks, 1978; Gonnermann & Manga, 2007). The exsolution of those volatiles subsequently increases the temperature at which

mineral phases form (Swanson, 1977; Wilson, 1980; Eichelberger, 1995; Eichelberger *et al.*, 1986) and therefore influences crystallization processes. This phenomenon is known as the effective undercooling, which represents the temperature difference between magma and the liquidus (e.g., Martel & Schmidt, 2003; Hammer, 2008).

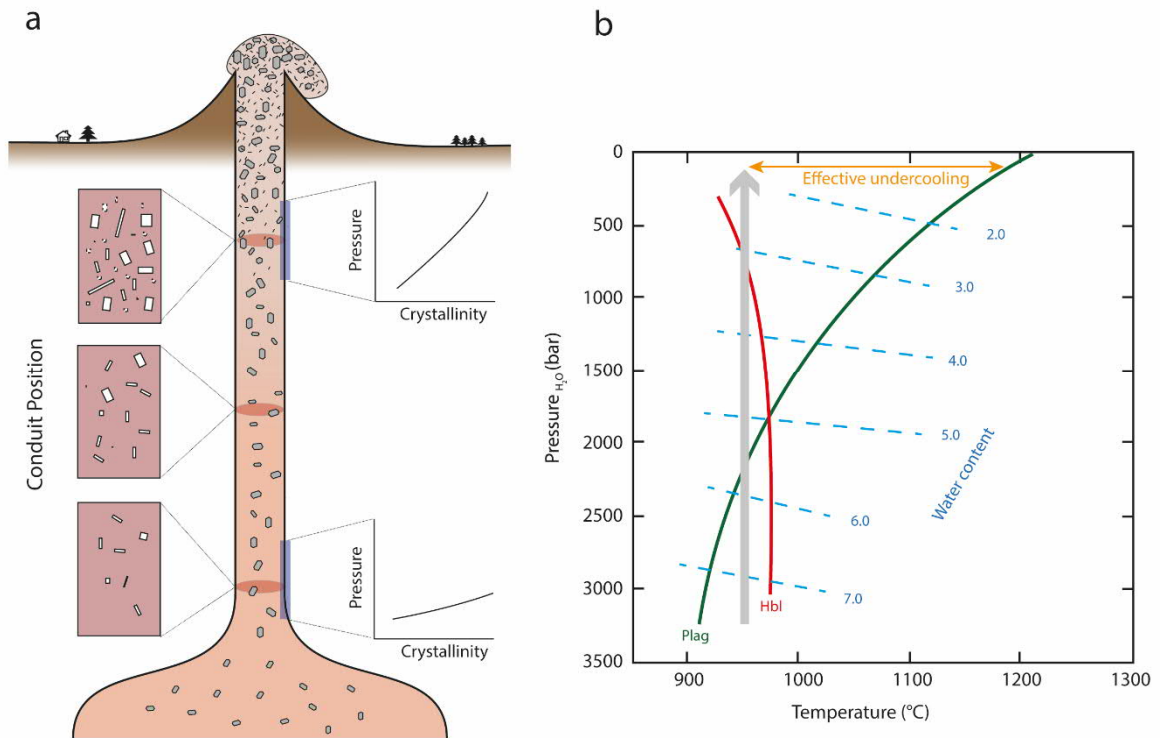


Figure 32: (a) Schematic cross-section of a volcanic conduit showing the crystallinity development at arbitrary low, middle, and upper levels in the conduit, depicting the expected textural changes of silicic magma that is undergoing degassing due to decompression.

When explosive eruptions are initiated, the magma chamber overpressure is usually highest, leading to fast ascent rates (Jaupart & Allegre, 1991). If there is no time for the exsolved gas phase to escape into the country rock, magma and gas phase hence act as a *closed system* (Newman *et al.*, 1988) leading to expansion, fragmentation and acceleration of a bubbly foam (Sparks, 1978; Wilson, 1980; Jaupart & Allegre, 1991). In the event of slower ascent rates, the volcanic conduit is able to divert the exsolved gases (often by means of fumaroles (Heiken *et al.*, 1988; Hammer *et al.*, 1999) or ash-charged vents known as tuffisites (Stasiuk *et al.*, 1996; Tuffen *et al.*, 2003)) or the ascending magma reaches some degree of permeability due to bubble nucleation, which allows the volatiles to degas through the bubble network (Eichelberger *et al.*, 1986; Klug & Cashman, 1996). This leads to *open system* conditions and consequently to an effusive eruption style (Eichelberger *et al.*, 1986; Newman *et al.*, 1988; Jaupart & Allegre, 1991; Klug & Cashman, 1996). Whether a (volatile-rich) volcanic system degasses as an open or closed

system is also influenced by viscosity of the magma, volatile diffusivity as well as bubble interconnectivity (e.g., Burnham & Davis, 1971; Eichelberger *et al.*, 1986; Woods & Koyaguchi, 1994; Moore *et al.*, 1998; Mangan *et al.*, 2004; Papale *et al.*, 2006; Gonnermann & Manga, 2007).

The fact that magmas undergo complex storage, ascent and decompression histories prior to an eruption may result in equally complex magmatic textures comprising crystals and vesicles in contact with quenched silicate melt (glass). Especially the pre-eruptive storage conditions, namely the position, temperature, pressure, and oxygen fugacity (fO_2) of a magma chamber dictate the initial rheological conditions of a magma. Once magma rises from its storage chamber, it may undergo several important chemical and physical changes that are directly linked to its position within the crust affecting the rheology of ascending magmas. Due to crystal growth and the profound influence of particle concentration, size distribution, and shape on suspension rheology, it is expected that rheology will change with time and position within the volcanic conduit. (Figure 32).

Crystal sizes are often bi- or multimodally distributed, e.g., with a population of phenocrysts embedded in a microlite-rich matrix (Marsh, 1988a; 1988b; 1998; Hammer *et al.*, 2000, 2002; Martel *et al.*, 2000; Castro *et al.*, 2003; Mock & Jerram, 2005; Morgan & Jerram, 2006; Castro & Gardner, 2008; Rannou & Caroff, 2010). Phenocrysts, by virtue of their larger size and common enclosure of silicate glass inclusions, are believed to represent crystallization at magma chamber conditions, while microlites, by contrast, may grow dominantly during magma ascent within the conduit, in response to changes in pressure, temperature, and melt-H₂O concentration. Thus, the microlite population is likely to be a key indicator of magma ascent conditions, including distance travelled and velocity (e.g., Hammer & Rutherford, 2002).

The intention of the second part of this thesis is to measure the CSDs in experimentally grown crystal populations in order to gauge when and at what P-T conditions microlite crystallization occurs in a volcanic conduit. Once it is established how magma composition, temperature and decompression (rise) rate scale with CSDs, it might be possible to develop curves showing the time- and pressure (depth)-dependent crystal contents in the volcanic conduit. Such information will in turn, serve as a basis to predict rheological transitions in active volcanic conduits. The target composition of this study is a

rhyodacite from the Minoan eruption of Santorini volcano, a volcanic system for which the erupted products are well characterized and whose magma storage reservoirs and plumbing systems are already well documented in terms of position and starting magma temperature (e.g., Cottrell *et al.*, 1999; Druitt *et al.*, 1999 - see chapter 6). Using these initial storage conditions as starting points, the aim is to map out how crystallinity changes as a function of pressure, or depth beneath the volcanoes and subsequently the rheological shifts expected to occur during the rise of magma from a variety of different storage positions to the point of eruption.

As summarized and reviewed by Riker *et al.* (2015), experiments simulating magmatic decompression provide a means of calibrating textures against known ascent conditions. While early work established the relevance of degassing-induced crystallization on magmatic and volcanic timescales (Fenn, 1977; Swanson, 1977; Muncill & Lasaga, 1988; Geschwind & Rutherford, 1995), a lot of research has aimed to correlate quantitative descriptors of crystal texture (i.e. abundance, number density, size, and morphology) with kinetic variables such as undercooling (the difference between the phase liquidus temperature and the experimental run temperature), decompression rate (dP/dt), and time (Hammer & Rutherford, 2002; Couch *et al.*, 2003a; Martel & Schmidt, 2003; Pupier *et al.*, 2008; Brugger & Hammer, 2010a; Cichy *et al.*, 2010; Martel, 2012; Mollard *et al.*, 2012; Arzilli & Carroll, 2013; Shea & Hammer, 2013). As a result these studies establish baseline crystallization kinetics of common magmatic minerals (Hammer & Rutherford, 2002; Martel & Schmidt, 2003; Mollard *et al.*, 2012), provide a context for linking groundmass crystal textures to specific eruptive events (Couch *et al.*, 2003a; Szramek *et al.*, 2006; Suzuki *et al.*, 2007; Blundy & Cashman, 2008; Martel, 2012) and compare the textural 'fingerprints' of decompression- and cooling-induced crystallization (Arzilli & Carroll, 2013; Shea & Hammer, 2013). Additionally the results of dynamic decompression experiments also suggest the potential for applications as geospeedometers (Toramaru, 1989; Rutherford & Hill, 1993) and geobarometers (Blundy & Cashman, 2008; Mollard *et al.*, 2012) and provide an essential reference for numerical models of magma ascent (e.g., Melnik & Sparks, 2005).

5.2. Experimental Strategy

By having the well-constrained mineral and glass compositional and textural database at hand, this data can be used as starting points for controlled petrological experiments. This set of experiments has two primary goals: (a) to establish the pressure, temperature, and crystal texture relations in magma conduits (*phase equilibrium experiments*), as well as (b) to simulate a range of magma rise scenarios, which will investigate the effects of magma rise speed and total decompression on the ensuing textural and chemical signatures in the eruptive materials (*decompression experiments*).

5.2.1. Phase Equilibrium Experiments

In order to map the evolution of CSD and crystal texture in a volcanic conduit with depth, it is necessary to perform petrological experiments at different pressures and temperatures representing different depth within the conduit in the first place. Allowing the system to fully equilibrate at each set of conditions, these conditions correspond to the pre-ascent and pre-eruptive magma storage conditions. Using samples of rhyodacitic pumice from Santorini volcano provides well-constrained information of the magma storage reservoir and plumbing system in terms of position and starting magma temperature (Figure 33; Cottrell *et al.*, 1999) and therefore establish the run temperature (900°C) and the amount of decompression later applied to the melt. Using these initial storage conditions as starting points, isothermal experiments of different pressures simulate how crystallinity changes as a function of pressure, or depth beneath the volcanoes and can be used as correlation for the decompression experiment runs.

In the phase equilibrium experiments, aliquots of crushed pumice powder are loaded into Ag-Pd capsules with enough water to ensure H₂O-saturated conditions. The assumption is that natural magmas were water-saturated at the time of storage and eruption (Eichelberger, 1995). Capsules will then be sealed, welded shut, and weighed prior to experiments in horizontal tube furnaces and Ni-Co-alloy (Waspaloy and René-41) “cold-seal” pressure vessels (autoclaves). The exact experimental procedure, as well as sample preparation and analysis will be discussed in the upcoming chapter 6.

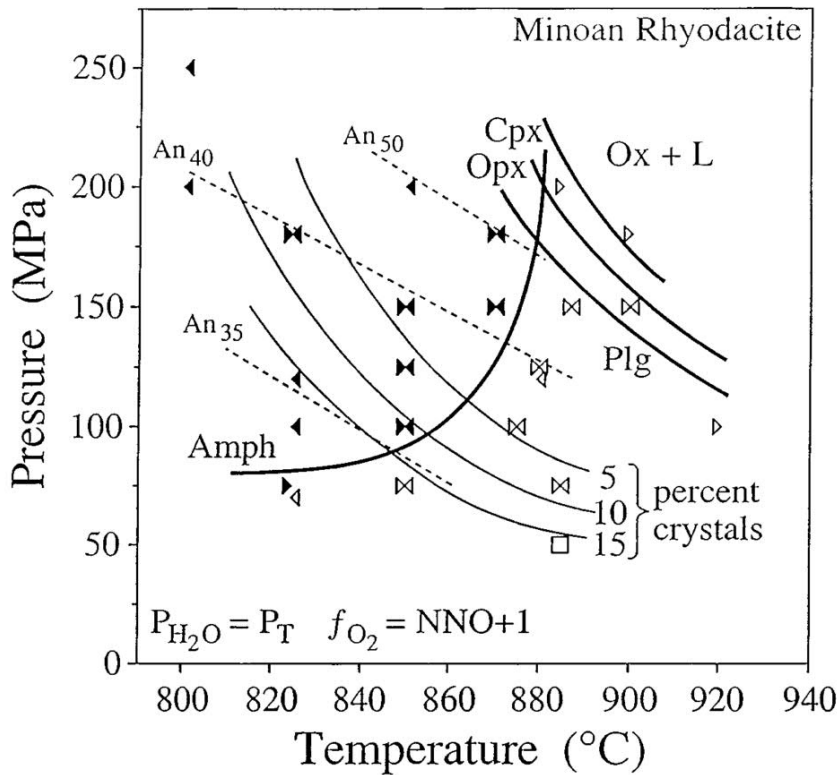


Figure 33: Phase equilibria diagram for hydrothermal experiments on Minoan rhyodacite from Cottrell et al., 1999)

5.2.2. Dynamic Decompression Experiments

In order to establish a relationship between decompression rate and magma crystal texture, decompression experiments simulate the rise of magma in the conduit. Since crystallization in magmatic rocks occurs in response to a change in temperature and/or a change in melt composition, decompression dynamics might influence the crystallinity and therefore the CSD of the sample drastically.

Because the changes in temperature due to cooling of an ascending magma batch are expected to be minor compared to the effects of decompression-induced volatile loss (degassing), the crystallization trigger investigated in this project part will be restricted to devolatilization-driven crystallization. The primary volatile species is H₂O, arguably the most important volatile component in arc magmas (Luhr, 2001; Wallace *et al.* 2002). Many if not most arc magmas are believed to exist at some point in their pre-eruptive history in an H₂O-saturated state and under these conditions when the magma rises, bubbles grow thereby sequestering exsolved H₂O from the silicate melt phase. As this happens, the chemical undercooling “felt” by the silicate melt phase increases, and consequently, provided there is enough time for crystals to nucleate and grow, mineral phases precipitate in the melt (Figure 32b). In general, the larger the degree of undercooling, the more the melt is inclined to respond by growing crystals. So, it is expected that the crystallinity (volume percent of crystals), size, and number density (number of crystals per unit volume) will all increase with time and position in the volcanic conduit. Thus the experimental strategy is to grow crystals in natural silicate melts under different yet controlled amounts of undercooling driven by different decompression rates under water-saturated conditions.

Since crystals need time to grow and in the natural system this time is offered by the amount of time the magma spends on its way to the surface (i.e., pre-quench time), experiments will be conducted across a range of realistic magma ascent rates (~0.05 - 0.2 m sec⁻¹). That ascent rate is given by the quotient of total decompression and experiment runtime. The isothermal decompressions will be conducted to an end-point pressure of 20MPa, corresponding to a relative shallow conduit depth. The differing decompression amounts correspond to specific pressure points and therefore depths in the chamber-conduit system as appropriately scaled to the approximate density profile of the sub-volcanic crust.

The set of decompression experiments are performed in the aforementioned apparatus. However, these experiments first involve an equilibration stage, in which the starting materials are subjected to a constant P-T dwell period of between 1 and 6 days to homogenize the starting material and simulate magma storage prior to ascent. Decompression will be induced by a continuously release of pressure at a rate governed by

a pressure intensifier system. Again, the exact experimental procedure, as well as sample preparation and analysis will be discussed in the upcoming chapter 6.

The results of those decompression experiments are commonly compared with textural characteristics of natural rocks to make interpretations about magma ascent rates (e.g., Rutherford & Hill, 1993; Hammer & Rutherford, 2002; Couch *et al.*, 2003a; Nicholis & Rutherford, 2004; Cashman & McConnell, 2005; Brugger & Hammer, 2010b; Riker *et al.*, 2015, etc.). Natural ascent rates cover a wide range, from 0.001 to 0.015 m·s⁻¹ for felsic and intermediate magmas in the crust, 0.1–10 m·s⁻¹ for effusive MORBs and more than 200 m·s⁻¹ for kimberlites and explosive eruptions (e.g., Paonita & Martelli, 2006; Sparks *et al.*, 2006; Rutherford, 2008; Misiti *et al.*, 2011). As shown by the aforementioned studies, decompression rate exerts a first-order control on crystal microtextures. However, as stated by Brugger and Hammer (2010a) the nature of magma ascent during or prior to an eruption is not fully understood. It is thought to be at times intermittent and pulsatory, with rapid accelerations followed by irregular pauses, whereas at other times it may consist of steady fluid flow (Smith, 1997; Tuffen *et al.*, 2003; Roman *et al.*, 2006; Scandone *et al.*, 2007;).

The way and style of the actual decompression is a huge issue when simulating magma ascent. As summarized by Brugger and Hammer (2010a) or Marxer *et al.* (2015), due to technical limitations and simply out of necessity, most decompression-induced crystallization experiments have utilized a *step-wise decompression* (SD) method consisting of either a single-step decompression (SSD) or multi-step decompression (MSD) (e.g., Hurwitz & Navon, 1994; Lyakhovsky *et al.*, 1996; Hammer & Rutherford, 2002; Coombs *et al.*, 2003; Couch *et al.*, 2003a; Martel & Schmidt, 2003; Larsen & Gardner, 2004; Nicholis & Rutherford, 2004; Gardner, 2007; Suzuki *et al.*, 2007; Castro & Gardner, 2008; among others). In those kind of experiments, pressure is changed manually from an initial pressure instantaneously to a final pressure or with the help of a series of small pressure drops and dwell periods before the sample is quenched. Experiments employing a *continuous decompression* (CD) make use of a constant release of pressure given by a distinct decompression rate imposed by a hydraulically driven screw pump pressure variator with programmable controller as for example demonstrated by Brugger and Hammer (2010a). Even though, according to Riker *et al.* (2015), only few continuous decompression experiments were performed with reasonable decompression rates (e.g.,

Brugger & Hammer, 2010a; Pichavant *et al.*, 2013; Riker *et al.*, 2015) in order to investigate crystal growth dynamics. Most experiments primarily focused on studies of volatile exsolution, bubble nucleation, and bubble growth processes (e.g., Gardner *et al.*, 1999; Mangan & Sisson, 2000; Martel & Schmidt, 2003) and imposed very rapid decompression rates (typically 450 MPa h^{-1}). Following Brugger and Hammer (2010a), the MSD approach is thought to closely approximate natural magma ascent because the small steps in pressure are regarded as insignificant in comparison with the total amount of decompression. However, they argue that effects of varying pressure- and time-step size on resulting crystal textures has never been investigated.

5.3. Textural characterization - Crystal-size distributions (CSD)

Many authors made use of textural analyses to characterize the processes before and during volcanic eruptions (e.g., Marsh, 1988a; 1988b; Cashman, 1992; Higgins, 1994; Hammer *et al.*, 1999; Cashman & Blundy, 2000; Hammer & Rutherford, 2002; Couch *et al.*, 2003; Martel & Schmidt, 2003; among others). Aspects of a natural sample's crystallization history (e.g., nucleation and growth rates, cooling and residence time, qualitative degassing patterns) can be extracted from the form of a crystal size distribution (Cashman & Marsh, 1988). It is typical to plot the CSD as the logarithm of the population density $n(L)$ (n = number of crystals per unit volume per unit length) as a function of size (measured as either the length or breadth of the crystal in two or three dimensions), because in most natural cases, $n(L)$ is observed to be an exponentially decreasing function of L (Marsh 1988 a; 1988b). The basis for plotting a CSD is the standard histogram, and methods to convert a histogram to a CSD are presented by Higgins (2006a). Once plotted, data typically fall onto straight or curved lines in CSD space and the slopes and y-intercepts of these lines can be used to distinguish different crystal populations within the rock and the time evolution of the crystal population (Figure 34; e.g., Hammer *et al.*, 1999, Higgins & Roberge, 2007).

Initially developed in chemical engineering by Randolph and Larson (1971), a theoretical basis for the concept of CSDs was established by Cashman & Marsh (1988) and Marsh (1988a; 1988b) by the application to igneous rocks of the corresponding industrial models. They proposed to study the numbers of crystals (per unit volume) in magmatic rocks in a semi-logarithmic fashion, by plotting them against their representative sizes

(Armienti, 2008; Rannou & Caroff, 2010) and showed that in an open, steady-state system with continuous crystallization, the CSD is a straight line with negative slope on a graph of \ln (population density) versus length. As shown by Pupier *et al.* (2008), based on the Avrami approach (1939, 1940) it can be considered that in order to achieve a given crystalline fraction ϕ corresponding to thermodynamic equilibrium in a given amount of time t , growth rate G and nucleation rate J are adjusted automatically according to the so-called Avrami equation:

$$\phi = 1 - \exp(-k_v J G^3 t^4) \quad (5.1)$$

where k_v is a volumetric factor. The relationship between the characteristic time necessary for crystallization, characteristic growth and nucleation rates, and CSD parameters have been quantified by Cashman (1992), Marsh (1998) and Zieg and Marsh (2002). The slope of a CSD can generally be equated with

$$slope = \frac{-1}{G * t} \quad (5.2)$$

while the intercept is the nucleation density. Nucleation and growth rates of crystals are controlled by the magnitude of the crystallization driving force, which can be expressed thermally as undercooling or chemically as saturation (Higgins and Roberge, 2007). As discussed by Marsh (1998) the typical log-linear decrease in population density as a function of crystal size can be explained, in a closed system, by two end-member scenarios. Either (i) the nucleation rate J (number of crystals $m^{-3} s^{-1}$) increases exponentially as a function of time, while growth rate G ($m s^{-1}$) is constant:

$$J(t) = J_0 \exp(C_j * t) \quad (5.3)$$

where J_0 and C_j are constants; or (ii) growth rate G increases exponentially as a function of crystal size, while the nucleation rate is constant. In this case:

$$G(L) = G_0 \exp(C_g * L) \quad (5.4)$$

where G_0 and C_g are constants.

As further discussed by Pupier *et al.* (2008), although significant progress has been made concerning the theoretical links between the CSD and the physical processes accompanying crystallization (e.g., Resmini 2007; Higgins 2002; Hort & Spohn 1991; Marsh 1988a, 1988b) consideration of these simple idealized cases illustrates that there is no unique quantitative interpretation of a given log-linear CSD. On the other hand, if time constraints are available (i.e. knowledge of the cooling history of the sample), values of G and J may be derived. In conclusion, in the batch closed system constituted by an experimental charge, the evolving shape of the CSD will provide insights into the nucleation and growth processes, whereas the CSD parameters (slope and intercept) will allow the determination of mean growth and nucleation rates. Additionally Rannou and Caroff (2010) showed, that although magmatic systems are always multiphase, most of the published CSD analyses concern only one selected mineral (e.g., Turner *et al.*, 2003; Higgins & Chandrasekharam, 2007; Morgan *et al.*, 2007). Only a few CSD studies deal with several comagmatic phases (e.g., Armienti *et al.*, 1994; Higgins, 2002a, 2002b; Higgins & Roberge, 2003; Mock *et al.*, 2003; Simakin & Bindeman, 2008).

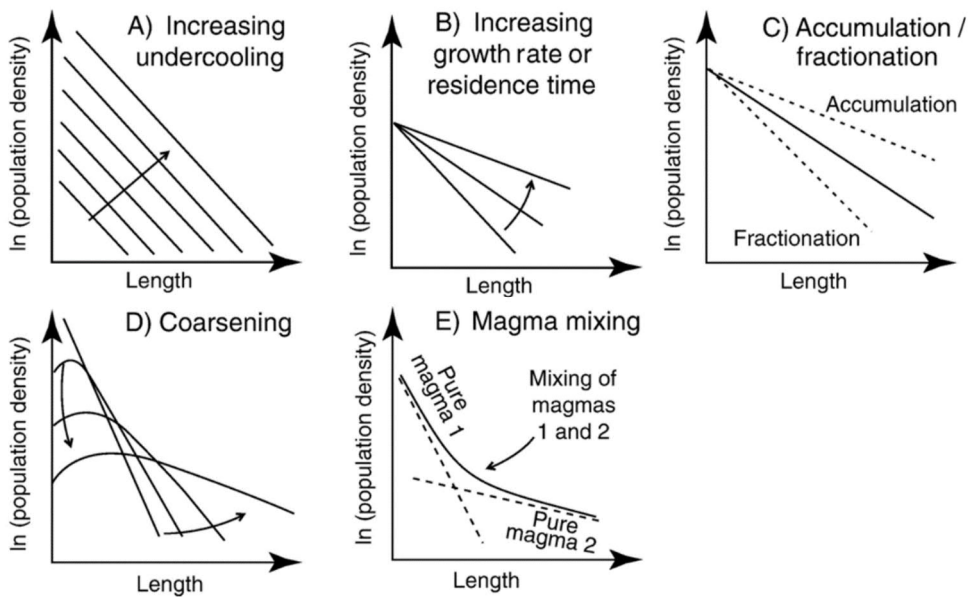


Figure 34: Examples of processes that can affect the shape of the CSD.

Higgins (2006a) proposed a CSD classification based on the shape of the distribution when plotted on relevant diagrams. Changes in intensive parameters, like temperature and pressure, will change the value of the crystallisation driving force. For constant conditions, however, there will only be one CSD, while a decrease in temperature will be represented on that graph by a family of straight lines with the same slope but different intercepts representing nucleation density (Figure 34a; Higgins, 2006a).

Furthermore, for a similar growth rate, a longer residence time will favour the growth of larger crystals; therefore, it will produce a change in the CSD slope but with the same intercept (Figure 34b). A change in growth rate will produce the same effect and if the crystal growth rate can be established then residence times can be calculated (Higgins & Roberge, 2007). Accumulation and fractionation processes can also change the overall shape of CSDs (Figure 34c). Both analytical and stochastic approaches have shown that crystal accumulation produces a gentler CSD slope because larger crystals descend faster than smaller crystals (Marsh, 1988a, 1988b; Higgins, 2002b). The complementary fractionated magma will have a steeper slope as more big crystals have been removed than small crystals (Higgins & Roberge, 2007).

Figure 34d shows theoretical CSDs for magma that is experiencing coarsening following the Communicating Neighbours model of DeHoff (1991). It has been proposed that coarsening (Ostwald Ripening, textural equilibration) is an important process in plutonic rocks (Hunter, 1987, 1996; Higgins, 1998, 2002), and might also be important in the development of some volcanic rocks (e.g., Higgins & Roberge, 2003). Coarsening in an igneous context is a process by which small crystals are resorbed while the larger crystals grow so that the total surface energy is minimized (see review by Voorhees, 1992). It occurs when magmas are held near their liquidus temperature for a long period. The turn down of the left side of the CSD curve in figure 34d represents the disappearance of the small crystals, whereas the right side of the CSD flattens during textural coarsening indicating that the growth rate of crystals increases to a maximum with grain size (Higgins, 1998). Thus, both the slope and intercept of the CSD diminish during this process (Higgins & Roberge, 2007).

Another process affecting overall shape of CSDs is magma mixing or the existence of multiple parental magmas. The terms used to describe these processes depend on the ratio of the mixing scale to the system size. If this value is small then the final product is homogeneous and the process is termed mixing. If the scale is larger, heterogeneities may be observed and the process is then termed mingling. If the components share a conduit or pluton then the term composite body or multiple magmas is used (Higgins & Roberge, 2007). Mixing of two magmas with non-collinear straight CSDs will produce a concave up curved CSD (Figure 34e; Higgins, 2006a). This is because the vertical scale on a classic CSD diagram is logarithmic. In detail, the CSD has straight segments at small and great

sizes parallel to the original CSDs, but displaced downwards between the two original CSDs. The degree of curvature will depend on the differences in CSD slope between the two magmas. On simple, linear, bivariate geochemical diagrams, mixing will produce a straight-line variation. This is not easy to distinguish from the curved distributions of fractional crystallization if there is little compositional variation (Higgins & Roberge, 2007).

6. Methodology

This chapter describes and summarizes the systematic experimental effort and techniques in terms of sample preparation, the actual experimental routine and the textural analysis used in the second part of this thesis.

6.1. Petrological experiments – procedure and methods

The series of isothermal equilibrium HP/HT-experiments as well as decompression experiments were carried out for textural analysis and comparison with natural samples follow the method described by Castro *et al.* (2013). The starting material of all experiments was a finely crushed powder of pumices that were sampled in the fallout deposits of Santorini Minoan eruption (A-layer). 50 to 70 mg of this powder was filled into gold tubes of 20 mm length and 4 mm diameter that were already welded shut on one side. Along with that, a sufficient amount of distilled water (~5 to 8 mg) was added to the powder to ensure water saturation at the intended pressure and temperature conditions of the following experiment (see Table 3). The capsules were then welded shut with an acetylene–oxygen torch. To enable heat conduction during welding and hence reduce the effect of vaporization of water within the capsule, the capsules were wrapped in water-saturated paper and partly submerged in a larger water reservoir. After welding, the capsule was heated on a hot plate at about 120 °C for 30 seconds and then reweighed to ensure that the capsules were reliably sealed. This process was repeated twice. If the weight was stable during the entire heating process, the capsules were ready for the experiment. Otherwise, the capsules were discarded.

All experiments were performed in horizontal tube furnaces and Ni-Co-alloy (Waspaloy and René-41) “cold-seal” pressure vessels (autoclaves). The autoclaves were first filled with distilled water before the gold capsule was added. Along with that, a Ni-metal filler rod was placed in the “free space” above the experimental capsule. This configuration prevents convection of the pressurizing fluid and fixes the oxygen fugacity (f_{O_2}) at about NNO+1 (e.g., Geschwind & Rutherford 1992, 1995).



Figure 35: Different stages of sample conditions during preparation

The autoclaves are connected to the pressurizing system of a rotary vein pump and a network of water-filled stainless steel pressure tubes. To check for any leaks, the autoclaves were pressurized to a pressure above the target value. If no leaking was observed, the furnaces were heated and pressurized to the desired P-T conditions. During the heating process, the pressure had to be monitored carefully, as the pressure builds up rapidly during heating-induced expansion of the fluid. When the target temperature of 900°C was reached, the system was left to equilibrate for half an hour before the actual experiment was started.

In the case of the equilibrium experiments with stable P-T conditions, the system was left at the initial pressure and temperature conditions until the end of the experiment for between 54 and 160h depending on the temperature and PH_2O and the need to preserve the mechanical integrity of the autoclaves. Following Pichavant and Macdonald (2007) or Cottrell *et al.* (1999) this duration is generally sufficient time to achieve local equilibrium between silicate melt and crystalline rims. For the series of decompression experiments, each experiment was left for several days (26 to 144h) to equilibrate and stabilize the mineral assemblage in presence of the surrounding silicate melt, before the actual decompression was started. The continuous decompression of the system was controlled

and performed by a PID modulator that controls the pump and decompresses the pressure system.

The individual decompression has to be set and the system runs automatically. Different decompression rates (15, 7.5, 3 and 0.5MPa/s) were chosen to imitate different ascent rates, i.e. eruption styles (explosive vs. effusive) and thus reproduce the textural properties of natural samples. The slowest decompression rate corresponds to an ascent rate ($\sim 0.01\text{m s}^{-1}$) typical of a dome-building effusive eruption (e.g., Mount St Helens), whereas the fastest decompression simulates an ascent rate ($\sim 0.17\text{m s}^{-1}$) corresponding to that preceding low-intensity explosive activity (Rutherford *et al.*, 2000). Assuming a lithostatic pressure gradient, each 10MPa pressure step corresponds to instantaneous ascent of $\sim 300\text{m}$.

The pressure and temperature during both equilibrium and decompression experiments were monitored daily to ensure stable equilibrium conditions. Pressure was checked by a factory-calibrated Bourdon-tube gauge, and also with a pressure transducer. The associated errors in pressure readings are $\pm 0.5\text{MPa}$ (Castro *et al.*, 2013). An inconel-sheathed K-type thermocouple was inserted into a bore at the end of the bomb to measure the temperature at a point closest to the capsule, in addition to an onboard thermocouple in the furnace that measured the temperature at the mid-point of the bomb. Little to no difference in temperature was noted between the bomb center and its end where the capsule would rest, although each thermocouple carries an error of $\pm 5^\circ\text{C}$.

At the end of an experiment, the autoclaves were quenched rapidly to inhibit thorough crystallization of the glass phase by a combination of blasting with compressed air (1–2 min) and submersion in a circulating cold-water bath. To mitigate significant pressure loss upon cooling by overpressurizing the experiments by 30 bars above the target point shortly before the air-cooling phase. After quenching, the capsules were removed and cleaned in an ultrasonic bath, dried and weighed again to check for leakage during the experimental run. The gold capsules were then cut open with a razor blade, and the experimental materials were removed. In each case, fluid fizzing out of the capsule was observed when opening the experimental charges. The run products were then prepared for electron probe microanalysis.

experiment	equilibrium			decompression						
	temperature [°C]	pressure [MPa]	duration [hrs]	rate				time		final pressure [MPa]
				[bar/h]	[MPa/h]	[m/h]	[m/sec]	[hrs]	[days]	
SP1	900	200	54,25	-	-	-	-	-	-	-
SP6	900	175	122,5	-	-	-	-	-	-	-
SP2	900	150	163	-	-	-	-	-	-	-
SP3	900	125	140,5	-	-	-	-	-	-	-
SP7	900	100	120	-	-	-	-	-	-	-
SP4	900	75	142	-	-	-	-	-	-	-
SP5	900	50	118	-	-	-	-	-	-	-
SP8	900	20	141	-	-	-	-	-	-	-
DC14	900	175	26	30	3	122,32	0,03	48,33	2,01	30
DC11	900	175	48	5	0,5	20,39	0,01	290,00	12,08	30
DC1	900	150	112	150	15	611,62	0,17	8,67	0,36	20
DC2	900	150	121,5	75	7,5	305,81	0,08	17,33	0,72	20
DC8	900	150	119	30	3	122,32	0,03	43,33	1,81	20
DC3	900	150	144	5	0,5	20,39	0,01	260,00	10,83	20
DC4	900	125	116,5	150	15	611,62	0,17	7,00	0,29	20
DC5	900	125	121,75	75	7,5	305,81	0,08	14,00	0,58	20
DC6	900	125	118,25	30	3	122,32	0,03	35,00	1,46	20
DC7	900	125	119,75	5	0,5	20,39	0,01	210,00	8,75	20
DC12	900	100	50	30	3	122,32	0,03	26,67	1,11	20
DC13	900	100	126	5	0,5	20,39	0,01	160,00	6,67	20

Table 3: Overview of petrological experiments - equilibrium and decompression experiments

6.2. Sample preparation

After the completion of the equilibrium, as well as the decompression experiments, the quenched products were examined with a range of chemical and microanalytical methods. With the help of thorough textural characterizations of the run products it is possible to determine their CSDs and the geometrical properties of the crystals (aspect ratio). The technique for sample preparation of the experimental samples follows standard procedures: The sample fragments were mounted in round hard-plastic pucks and embedded in epoxy resin. Meticulous preparation of the epoxy is key to forthcoming analyses since it has to be prevented to mix any bubbles into the puck. This applies especially for the very porous natural pumice samples. Bubbles can be brought to the surface with a small needle or if needed with the help of a vacuum chamber. For good results and image acquisition with electron microprobe (EMPA) it is essential, that the sample surface is clean and very well polished. Even small irregularities may lead to scattering of electrons. If the epoxy is hardened, the mounted sample has to be ground and polished. There are two grinding steps using diamond grits of different grain sizes, followed by three polishing steps using either polyester or silk cloth in combination with diamond suspensions of the appropriate grain size. After each polishing step, the puck has to be cleaned in an ultrasonic bath, and the spinning table is cleaned to prevent contamination. Prior to EMPA analyses, a carbon coating of about 20nm must be applied to the polished samples. The carbon coating ensures conductivity during the measurements and inhibits any charges building up (e.g., Reed, 1996). There is no influence of the carbon coating on the measured results.

6.3. Electron microprobe analyses (EMPA)

The electron microprobe analysis (EMPA) was used to acquire BSE pictures, visually enhancing chemical variations within samples, and to chemically analyze the phenocrysts composition in order to compare the results to natural samples (Cottrell *et al.*, 1999). All microprobe analyses were obtained with a *JEOL JXA 8900 RL* at the Johannes Gutenberg-University of Mainz. It is one of the most widely used and most efficient non-destructive analytical techniques in the determination of major and minor element chemistry of solid rock samples due to the fact of its excellent spatial resolution in the order of 1 μm . The sample is analysed by characteristic x-ray lines, which are excited by a focussed electron

beam in a non-destructive way so that quantitative analysis can be obtained in many cases with an accuracy of the order of 1-2 % of the amount present for a given element. (Goldstein *et al.*, 1992; Rollinson, 1993; Reed, 1996).

The EMPA is based on the interaction of electrons and the surface of a specific rock sample and is basically comparable to an X-ray tube. Here, an electron beam is generated and focused on the sample, whereby the atoms of the sample are excited due to the power of the electrons. The electrons of the inner shells of the atoms are elevated to higher energy levels or pushed out of the atom while electrons of the outer shells immediately fill the vacancy and element specific radiation occurs (Reed, 1996). In fact, this radiation can be analysed by two distinctive methods: (a) an energy dispersive system (EDS) and (b) a wavelength dispersive system (WDS). The EDS is used to count the electron quanta and simultaneously records the associated energy in a relatively short amount of time. In principle, the detector measures "all" elements simultaneously, while comparing and matching the characteristic radiation or the element-specific peaks with standards to obtain the qualitative (and partly the quantitative) composition of the sample. Problems only occur due to electronically induced artifacts. On the other hand the WDS is characterised by a better resolution and better detection limits. An analyser crystal is placed between sample and detector to decompose the polychromatic X-ray radiation into its wavelengths after Bragg's law. Because of the fact that different detectors are used to detect the individual wavelength ranges, the time of measurements are increased significantly. By comparing and converting the intensities of the signal to concentration in reference to a standard, the quantitative composition of the sample can be obtained just as for EDS (Goldstein *et al.*, 1992; Reed, 1996).

Another feature of EMPA is the detection of two sorts of electrons in which the radiation can be separated: the secondary electrons (SE) and the back scattered electrons (BSE). This can be used as an imaging tool. In this case, the electron beam constantly scans a discrete area. The SE and especially BSE images can be used as an indicator for the chemical composition and / or for differences in the composition. Areas rich in elements with a higher atomic number scatter more electrons and are visualized brighter. (Goldstein *et al.*, 1992; Reed, 1996).

6.4. Image analysis

6.4.1. ImageJ and Adobe Photoshop

The textures and mineral assemblages of the samples provided by the petrological experiments represent a “snapshot” into prevailing crystallization regimes at certain experimental conditions. To analyze and compare the crystallinity and textural characteristics of those samples, images were taken in the BSE mode of the electron microprobe. In order to compare different samples to each other, pictures were taken with the same magnification (100x). Since the grains were bigger than the image section of the EMPA with that magnification several pictures per sample were taken and stuck together with *Adobe Photoshop*. That software was also used to prepare and edit the images prior to further analysis with *ImageJ*. This software is a free image analysis and processing application based on “Java”, provided by the U.S. National Institute of Health (<http://rsb.info.nih.gov/ij/index.html>; Abràmoff *et al.*, 2004). *ImageJ* offers different tools and applications that are frequently used in various sciences. In this thesis, it was used to automatically measure crystal number, area, and size (calculated as the major and minor axes of an equivalent ellipse) in each binary image of the experimental samples (e.g., Riker *et al.*, 2015).

In order to do so and detect the crystals, the BSE images were edited with *Adobe Photoshop*. The procedure follows Shea *et al.* (2010) who summarized helpful hints how to process images with that software for size analysis. Distinctive phases in the sample are relatively simple to select by their grey value and thresholding functions. However, especially the relevant plagioclase microlites do not differ significantly in their grey value from the surrounding glass matrix and no automatic thresholding process could be used. Nonetheless, plagioclase microlites are easily distinguishable from the glass matrix with the naked eye, so that each microlite had to be treated manually. Despite being very time consuming, the advantage of the manual selection is that no false grey values are incorporated into the analysis and that the shape of really awkward shaped crystals could be selected with great accuracy. To ensure appropriate treatment of edge-intersecting crystals, each image was processed twice following Riker *et al.* (2015): once including crystals in contact with the image boundary (for determination of the total crystal area), and once excluding these crystals (for complete crystal size distributions; Higgins, 2006b; Hammer, 2008). After completely selecting all crystals, a threshold image and afterwards a

binary image was created, so that only the crystals are displayed as black particles. This binary image is then uploaded to *ImageJ*. After setting the scale the image can be analyzed with the “Analyze Particles” application, which presents data regarding the area, length and width of a crystal determined via the “Fit Ellipse”. The area of vesicles and phenocrysts were determined in a separate analyzing step and subtracted from the image area (Hammer *et al.*, 1999).

6.4.2. CSD corrections

The application of CSD theory to natural (or experimentally produced) datasets requires conversion of areal (apparent) crystal dimensions to true three-dimensional crystal shapes. These conversions, as well as the data procession were executed using the software program *CSD Corrections*. That program is designed by Michael Higgins and based on his publications concerning textural analysis and crystal size distribution (CSD; e.g., Higgins 2000, 2002a, 2002b, 2006a, 2006b). It is now widely used in the geological community for the generation of crystal size distributions and readily presents crystal size distribution plots and histograms as well as distribution of crystal orientation. The application of CSD theory to natural datasets requires conversion of areal (apparent) crystal dimensions to true three-dimensional crystal shapes which were using this software. The program attempts to account for three sources of stereological error (e.g., Hammer *et al.*, 1999): (1) cut effects, which result from planar sectioning of crystals at different orientations; (2) intersection probability, which means that small crystals are less likely to be sectioned than larger ones; and (3) deviations arising from nonspherical crystal habit (Riker *et al.*, 2015). Key inputs for *CSD Corrections* are measured crystal sizes, L , here defined as the long axis of a best-fit ellipse, as output by *ImageJ*. Additional required inputs include crystal shape (the ratios of short to intermediate to long axes), sample fabric, and grain roundness. Therefore *.csd*-files with the required data from *ImageJ* analysis may be imported directly. *CSD Corrections* will recognize the image area [mm^2], pixel size [mm], number of analyzed crystals, as well as parameters of the “fit ellipse” with rough crystal shape dimensions. The user only has to control the inherited data and must enter a correcting value for the texture (foliation / lineation) and particle shape (roundness). Since there is no obvious foliation or lineation in the analysed samples this value was set = 0. The roundness value = 0.1 follows the example given by Brugger and Hammer (2010b). Shape factors were determined using the Excel database *CSDSlice* (Morgan & Jerram, 2006), which compares the distribution

of area-based crystal aspect ratios with those generated by random sectioning of known crystal shapes to determine the best-fit three-dimensional habit. Importantly, this assumes that a single shape factor applies to the entire crystal population.

The most delicate matter is to choose the size scale of the bins (i.e. logarithmic, linear, custom), which results in distinct changes regarding the shape of the CSD plots and histograms. In this study, a linear size scale was selected so that all bins share the same interval ($d = 0.005$ mm). *CSD Corrections* also provides the possibility to provide pseudo-3D data (Brugger & Hammer, 2010). Therefore a value for the 3D component has to be set = 1 representing the shortest axis of the crystal. In order to calculate 3D information, the length and width of the particle is corrected using the “interseccion - probability effect”, as well as the “cut - section effect” (Higgins, 2000). While the first one assumes that larger particles are more often affected by 2D sections, the latter of describes the possibility to cut a particle at its widest point in 2D. However, this is only an approximation and no real 3D information. Other methods like tomography or procedures involves collecting a series of optical photomicrographs at successive levels in a transparent thin section with a petrographic microscope and digital camera) have proven to be more effective for that (e.g., Castro *et al.*, 2003).

7. Results and Discussion petrological experiments

This chapter summarizes the results of the preliminary set of petrological HP/HT-experiments. Following the preparation steps presented in *chapter 6*, the first approach for these experiments was to synthesize and analyse samples with fixed temperature and pressures (equilibrium experiments) prior to the decompression experiments simulating the ascent of magma at fixed decompression rates. The subsequent sections present the phenomenological observations, as well as the textural analysis (CSD's) of the equilibrium and the decompression experiments respectively. A discussion of possible sources of error are also discussed, as well as a and a test of the model derived in chapter 4 on the here produced data. Finally, those results are put into context and possible further steps for future research are presented.

7.1. Equilibrium experiments

The set of equilibrium experiments consists of eight isothermal HP/HT-experiments with varying pressures (20 MPa to 200 MPa) at 900°C following the phase diagram initially developed by Cottrell *et al.* (1999; figure 36i, table 4). The duration of these experiments were set on an average of about 5 days so that each sample had enough time to become fully equilibrated in terms of its p-T-conditions. This dataset is thought to serve as reference analyses for the upcoming decompression experiments in order to estimate growth and nucleation rates.

Due to the initial setup of the experimental dataset, the individual experiments represent different stages in the phase diagram of the given melt composition of the Santorini pumice. While sample SP1 at 200 MPa is above the liquidus temperature and therefore contains only oxides and no further minerals, decreasing pressures in the samples SP2 to SP8 put the given experiment below the liquidus temperature introducing clinopyroxene, orthopyroxene and plagioclase minerals respectively (figure 36). However, this set of equilibrium experiments reproduced the phase diagram of Cottrell *et al.* (1999) adequately good to serve as a reference for further experiments. In addition to that, decreasing pressures also increases the crystal content of the given samples (from $\sim 0.3\% \pm 1\%$ up to $\sim 5\% \pm 1\%$; table 4). Most crystals have a euhedral shape reflecting the

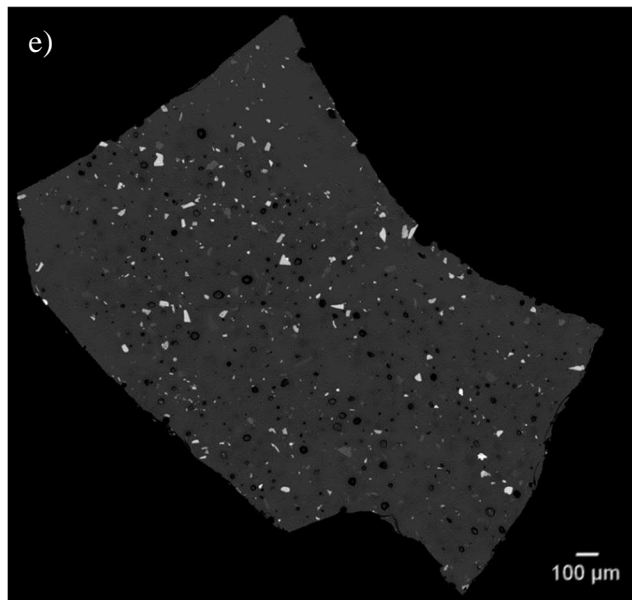
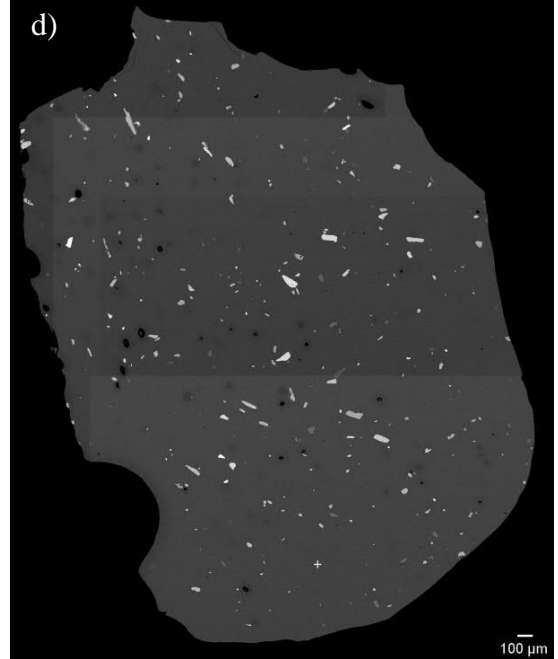
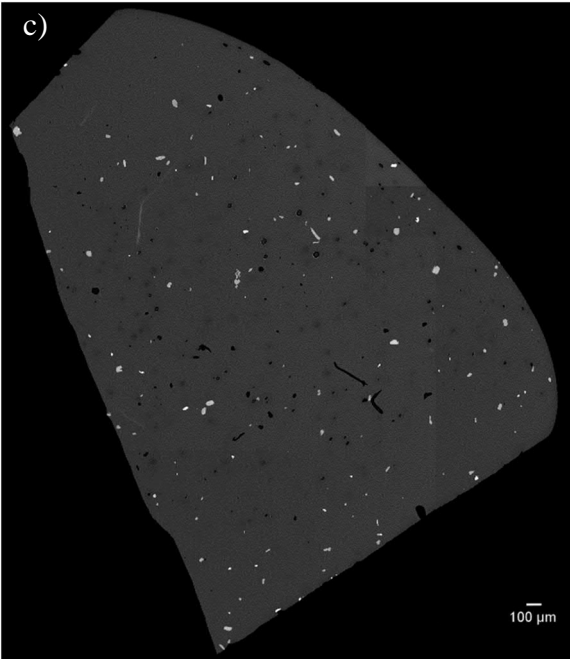
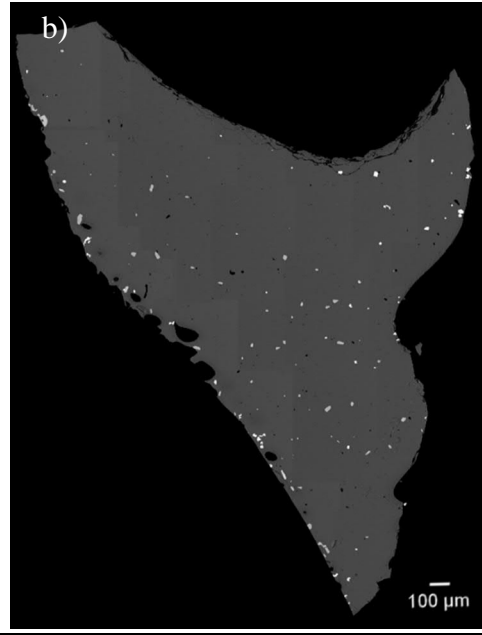
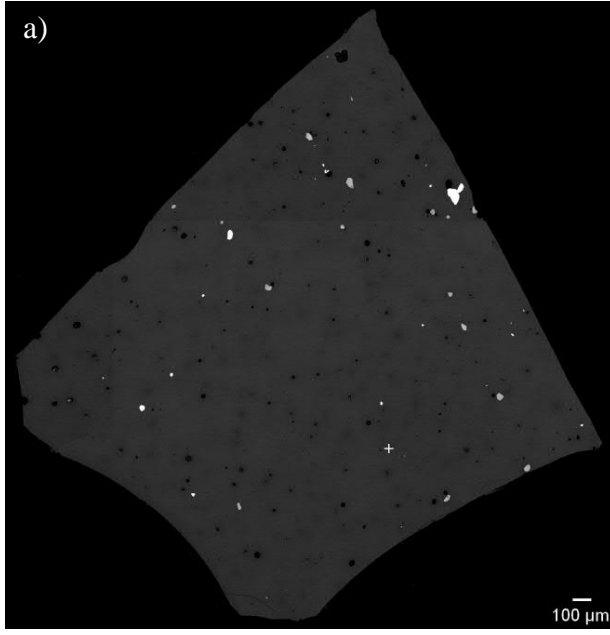
Exp	temp [°C]	pressure (init) [MPa]	duration [h]	decomp. rate		pressure final [MPa]	ϕ [%]	mean aspect ratio	ϕ_m eq. 4.4	polydispersity γ	relative viscosity
				[MPa/h]	[m/s]						
SP1	900	200	54.25	-	-	-	0.317	1.6028	0.7036	0.2661	1.0091
SP6	900	175	122.5	-	-	-	0.670	1.7636	0.6748	0.4259	1.0202
SP2	900	150	163	-	-	-	0.550	1.8961	0.6652	0.4763	1.0168
SP3	900	125	140.5	-	-	-	1.524	1.9676	0.6992	0.2485	1.0451
SP7	900	100	120	-	-	-	2.112	1.7521	0.6951	0.2949	1.0637
SP4	900	75	142	-	-	-	4.283	1.8214	0.6859	0.3397	1.1377
SP5	900	50	118	-	-	-	4.270	1.6874	0.6997	0.2775	1.1342
SP8	900	20		-	-	-					
DC14	900	175	26	3	0.03	30	3.694	2.0679	0.6749	0.3721	1.1192
DC11	900	175	48	0.5	0.005	30	10.733	2.4690	0.6633	0.3812	1.4233
DC1	900	150	112	15	0.17	20	1.686	1.9128	0.6888	0.3097	1.0508
DC2	900	150	121.5	7.5	0.075	20	1.796	2.2619	0.6822	0.2993	1.0548
DC8	900	150	119	3	0.03	20	6.630	3.2873	0.6628	0.2729	1.2347
DC3	900	150	144	0.5	0.005	20	25.191	4.1710	0.6382	0.2968	2.7294
DC4	900	125	116.5	15	0.17	20	1.991	2.2728	0.6696	0.3731	1.0622
DC5	900	125	121.75	7.5	0.075	20	1.949	1.9372	0.6795	0.3635	1.0599
DC6	900	125	118.25	3	0.03	20	16.897	2.6555	0.6734	0.2946	1.7821
DC7	900	125	119.75	0.5	0.005	20	22.458	2.7585	0.6520	0.4072	2.3270
DC12	900	100	50	3	0.03	20	24.968	2.0186	0.6668	0.4384	2.5553
DC13	900	100	126	0.5	0.005	20	35.248	2.0541	0.6723	0.3922	4.4190

Table 4: Results of petrological experiments - equilibrium and decompression experiments

equilibrium conditions of the system, while some crystals (mainly pyroxenes) show features of growth margins. Especially occurring in the runs at lower pressures, this phenomenon might be due to the fact that the initial conditions of the experimental run were in the range of temperatures and pressure where the minerals are yet stable and could not be molten again during the experiment. Consequently, the existing crystal acted as a nucleation point at which the crystallization of the crystals could start (again) to grow. This might be even more interesting for the upcoming decompression experiments where an increased number of nuclei influences the nucleation rate of crystals in the melt quite drastically.

The crystal size distributions of the individual equilibrium experiments have been calculated following the procedure discussed in section 6.4. The area of vesicles in each sample was subtracted from the total measured area in order to get accurate values of mineral CSDs in the magma before vesiculation (dense rock equivalent). The resulting CSD data were plotted on a diagram of \ln (population density) versus size (L =longest dimension) shown in figure 37. All equilibrium experiments produce non-linear CSDs with concave-upward and/or slightly kinked forms.

Since the CSDs determined here are only slightly curved on a classical CSD diagram (S -type distribution of Higgins, 2006b), similar to Higgins and Roberge (2007) meaningful values for the slope and intercept of the CSD could be determined by linear regression using the methods of Higgins (2006b). The characteristic length (LD) of each CSD was calculated as $-1/\text{slope}$. This parameter has the dimension of length and is equal to the mean crystal length for a straight CSD that extends to all crystal sizes (Marsh, 1988). The exact values can be found in die appendix.



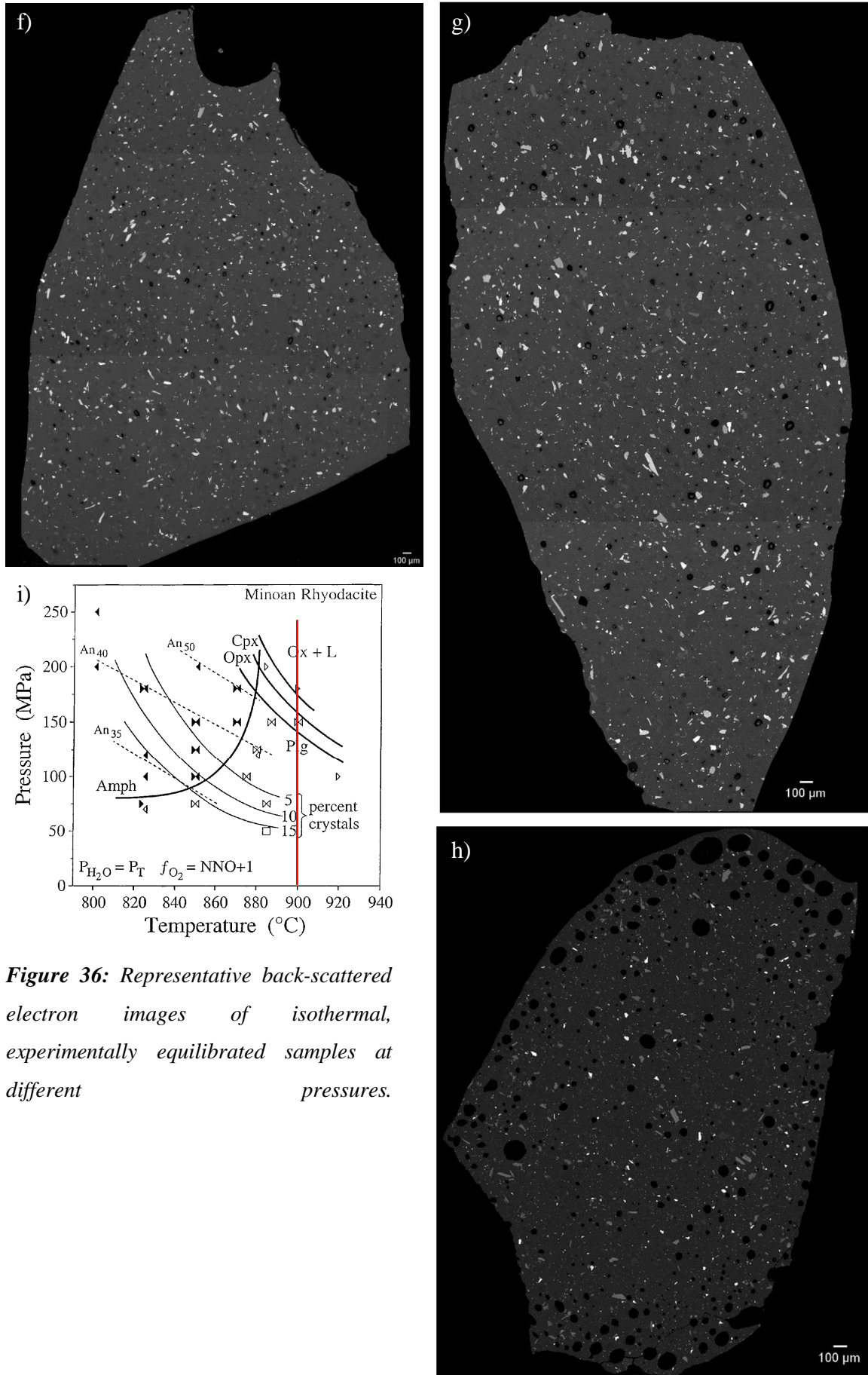


Figure 36: Representative back-scattered electron images of isothermal, experimentally equilibrated samples at different pressures.

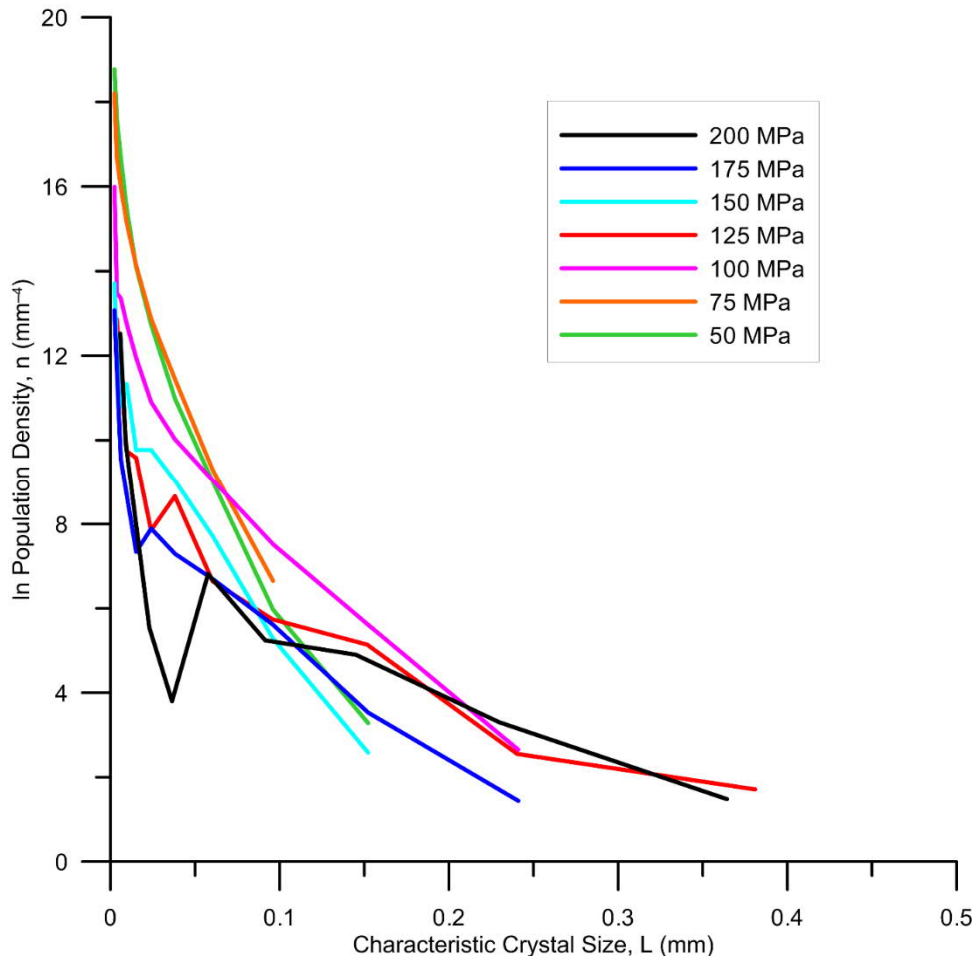


Figure 37: Crystal size distributions of experimentally equilibrated samples

7.2. Decompression experiments

The set of decompression experiments consists of 12 isothermal HP/HT- experiments with four varying decompression rates (15 MPa/h, 7.5 MPa/h, 3 MPa/h and 0.5 MPa/h) starting from four individual initial pressures P_{init} (175 MPa, 150 MPa, 125 MPa and 100 MPa) at 900°C (figures 38-41, table 3). A decompression rate of 15 MPa/h corresponds to a relatively fast ascent rate of about $0,17\text{ms}^{-1}$ and is related to a low-intensity explosive activity (Rutherford & Gardner, 2000; Rutherford, 2008), while a decompression rate of 5 MPa/h corresponds to a relatively slow ascent rate of about 0.005m s^{-1} . The following sections are structured following the individual initial pressures.

7.2.1. Initial pressure 175 MPa

Following the phase diagram for rhyodacitic pumice of the Minoan eruption derived by Cottrell *et al.* (1999), the initial pressures of 175 MPa at 900°C represent a regime right above the liquidus temperature. After a given annealing time, the two experiments were decompressed at decompression rates of 3 MPa/h (DC14) and 0.5 MPa/h (DC11) to a final pressure of 30 MPa (Figure 38). Compared to the equilibrium experiment at 175 MPa, the crystal content on the decompressed samples is much higher ($\sim 3.7\% \pm 0.5\%$ for DC 14 and $\sim 10.8\% \pm 0.5\%$ for DC11). Clinopyroxene and orthopyroxene with a euhedral shape and to a much smaller extent oxides, as well as elongated, skeletal shaped plagioclase crystals represent the mineral phases. Since some of the pyroxenes show features of growth margins, it can be assumed that not all crystals were newly formed during decompression but were not molten during annealing prior to the decompression and served as nuclei. In addition, both decompression experiments produce non-linear CSDs with concave-upward and/or kinked forms (Figure 42a).

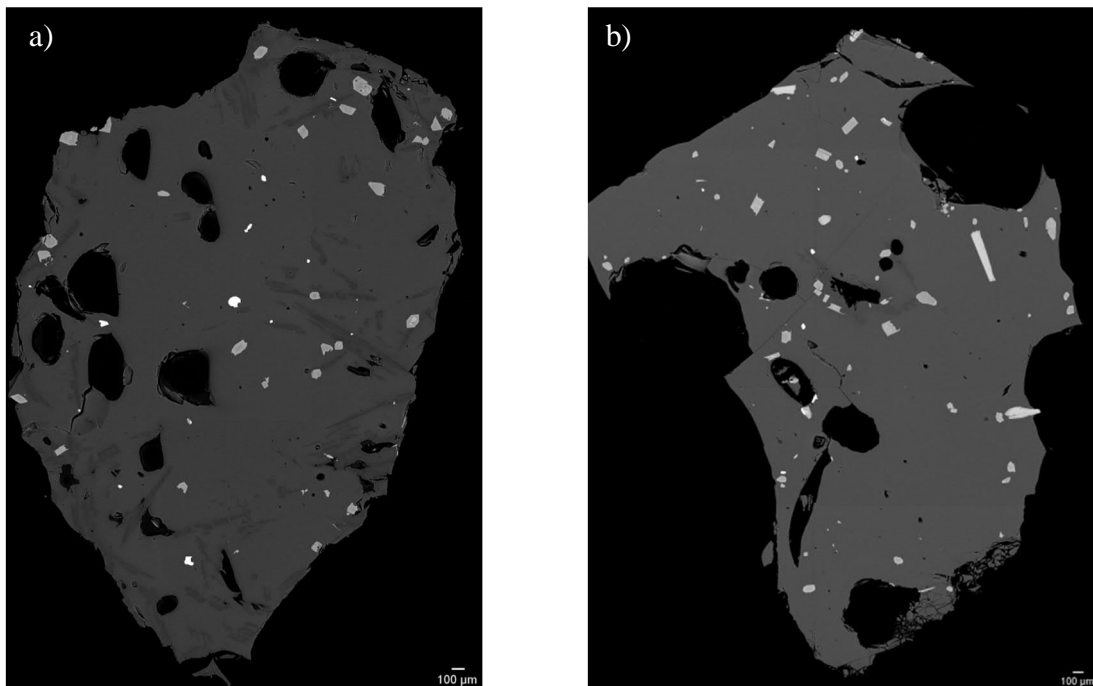


Figure 38: Representative back-scattered electron images of isothermal, experimentally decompressed samples - initial pressure 125MPa.

7.2.2. Initial pressure 150 MPa

Starting from an initial pressure of 150 MPa at 900°C, the experiments represent a regime where clinopyroxene and orthopyroxene are yet stable. After a given annealing time, the four experiments were decompressed at decompression rates of 15 MPa/h (DC1), 7.5 MPa/h (DC2), 3 MPa/h (DC8) and 0.5 MPa/h (DC3) to a final pressure of 20 MPa (Figure 39). Decreasing the decompression rate, increases the crystal content of each sample respectively ($\sim 1.7\% \pm 0.5\%$ for DC1, $\sim 1.8\% \pm 0.5\%$ for DC2, $\sim 6.6\% \pm 0.5\%$ for DC8 and $\sim 25.2\% \pm 0.5\%$ for DC3). While most clinopyroxene and orthopyroxene crystals have a euhedral shape, the experimental runs with the smallest decompression rates feature elongated and skeletal shaped plagioclase crystals. This phenomenon is even more pronounced than in the samples with an initial pressure of 175 MPa. Again, some of the pyroxenes show features of growth margins. The experiments with higher decompression rates (DC1 and DC2) produce slightly more linear CSD's, whereas the slower rates (DC8 and DC3) produce more concave-upward and/or kinked formed CSD's (Figure 42b). The abundance of the most elongated plagioclase crystals in sample DC3 is also illustrated and results in the most concave-upward formed CSD.

7.2.3. Initial pressure 125 MPa

Starting from an initial pressure of 125 MPa at 900°C, the experiments represent a regime where not only clinopyroxene and orthopyroxene are yet stable, but also plagioclase becomes a stable phase to crystallize. Similar to the set of experiments before, the four experiments were decompressed at decompression rates of 15 MPa/h (DC4), 7.5 MPa/h (DC5), 3 MPa/h (DC6) and 0.5 MPa/h (DC7) to a final pressure of 20 MPa after a given time of annealing (Figure 40). The crystal content of each sample increases with decreasing the decompression rate, respectively ($\sim 2\% \pm 0.5\%$ for DC4, $\sim 2\% \pm 0.5\%$ for DC5, $\sim 16.9\% \pm 0.5\%$ for DC6 and $\sim 22.5\% \pm 0.5\%$ for DC7). Most clinopyroxene and orthopyroxene crystals are characterized by a euhedral shape and show features of growth margins. Plagioclase minerals of this set of experiments show those rims as well, while the relatively high amount of elongated and skeletal shaped crystals as in the decompressed samples with an initial pressure of 150 MPa, however, is only represented in sample

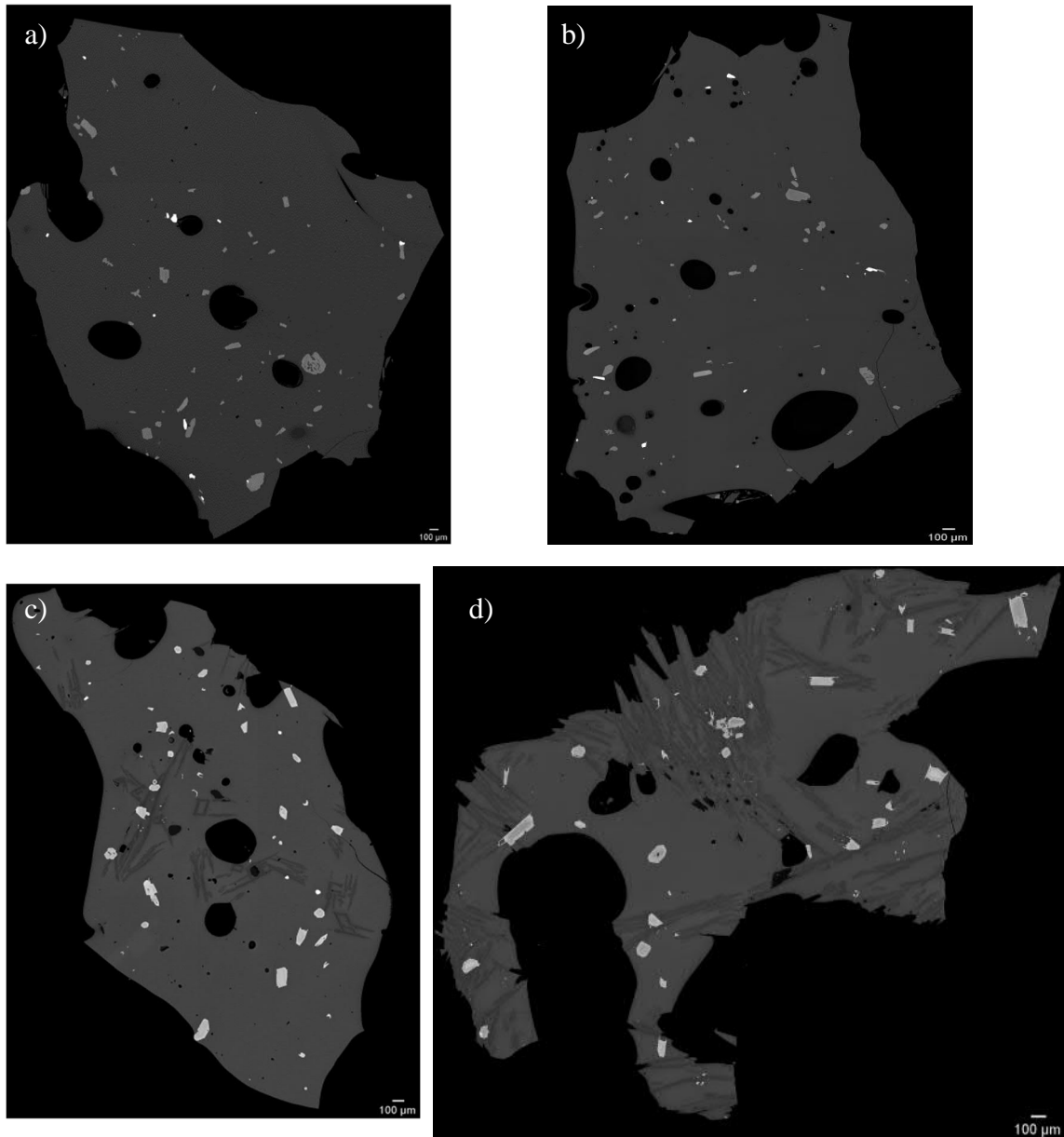


Figure 39: Representative back-scattered electron images of isothermal, experimentally decompressed samples - initial pressure 150MPa.

DC6. The CSD's of this set of experiments are similar to the ones of the previous set. The experiments with higher decompression rates (DC4 and DC5) produce slightly more linear CSD's, whereas the slower rates (DC6 and DC7) produce more concave-upward and/or kinked formed CSD's (Figure 42c). Again, the abundance of the most elongated plagioclase crystals in sample DC6 is also illustrated and results in the most concave-upward formed CSD.

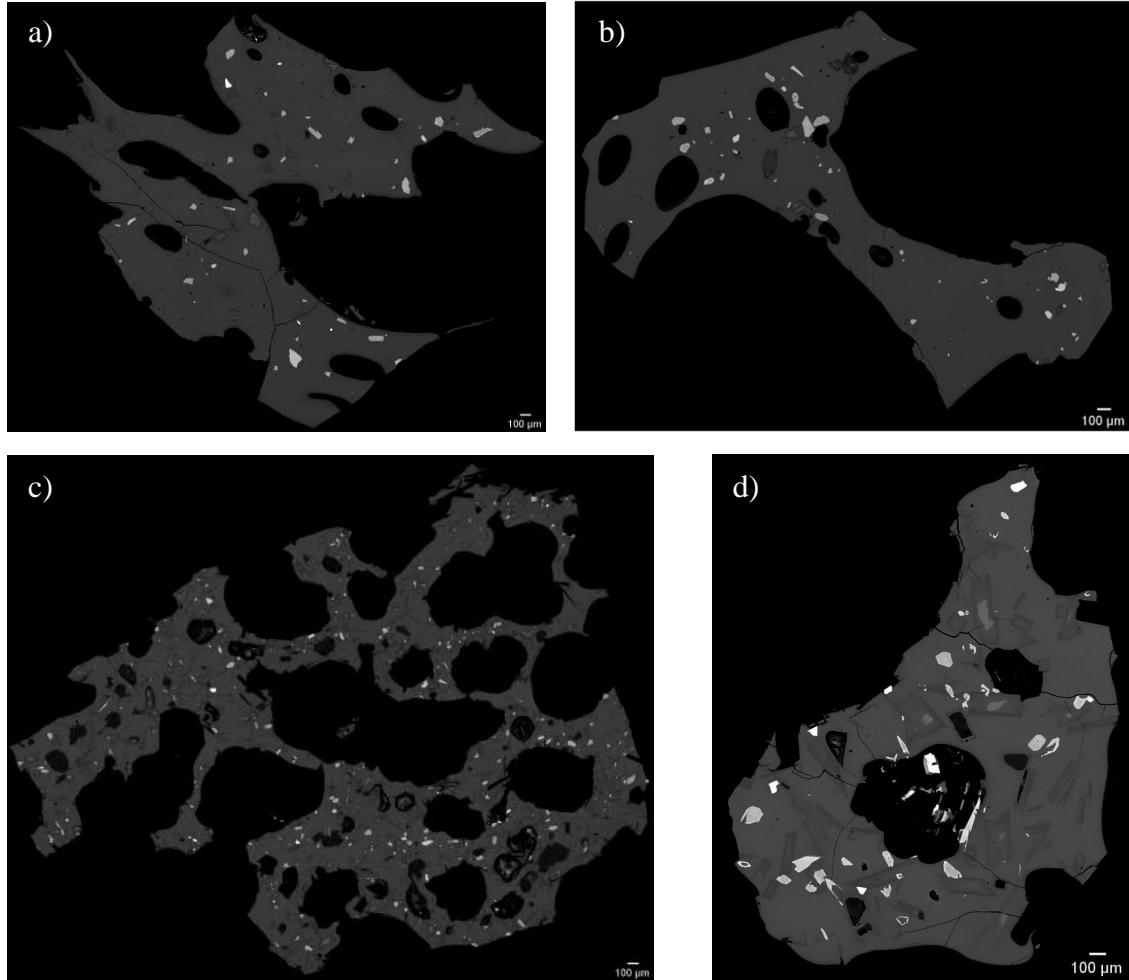


Figure 40: Representative back-scattered electron images of isothermal, experimentally decompressed samples - initial pressure 125MPa.

7.2.4. Initial pressure 100 MPa

The set of experiments starting from an initial pressure of 100 MPa at 900°C, represent a regime where clinopyroxene, orthopyroxene and plagioclase are stable and have crystallized to certain amount of up $\sim 2\text{vol.}\%$ in the melt. After a given time of equilibration, the two experiments were decompressed at decompression rates of 3 MPa/h (DC12) and 0.5 MPa/h (DC13 - Figure 41). Following the same pattern as the other samples, a decrease of the decompression rate, increases the crystal content of each sample respectively ($\sim 25\% \pm 0.5\%$ for DC12 and $\sim 35.2\% \pm 0.5\%$ for DC13). The pyroxenes have a euhedral shapes and show features of growth margins, as well as the plagioclase crystals.

Those crystals, however, are far less elongated and skeletonized than plagioclase from the other experimental sets. In addition, both decompression experiments produce slightly non-linear CSDs with concave-upward and/or kinked forms (Figure 42d).

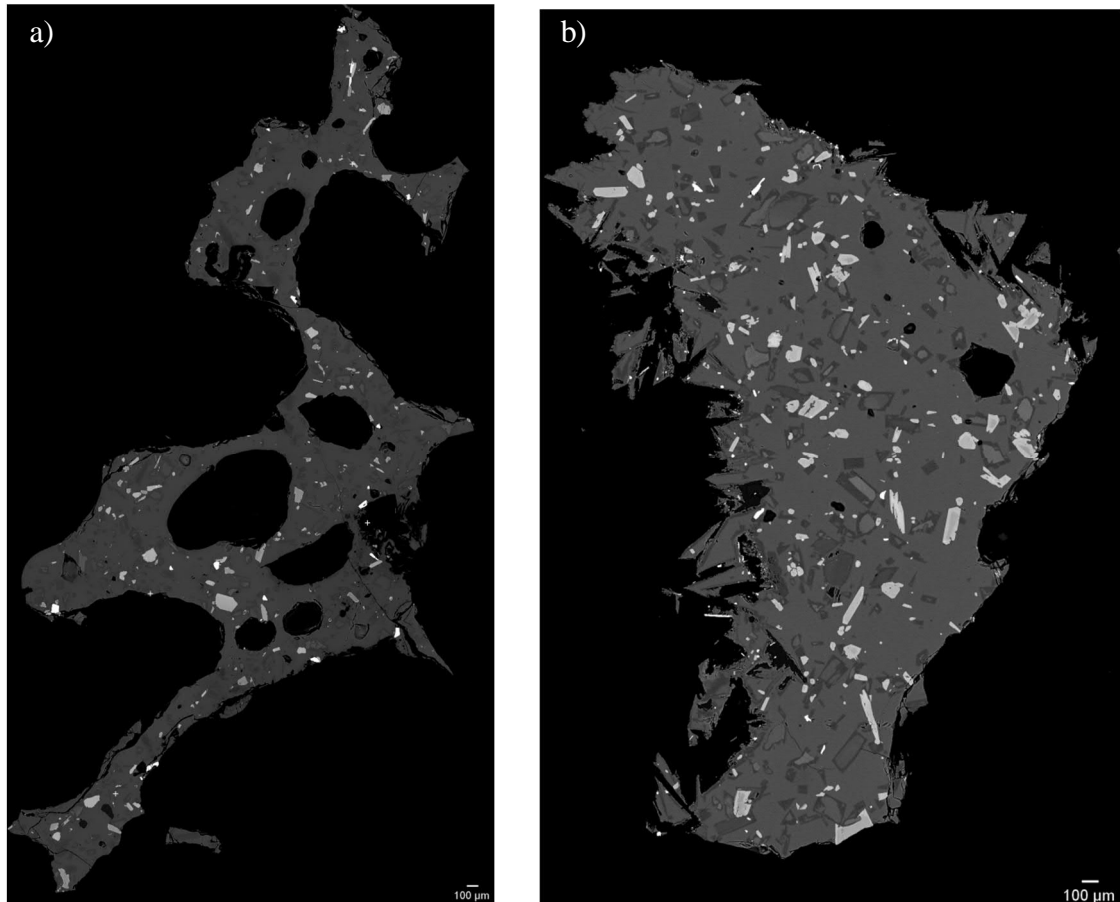


Figure 41: Representative back-scattered electron images of isothermal, experimentally decompressed samples - initial pressure 100 MPa.

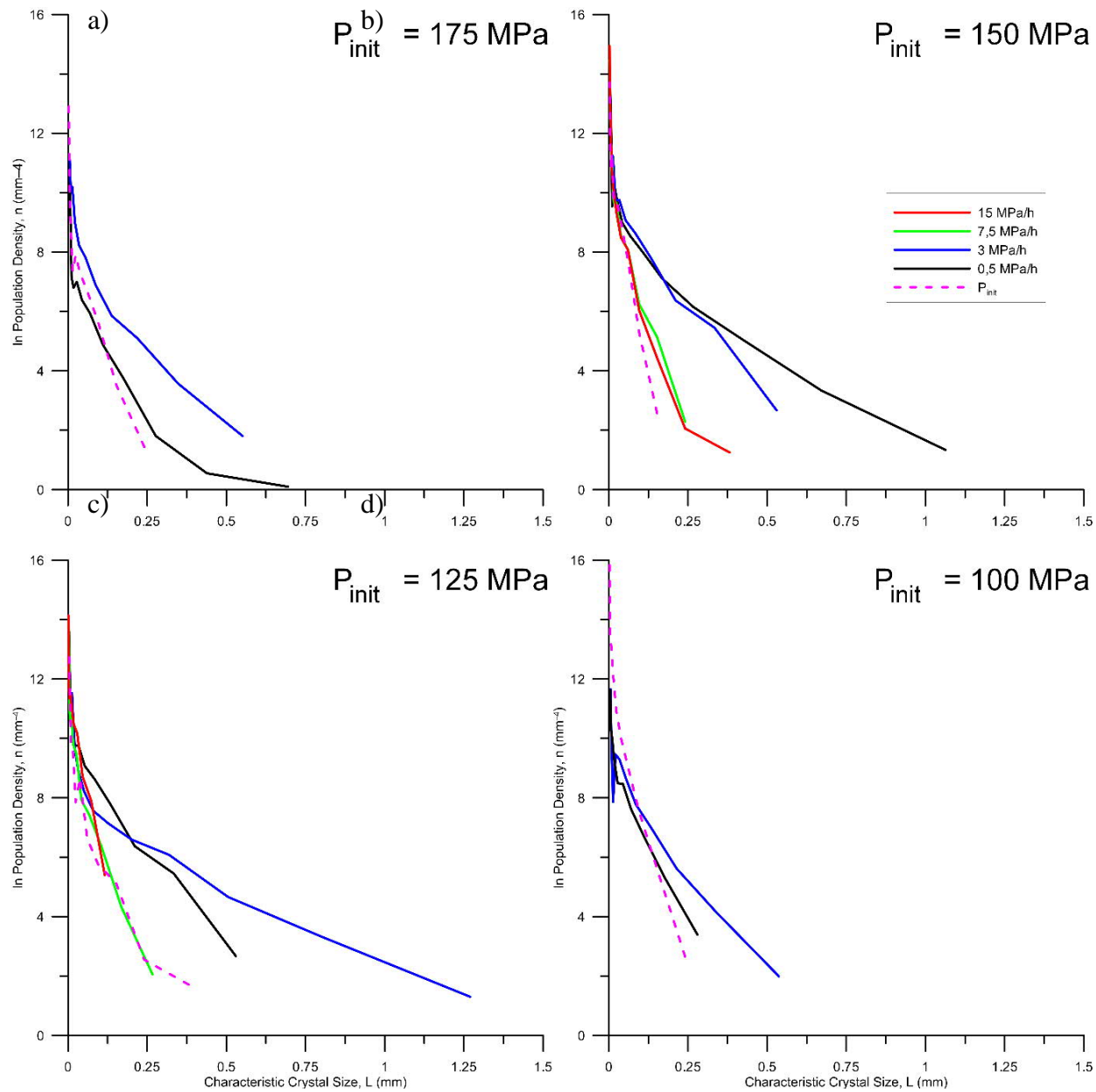


Figure 42: Crystal size distributions of experimentally decompressed samples

7.3 General remarks

As widely discussed before, crystallization in magmatic rocks occurs in response to a change in temperature and/or a change in melt composition. The crystallization trigger investigated in this thesis, however, is restricted to devolatilization-driven crystallization. Due to bubble growth during magma ascent sequestering exsolved H₂O from the silicate melt phase, the chemical undercooling “felt” by the silicate melt phase increases, and consequently, provided there is enough time for crystals to nucleate and grow, mineral phases precipitate in the melt. In general, the larger the degree of undercooling, the more the melt is inclined to respond by growing crystals. As a result, crystallinity, size, and number density will increase with time and position in the volcanic conduit, which is shown by the equilibrium experiments of this thesis (section 7.1) Apart from the two experiments with the highest pressures, the CSD’s of the experiments are fairly linear and represent the equilibrium conditions of the given experiments.

The experimental strategy to grow crystals in natural silicate melts under different yet controlled amounts of undercooling driven by decompression under water-saturated conditions is shown by the results in section 7.2. As for these decompression experiments, it can be seen that all decompression experiments produce non-linear CSDs with concave-upward and/or kinked forms (Figure 43) that might be attributed to the combined effect of crystals formed during equilibration and nucleated during decompression. The curvature, however, changes with decompression rate, path, and fluid composition. A noticeable overturn in population density is observed in the smallest sizes, whereas the largest size class (or classes) of some samples exhibits a slight downturn. As discussed by Riker *et al.* (2015) the latter may be an artifact of the imaging process, reflecting magnification scales too high to capture statistically meaningful numbers of the largest crystals; it may also record a lack of late nucleation. Overturns at small size classes have been variously attributed to ripening (e.g. Higgins & Roberge, 2003; Pupier *et al.*, 2008), under-compensation for intersection probability (e.g. Brugger & Hammer, 2010b), or insufficient resolution (e.g. Cashman & Ferry, 1988; Hammer *et al.*, 1999), although image resolution of this thesis is more than adequate to capture crystals >1 μm in length.

The curvature of the CSD, however, has been ascribed to a variety of natural processes in volcanological literature: e.g. magma mixing, crystal accumulation, textural

coarsening, two-stage crystallization, or accelerating nucleation and growth (Marsh, 1988; Armienti *et al.*, 1994; Higgins, 1998; Bindeman, 2003; Higgins & Roberge, 2003; Shea *et al.*, 2010), or to artifacts produced by the 2D–3D conversion because of variations in crystal shape (Castro *et al.*, 2004). Following Brugger & Hammer (2010b), the curvature of experimentally derived CSD's might be interpreted based on the known experimental histories of these samples, which include two separate crystal populations (those formed during the initial anneal period and those formed during decompression) with distinct nucleation regimes. As shown by Riker *et al.* (2015) the strength of this curvature, and the crystal size, L , at its inflection point, vary with changing decompression conditions and probably reflect the shifting contributions of nucleation and growth to the evolution of each population.

Similar to other studies, the most important crystallization process during the experiments is the crystallization of plagioclase. The crystal size distributions show that crystallization is dominated by either nucleation (slow decompression) or growth (fast decompression) depending on the decompression rate. Brugger & Hammer (2010a) showed the dependence of the growth rate on decompression, while it has long been recognized that plagioclase growth rates vary as a function of cooling rate (Walker *et al.*, 1978; Cashman, 1993; Leshner *et al.*, 1999; Conte *et al.*, 2006). Hammer & Rutherford (2002) investigated the different crystallization regimes of plagioclases and the dependence on the degree of undercooling was determined.

If, however, ascent rate varies during decompression, which is extremely likely for natural magmas undergoing closed-system degassing, then growth rates may likewise vary by several orders of magnitude during ascent (Hammer & Rutherford, 2002; Couch *et al.*, 2003b). Following Brugger & Hammer (2010), the microlith number density and the crystal morphology of the microliths are mentioned as the best indicators for the ascent rate in natural systems, although an average ascent rate might not be a sufficient description. The variation has important implications for calculations of magmatic timescales that utilize crystal growth rates (Brugger & Hammer, 2010). Just as magma ascent rates vary widely across volcanic systems, ascent styles probably span a wide range from purely continuous to entirely pulsatory (Hammer & Rutherford, 2002). In addition, the style of magma ascent almost certainly varies between various magmatic systems and perhaps temporally within any given system. Thus, consideration of ascent style in addition to rate

will undoubtedly strengthen the interpretive power of experimental studies for constraining natural magma ascent processes (Brugger & Hammer, 2010). Similar to Riker *et al.* (2015), the experiments suggest that, at a wide range of experimental conditions, growth on pre-existing crystals represents a significant proportion of the additional crystallization owing to decompression (25–50%).

A distinctive feature of the slowly decompressed samples is the shape of the grown plagioclase crystals. As can be seen in figure 43, the crystals show features of swallowtail and/or skeletal shape. Following Vernon & Clarke (2008) skeletal is a term used to describe the habit of euhedral to subhedral crystals in igneous rocks containing crystallographically orientated hollows and gaps, while the voids within the crystals are filled with groundmass material. Skeletal morphologies are relatively common in olivine and plagioclase crystals in volcanic rocks and thought to form under large super-cooling and indicate disequilibrium (Gornitz, 1981). Because of such a melt disequilibrium, crystals form by a diffusion controlled growth process, where atoms are added more rapidly to the edges and corners of a growing crystal than to the centers of crystal faces, resulting in either branched, tree-like forms or hollow, stepped depressions (Vernon & Clarke, 2008).

These disequilibrium features become increasingly abundant with increasing decompression rate. A trend, which is consistent with previous studies that map morphological changes with increasing effective undercooling: from compact euhedral, to tabular, then swallowtail and hopper (Lofgren, 1974; Corrigan, 1982; Hammer & Rutherford, 2002). As shown by Hammer & Brugger (2010) faster decompression produces high microlite number densities that record late-stage high instantaneous effective undercooling, whereas the euhedral morphologies of growth-dominated crystallization reflect smaller instantaneous undercooling throughout slow decompression. This trend, however, is not as clearly shown in my experiments as in those studies. , the fact that those “chains” of skeletal plagioclase crystals affect the shape of the CSD enormously

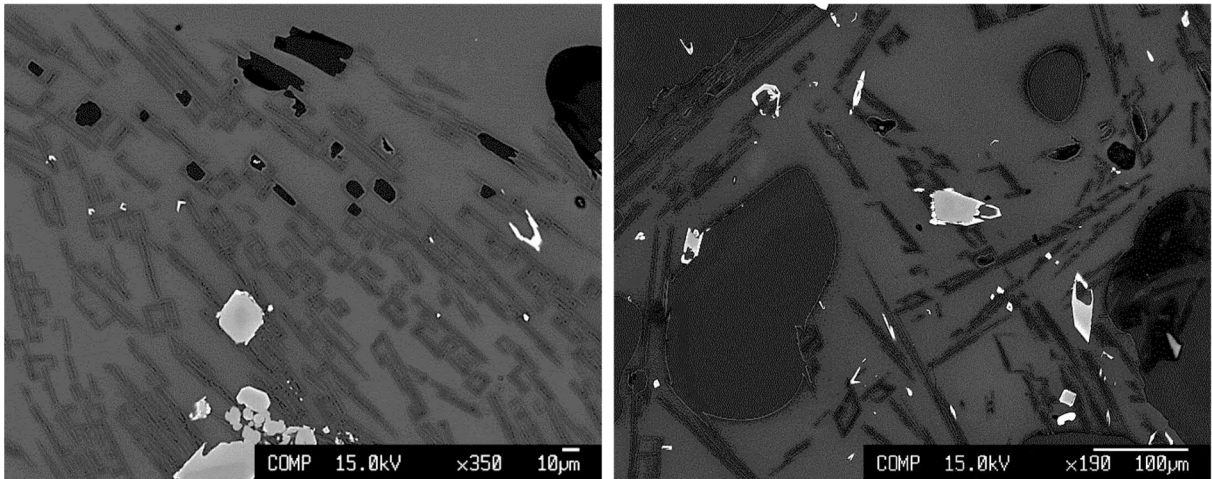


Figure 43: Representative back-scattered electron images of skeletal shaped and elongated plagioclase crystals in sample DC3.

The application of the previously derived model on the artificial CSD's of these experiments is illustrated in figure 44. By analyzing the 2D binary BSE images of the respective experimental samples, it is possible to gather textural data of those rocks in order to estimate the variables needed for the use of equation (4.6) and the calculation of relative viscosity $\eta_{r,*}$ (Table 4).

The present example (Figure 44) illustrates that both the equilibrium and the decompression samples are characterized by relatively high polydispersity values γ ($0.2 < \gamma < 0.5$). In addition to a relatively low crystallinity for the equilibrium samples, that results in relatively low relative viscosity values $\eta_{r,*}$ (< 1.3). By contrast, due to the higher crystallinity of the decompressed samples relative viscosity values $\eta_{r,*}$ are considerable higher.

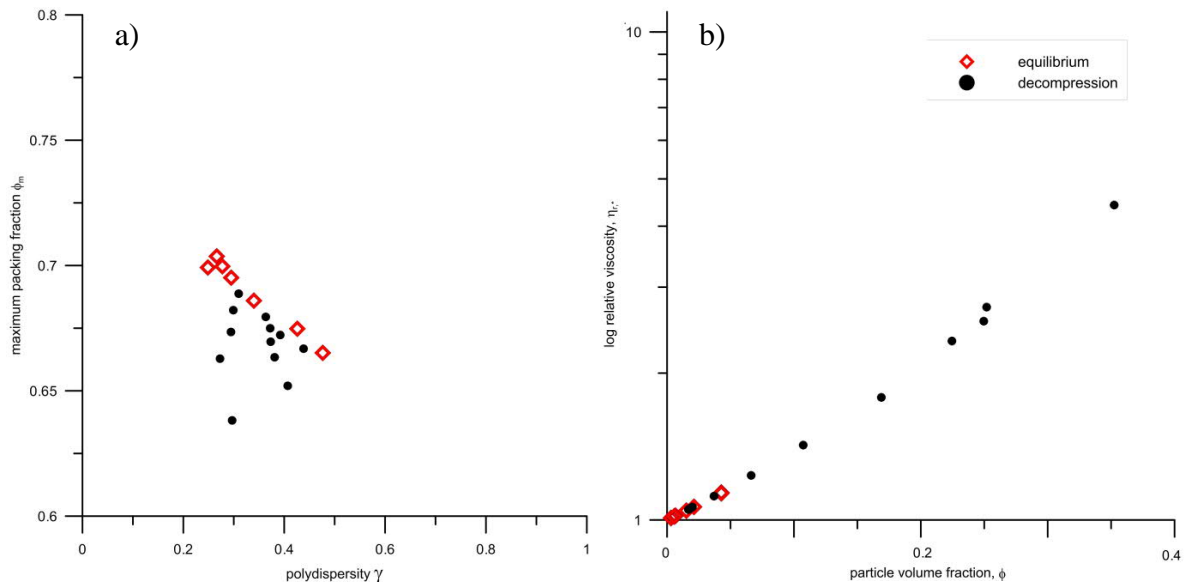


Figure 44: Application of the aforementioned model derived in this thesis (chapter 4) on the samples of the HP/HT-experiments.

7.4. Sources of error and routes for future work

As this second part of this thesis is mostly based upon decompression experiments and textural characterization with the help of CSD's, a variety of errors may be introduced along the way. The first source of a possible error is the pumice used as the basis of the petrological experiments. Although carefully crushed, the powder might have been inhomogeneous in terms of crystal fragments that served as nuclei for further crystallization in the decompression experiments. A statistically inhomogeneity in the powder therefore might result in textural differences.

Compared to natural processes a limitation of the experiments performed for this thesis is the static course of the decompression experiments. In nature, ascending magma is subject to physical phenomena like sudden pressurization and decompression, as well as local shear stress and flow gradients that might have a significant impact on the rheology and the crystallization behavior of magma. Thus, processes in nature respond to various and changing parameters and are more complex than any processes modeled in the lab.

The experiments of this thesis were performed with stable, isothermal conditions and with constant decompression rates. This, however, is only an approximation since varying degrees of decompression rates (ΔP), as well as stepwise or at least no constant decompression steps (Δt) might occur in natural systems, as well as a possible cooling of magma.

Compared to natural magma, the image analysis in this experimental effort neglects the vesicles in the samples. The area of vesicles was subtracted from the total measured area in order to get accurate values of mineral CSDs in the sample batch (dense rock equivalent). The reason for this limitation was due to combined effects of a bubble-size distribution and its interconnections with CSD's are barely studied. However, the amount of vesicles in the melt is an essential part governing the processes and behavior of the magma during its ascent and need to be taken into account.

Another important source of errors corresponds with the processing of the images prior to the textural analysis. Mounting and preparing a distinct chunk of the resulting experimental product affects the representativeness of the analyzed sample. Depending on the 2D cut through the sample it is not guaranteed that the section fully represents the sample and that large amounts of crystals in the sample are not even taken into account because they are not affected by the analyzed sample surface. In addition, the resolution of the individual images might be a relevant source of errors. A poor image resolution can lead to exclusion of small crystal sizes. Nevertheless, poor resolution can be ruled out as an error source, since the resolution of BSE images acquired with the electron microprobe is very good and the contrast between the crystals and glass matrix is strong enough for analysis.

However, detecting the individual crystals is a crucial point in processing the images. Distinctive phases in the sample are relatively simple to select by their grey value and thresholding functions. However, especially the relevant plagioclase microlites do not differ significantly in their grey value from the surrounding glass matrix and no automatic thresholding process could be used. Each microlite had to be treated manually and some grain boundaries were not pronounced enough to easily detect two minerals as one grain. Despite being very time consuming, the advantage of the manual selection is that no false

grey values are incorporated into the analysis and that the shape of awkward shaped crystals could be selected with great accuracy.

By using *CSD Corrections*, one crucial parameter is the bin size interval as it strongly affects the regression slope. Larger bin size intervals for instance can cause shallower slopes, because small variations are averaged. However, the regression slope is subsequently used to estimate the microlite growth duration, so that variations in the slope will result in differences in this value. The bin size interval was hence chosen small enough and consistently ($d=0.005$) for all analyzed samples to ensure comparability without neglecting relevant information. As mentioned before, the mere nature of the image analysis in 2D used in this thesis is also an important source of error. Following Higgins & Roberge (2007), the maximum 3D crystal size is an important characteristic of the CSD, but cannot be determined from two-dimensional data. Converting 2D information from a thin section into 3D information for instance using the “interseccion - probability effect”, or the “cut - section effect” (Higgins, 2000) is only an approximation and no real 3D data. Also the approximation by determining 3D-shape factors using the Excel database CSDSlice (v.5; Morgan & Jerram, 2006) is only a best-fit method, which gives only a slight impression of 3D information. In order to get real 3D data methods like tomography or procedures collecting a series of optical photomicrographs at successive levels in a transparent thin section with a petrographic microscope and digital camera) have proven to be more effective (e.g., Castro *et al.*, 2003).

In addition to the variety of possible errors that might have affected the analysis of the HP/HT-experiments along the way, the results of the experimental effort of this study have only preliminary characteristics. Due to the mere nature of this project's structure, the results presented in this study are only the first steps in the effort of mapping the textural evolution of magma in a volcanic conduit and relate its CSD to the rheology of the magma. In order to develop rheological conduit profiles and to set up a statistically sound database of the effects of magma rise speed and total decompression on the ensuing textural and chemical signatures in the eruptive materials, the simulation of a range of magma rise scenarios needs to be extended. In terms of different initial conditions, it would be particularly interesting to simulate a variety of different initial pressures, various decompression rates and different decompression intervals, as well as the extension of

these experiments to other initial magma compositions and the implementation of the volatile phase into the model.

Then again, another obvious route for future work is a more thorough comparison and combination of the results of the HP/HT-experiments with the findings of the analogue experiments. While in this thesis, the textural analysis of the experimental results were applied to the aforementioned model derived in this study, it would be particularly interesting to apply analogue experiments to model the crystallization history of natural magma based on the petrological CSD data obtained by HP/HT-experiments or by the analysis of natural rocks. Preparing analogue samples with a blend of artificial particles of comparable particle size and shape distributions, each set of experimental pressure and temperature conditions corresponds to a certain conduit depth or decompression history. Therefore, it would be possible to emulate the evolution of crystallinity of a magma during its ascent in analogue experiments, and quantify the concurrent evolution of natural magma rheology. Based on these experiments it would not only be possible to cross-reference both the findings of the experimental set-up, as well as of the analogue approach, but also to create more artificially created CSD's. Since literature lacks of those studies, there is a general need of more (artificially) CSD's in order to study its implications on volcanology and petrology.

8. Conclusions and Future work

In this work I have used both analogue experiments on particle-bearing silicone oil, as well as HP/HT-experiments on natural samples of Santorini pumice to investigate and simulate how crystal-size distributions influence the rheological behaviour of a crystal-bearing melt. In the course of this study I could show, that the maximum packing fraction ϕ_m of particles is not only an important parameter portraying the particle microstructure of a suspension, but that it is also seemingly the only parameter controlling the rheological behaviour of that suspension. Combining information about particle size and shape with all relevant statistical characteristics of the distribution, ϕ_m is mainly controlled by the polydispersity of the particles, as well as particle size, variance, skewness of the distribution.

Adopting the definition of polydispersity γ following Wadsworth *et al.* (2017, eq. 2.31), it was possible to fit the experimental data results to following equation:

$$\phi_m = 1 - \left((1 - \phi_{m,0}) \gamma^a \right) \quad (\text{eq. 4.4})$$

Combining this (semi-)empirical model with the ones given by Mader *et al.* (2013) and Maron and Pierce (1956) it is now possible to quantify and to make direct estimates of the relative viscosity of a given natural crystal-bearing melt on the basis of textural analysis readily obtained through image analysis with well-established techniques and software of rock samples:

$$\eta_{r,*} = \left(1 - \phi \left[1 - \left(\left(1 - \left\{ \phi_{m1} \exp \left[-\frac{(\log_{10} r_p)^2}{2 b^2} \right] \right\} \right) \gamma^a \right) \right]^{-1} \right)^{-2} \quad (\text{eq. 4.6})$$

As the main result of this thesis, this expression takes into full account the volume fraction or crystallinity ϕ , the mean aspect ratio r_p of the crystals, and the polydispersity γ , when predicting the relative viscosity of a particle-bearing liquid. For natural magmas, these parameters can be readily obtained through image analysis with well-established techniques and software of rock samples, as I have shown in a practical application. Hence, this equation provides, for the first time, a means to estimate relative magma viscosity purely based on a comprehensive textural description of a section sample.

Since an exact definition of ϕ_m is quite ambiguous and is still in discussion, the findings of this thesis also suggest the use of a distinguishing nomenclature concerning the nature of the maximum packing fraction:

$$\phi_{m,rcp} < \phi_{m,rheol} < \phi_{m,geom} \quad (\text{eq. 4.2})$$

In addition to that, this thesis presents the first experimental evidence that in multimodal suspensions the maximum packing fraction ϕ_m increases with increasing value of polymodality.

Nonetheless, the model (eq. 4.6) of this thesis also has its limitations. It only focuses on the relative effect of crystal-size distributions on the rheology of magmas systems and the occurrence of vesicles in natural rocks is not taken into account. As such, we envision that the predicted viscosity values could be applicable to vesicle-free domains of magmatic flow in either conduit margins or dense sections of active lava flows. As direct viscosity measurements on active lavas are exceedingly difficult if not impossible, this application provides a new and robust way to establish baseline data on magma rheology from samples of specific flow regimes in active or extinct volcanic systems. Future variants of the current model may incorporate the complex effects of bubbles on magma rheology (Manga et al., 1998). It is very likely that vesicles and their size distributions might not only affect the value of polydispersity but also the physical properties of the magma (e.g., Manga et al., 1998; Truby et al., 2015; among others). It would be particularly interesting to extend the model to three-phase systems and the resulting effects on the relative viscosity. That would make the model more robust and more "realistically" since magma is a three-phase system and the vesicles have a large influence on conduit processes. Also a crucial field of further research is to test the findings of this thesis in 3D.

The petrological HP/HT-experiments were used to measure the CSDs in experimentally grown crystal populations in order to test the finding of the analogue experiments. With the set of *phase equilibrium experiments* it was possible to reproduce the pressure, temperature, and crystal texture relations in the magma of the rhyodacitic pumice of the Minoan eruption of Santorini volcano that was used as the target

composition (e.g., Cottrell *et al.*, 1999). The set of *decompression experiments* simulates a range of magma rise scenarios in terms of magma rise speed and total decompression, which resulted in effects on the ensuing textural and chemical signatures in the eruptive materials. The textural analysis of the experimental results were applied to the aforementioned model derived in this study and calculations of the relative viscosity of the given experimental batch could be executed.

However, due to the mere nature of the structure of the project, the results presented in this study are only the first steps in the effort of mapping the textural evolution of magma in a volcanic conduit and relate its CSD to the rheology of the magma. It would be particularly interesting to simulate a variety of decompression intervals to set up a statistically sound database of textural evolutions of crystals during magma ascent. Another obvious route for future work would be to extent these experiments to other magma compositions. There is definitely a need of more artificially created CSD's, since literature lacks of those studies. In addition to that it is vital to compare those findings to natural rocks, even if the erupted materials represent end-members of the textural evolution.

Bibliography

- Abràmoff, M. D., Magalhães, P. J., & Ram, S. J.** (2004). Image processing with ImageJ. *Biophotonics international*, 11(7), pp. 36-42.
- Alidibirov, M., & Dingwell, D. B.** (1996). Magma fragmentation by rapid decompression. *Nature*, 380(6570), pp. 146. (<https://doi.org/10.1038/380146a0>).
- Alidibirov, M., Dingwell, D. B., Stevenson, R. J., Hess, K. U., Webb, S. L., & Zinke, J.** (1997). Physical properties of the 1980 Mount St. Helens cryptodome magma. *Bulletin of volcanology*, 59(2), pp. 103-111. (<https://doi.org/10.1007/s004450050178>).
- Applegarth, L. J., Pinkerton, H., James, M. R., & Calvari, S.** (2010). Lava flow superposition: The reactivation of flow units in compound 'a'a flows. *Journal of Volcanology and Geothermal Research*, 194(4), pp. 100-106. (<https://doi.org/10.1016/j.jvolgeores.2010.05.001>).
- Armienti, P., Pareschi, M. T., Innocenti, F., & Pompilio, M.** (1994). Effects of magma storage and ascent on the kinetics of crystal growth. *Contributions to Mineralogy and Petrology*, 115(4), pp. 402-414. (<https://doi.org/10.1007/BF00320974>).
- Armienti, P.** (2008). Decryption of igneous rock textures: crystal size distribution tools. *Reviews in Mineralogy and Geochemistry*, 69(1), pp. 623-649. (<https://doi.org/10.2138/rmg.2008.69.16>).
- Arzilli, F., & Carroll, M. R.** (2013). Crystallization kinetics of alkali feldspars in cooling and decompression-induced crystallization experiments in trachytic melt. *Contributions to Mineralogy and Petrology*, 166, pp. 1011-1027. (<https://doi.org/10.1007/s00410-0130906-1>).
- Avrami, M.** (1939). Kinetics of phase change. I General theory. *The Journal of chemical physics*, 7(12), pp. 1103-1112. (<https://doi.org/10.1063/1.1750380>).
- Avrami, M.** (1940). Kinetics of phase change. II transformation-time relations for random distribution of nuclei. *The Journal of Chemical Physics*, 8(2), pp. 212-224. (<https://doi.org/10.1063/1.1750631>).
- Bachmann, O., Dungan, M. A., & Lipman, P. W.** (2002). The Fish Canyon magma body, San Juan volcanic field, Colorado: rejuvenation and eruption of an upper-crustal batholith. *Journal of Petrology*, 43(8), pp. 1469-1503. (<https://doi.org/10.1093/petrology/43.8.1469>).
- Bachmann, O., & Bergantz, G. W.** (2004). On the origin of crystal-poor rhyolites: extracted from batholithic crystal mushes. *Journal of Petrology*, 45(8), pp. 1565-1582. (<https://doi.org/10.1093/petrology/egh019>).
- Bachmann, O., Miller, C. D., & De Silva, S. L.** (2007). The volcanic-plutonic connection as a stage for understanding crustal magmatism. *Journal of Volcanology and Geothermal Research*, 167(1-4), pp. 1-23. (<https://doi.org/10.1016/j.jvolgeores.2007.08.002>).
- Bachmann, O., & Bergantz, G. W.** (2008). Rhyolites and their source mushes across tectonic settings. *J of Petrology*, 49(12), pp. 2277-2285. (<https://doi.org/10.1093/petrology/egn068>).
- Bachmann, O.** (2010). The petrologic evolution and pre-eruptive conditions of the rhyolitic Kos Plateau Tuff (Aegean arc). *Open Geosciences*, 2(3), pp. 270-305. (<https://doi.org/10.2478/v10085-010-0009-4>).
- Bagdassarov, N., & Dingwell, D. B.** (1992). A rheological investigation of vesicular rhyolite. *Journal of volcanology and geothermal research*, (3), pp. 307-322. ([https://doi.org/10.1016/0377-0273\(92\)90099-Y](https://doi.org/10.1016/0377-0273(92)90099-Y)).
- Bagdassarov, N. S., & Dingwell, D. B.** (1993a). Frequency dependent rheology of vesicular rhyolite. *Journal of Geophysical Research: Solid Earth*, 98(B4), pp. 6477-6487. (<https://doi.org/10.1029/92JB02690>).
- Bagdassarov, N. S., & Dingwell, D. B.** (1993b). Deformation of foamed rhyolites under internal and external stresses: an experimental investigation. *Bulletin of Volcanology*, 55(3), pp. 147-154. (<https://doi.org/10.1007/BF00301512>).
- Bagdassarov, N., & Dorfman, A.** (1998a). Granite rheology: magma flow and melt migration. *Journal of the Geological Society*, 155(5), pp. 863-872. (<https://doi.org/10.1144/gsjgs.155.5.0863>).

- Bagdassarov, N., & Dorfman, A.** (1998b). Viscoelastic behavior of partially molten granites. *Tectonophysics*, 290(1-2), pp. 27-45. ([https://doi.org/10.1016/S0040-1951\(98\)00010-9](https://doi.org/10.1016/S0040-1951(98)00010-9)).
- Baranau, V., & Tallarek, U.** (2014). Random-close packing limits for monodisperse and polydisperse hard spheres. *Soft Matter*, 10(21), pp. 3826-3841. (<https://doi.org/10.1039/C3SM52959B>).
- Barnes, H. A., Hutton, J. F., & Walters, K.** (1989). *An introduction to rheology*. Elsevier.
- Barnes, H. A.** (1995). A review of the slip (wall depletion) of polymer solutions, emulsions and particle suspensions in viscometers: its cause, character, and cure. *Journal of Non-Newtonian Fluid Mechanics*, 56(3), pp. 221-251. ([http://dx.doi.org/10.1016/0377-0257\(94\)01282-M](http://dx.doi.org/10.1016/0377-0257(94)01282-M))
- Batchelor, G. K.** (1967). *An introduction to fluid dynamics*. Cambridge: Cambridge University Press, 1967
- Batchelor, G. K.** (1977). The effect of Brownian motion on the bulk stress in a suspension of spherical particles. *Journal of fluid mechanics*, 83(1), pp. 97-117. (<https://doi.org/10.1017/S0022112077001062>).
- Bernal, J. D. & Mason, J.** (1960). Co-ordination of randomly packed spheres. *Nature* 188, pp. 910-911.
- Berryman, J. G.** (1983). Random close packing of hard spheres and disks. *Physical Review A*, 27(2), pp. 1053. (<https://doi.org/10.1103/PhysRevA.27.1053>).
- Best, M. G., & Christiansen, E. H.** (2001). *Igneous petrology*. Blackwell Science.
- Bierwagen, G. P., & Sanders, T. E.** (1974). Studies of the effects of particle size distribution on the packing efficiency of particles. *Powder technology*, 10(3), pp. 111-119. ([https://doi.org/10.1016/0032-5910\(74\)80036-7](https://doi.org/10.1016/0032-5910(74)80036-7)).
- Bindeman, I. N.** (2003). Crystal sizes in evolving silicic magma chambers. *Geology*, 31(4), pp. 367-370. ([https://doi.org/10.1130/0091-7613\(2003\)031%3C0367:CSIESM%3E2.0.CO;2](https://doi.org/10.1130/0091-7613(2003)031%3C0367:CSIESM%3E2.0.CO;2)).
- Blott, S. J. & Pye, K.** (2001). GRADISTAT: a grain size distribution and statistics package for the analysis of unconsolidated sediments. *Earth surface processes and Landforms*, 26(11), pp. 1237-1248. (<http://dx.doi.org/10.1002/esp.261>)
- Blott, S. J. & Pye, K.** (2012). Particle size scales and classification of sediment types based on particle size distributions: Review and recommended procedures. *Sedimentology*, 59(7), pp. 2071-2096. (<http://dx.doi.org/10.1111/j.1365-3091.2012.01335.x>)
- Blundy, J., & Cashman, K. V.** (2008). Petrologic reconstruction of magmatic system variables and processes. *Reviews in Mineralogy and Geochemistry*, 69(1), pp. 179-239. (<https://doi.org/10.2138/rmg.2008.69.6>).
- Bourgue, E., & Richet, P.** (2001). The effects of dissolved CO₂ on the density and viscosity of silicate melts: a preliminary study. *Earth and Planetary Science Letters*, 193(1-2), pp. 57-68. ([https://doi.org/10.1016/S0012-821X\(01\)00491-5](https://doi.org/10.1016/S0012-821X(01)00491-5)).
- Brenner, H.** (1970). Rheology of two-phase systems. *Annual Review of Fluid Mechanics*, 2(1), pp. 137-176. (<https://doi.org/10.1146/annurev.fl.02.010170.001033>).
- Brophy, J. G.** (1991). Composition gaps, critical crystallinity, and fractional crystallization in orogenic (calc-alkaline) magmatic systems. *Contributions to Mineralogy and Petrology*, 109(2), pp. 173-182. (<https://doi.org/10.1007/BF00306477>).
- Brouwers, H. J. H.** (2006). Particle-size distribution and packing fraction of geometric random packings. *Physical review E*, 74(3), 031309. (<https://doi.org/10.1103/PhysRevE.74.031309>).
- Brouwers, H. J. H.** (2010). Viscosity of a concentrated suspension of rigid monosized particles. *Physical Review E*, 81(5), 051402. (<https://doi.org/10.1103/PhysRevE.81.051402>).
- Brouwers, H. J. H.** (2013). Random packing fraction of bimodal spheres: An analytical expression. *Physical Review E*, 87(3), 032202. (<https://doi.org/10.1103/PhysRevE.87.032202>).
- Brückner, R., & Deubener, J.** (1997). Description and interpretation of the two phase flow behaviour of melts with suspended crystals. *Journal of Non-Crystalline Solids*, 209(3), pp. 283-291. ([https://doi.org/10.1016/S0022-3093\(96\)00571-6](https://doi.org/10.1016/S0022-3093(96)00571-6)).
- Brugger, C. R., & Hammer, J. E.** (2010a). Crystallization kinetics in continuous decompression experiments: implications for interpreting natural magma ascent processes. *Journal of Petrology*, 51(9), pp. 1941-1965. (<https://doi.org/10.1093/petrology/egq044>).

- Brugger, C. R., & Hammer, J. E.** (2010b). Crystal size distribution analysis of plagioclase in experimentally decompressed hydrous rhyodacite magma. *Earth and Planetary Science Letters*, 300(3-4), pp. 246-254. (<https://doi.org/10.1016/j.epsl.2010.09.046>).
- Buranasrisak, P. & Narasingha, M. H.** (2012). Effects of particle size distribution and packing characteristics on the preparation of highly-loaded coal-water slurry. *International Journal of Chemical Engineering and Applications*, 3(1), 31. (<https://dx.doi.org/10.7763/IJCEA.2012.V3.154>)
- Burnham, C. W., & Davis, N. F.** (1971). The role of H₂O in silicate melts; I, PVT relations in the system NaAlSi₃O₈-H₂O to 10 kilobars and 1000 degrees C. *American Journal of Science*, 270(1), pp. 54-79. (<https://doi.org/10.2475/ajs.270.1.54>).
- Buscall, R., McGowan, J. I. & Morton-Jones, A. J.** (1993). The rheology of concentrated dispersions of weakly attracting colloidal particles with and without wall slip. *Journal of Rheology (1978-present)*, 37(4), pp. 621-641. (<http://dx.doi.org/10.1122/1.550387>)
- Buscall, R.** (2010). Letter to the Editor: Wall slip in dispersion rheometry. *Journal of Rheology (1978-present)*, 54(6), pp. 1177-1183. (<http://dx.doi.org/10.1122/1.3495981>)
- Caricchi, L.; Burlini, L.; Ulmer, P.; Gerya, T.; Vasalli, M. & Papale, P.** (2007). Non-Newtonian rheology of crystal-bearing magmas and implications for magma ascent dynamics. *Earth and Planetary Science Letters*, 264, pp. 402-419. (<http://dx.doi.org/10.1016/j.epsl.2007.09.032>)
- Caricchi, L., Giordano, D., Burlini, L., Ulmer, P., & Romano, C.** (2008). Rheological properties of magma from the 1538 eruption of Monte Nuovo (Phlegrean Fields, Italy): An experimental study. *Chem. Geology*, 256, pp. 158-171. (<https://doi.org/10.1016/j.chemgeo.2008.06.035>).
- Caricchi, L., Pommier, A., Pistone, M., Castro, J., Burgisser, A., & Perugini, D.** (2011). Strain-induced magma degassing: insights from simple-shear experiments on bubble bearing melts. *Bulletin of volcanology*, 73(9), pp. 1245-1257. (<https://doi.org/10.1007/s00445-011-0471-2>).
- Cashman, K. V., & Ferry, J. M.** (1988). Crystal size distribution (CSD) in rocks and the kinetics and dynamics of crystallization. *Contributions to Mineralogy and Petrology*, 99(4), pp. 401-415. (<https://doi.org/10.1007/BF00371933>).
- Cashman, K. V. & Marsh, B. D.** (1988). Crystal size distribution (CSD) in rocks and the kinetics and dynamics of crystallization. 2. Makaopuhi Lava Lake. *Contrib Min Petrol* 99 (3), pp. 292-305. (<http://dx.doi.org/10.1007/BF00375363>)
- Cashman, K. V.** (1992). Groundmass crystallization of Mount St. Helens dacite, 1980-1986: a tool for interpreting shallow magmatic processes. *Contributions to Mineralogy and Petrology*, 109(4), pp. 431-449. (<https://doi.org/10.1007/BF00306547>).
- Cashman, K. V.** (1993). Relationship between plagioclase crystallization and cooling rate in basaltic melts. *Contributions to Mineralogy and Petrology*, 113(1), pp. 126-142. (<https://doi.org/10.1007/BF00320836>).
- Cashman, K. V., & Blundy, J.** (2000). Degassing and crystallization of ascending andesite and dacite. *Philosophical Transactions of the Royal Society of London A: Mathematical, Physical and Engineering Sciences*, 358(1770), pp. 1487-1513. (<https://doi.org/10.1098/rsta.2000.0600>).
- Cashman, K. V., Sparks, R. S. J., & Hawkesworth, C. J.** (2004). Volatile controls on magma ascent and eruption. *The State of the Planet: Frontiers and Challenges in Geophysics*, 150, pp. 109-124. (<https://doi.org/10.1029/150GM10>).
- Cashman, K. V., & McConnell, S. M.** (2005). Multiple levels of magma storage during the 1980 summer eruptions of Mount St. Helens, WA. *Bulletin of Volcanology*, 68(1), pp. 57. (<https://doi.org/10.1007/s00445-005-0422-x>).
- Cashman, K. V., & Giordano, G.** (2014). Calderas and magma reservoirs. *Journal of Volcanology and Geothermal Research*, 288, pp. 28-45. (<https://doi.org/10.1016/j.jvolgeores.2014.09.007>).
- Cashman, K. V., Sparks, R. S. J., & Blundy, J. D.** (2017). Vertically extensive and unstable magmatic systems: a unified view of igneous processes. *Science*, 355(6331), 3055. (<https://doi.org/10.1126/science.aag3055>).

- Castro, J. M.; Cashman, K. V. & Manga, M.** (2003). A technique for measuring 3D crystal-size distributions of prismatic microlites in obsidian. *American Mineralogist* 88, pp. 1230–1240. (<http://dx.doi.org/10.2138/am-2003-8-906>)
- Castro, J. M. & Gardner, J. E.** (2008). Did magma ascent rate control the explosive-effusive transition at the Inyo volcanic chain, CA? *Geology* 36, pp. 279–282. (<http://dx.doi.org/10.1130/G24453A.1>)
- Castro, J. M., Schipper, C. I., Mueller, S. P., Militzer, A. S., Amigo, A., Parejas, C. S., & Jacob, D.** (2013). Storage and eruption of near-liquidus rhyolite magma at Cordón Caulle, Chile. *Bulletin of Volcanology*, 75(4), pp. 702. (<https://doi.org/10.1007/s00445-013-07029>).
- Castruccio, A.; Rust, A. C. & Sparks, R. S. J.** (2010). Rheology and flow of crystal-bearing lavas: insights from analogue gravity currents. *Earth and Planetary Science Letters*, 297, pp. 471–480. (<http://dx.doi.org/10.1016/j.epsl.2010.06.051>)
- Champallier, R., Bystricky, M. & Arbaret, L.** (2008). Experimental investigation of magma rheology at 300 MPa: From pure hydrous melt to 76 vol.% of crystals. *Earth and Planetary Science Letters*, 267(3), pp. 571–583. (<http://dx.doi.org/10.1016/j.epsl.2007.11.065>)
- Chang, C. & Powell, R. L.,** (1994). Effect of particle size distributions on the rheology of concentrated bimodal suspensions. *J Rheol* 38, pp. 85–98. (<http://dx.doi.org/10.1122/1.550497>)
- Chevrel, M. O., Cimarelli, C., deBiasi, L., Hanson, J. B., Lavallée, Y., Arzilli, F., & Dingwell, D. B.** (2015). Viscosity measurements of crystallizing andesite from Tungurahua volcano (Ecuador). *Geochemistry, Geophysics, Geosystems*, 16(3), 870–889. (<http://dx.doi.org/10.1002/2014GC005661>)
- Chianese, A., & Kramer, H. J.** (Eds.) (2012). *Industrial crystallization process monitoring and control*. John Wiley & Sons.
- Chong, J. S.; Christiansen, E. B. & Baer, A. D.** (1971). Rheology of concentrated suspensions. *Journal of Appl Polym Sci* 15, pp. 2007–2021. (<http://dx.doi.org/10.1002/app.1971.070150818>)
- Cichy, S. B., Botcharnikov, R. E., Holtz, F., & Behrens, H.** (2010). Vesiculation and microlite crystallization induced by decompression: A case study of the 1991–1995 Mt Unzen eruption (Japan). *Journal of Petrology*, 52(7–8), pp. 1469–1492. (<https://doi.org/10.1093/petrology/egq072>).
- Cimarelli, C.; Costa, A.; Mueller, S. P. & Mader, H. M.** (2011). Rheology of magmas with bimodal crystal size and shape distributions: insights from analog experiments. *Geochem Geophys Geosyst* 12. (<http://dx.doi.org/10.1029/2011GC003606>)
- Conte, A. M., Perinelli, C., & Trigila, R.** (2006). Cooling kinetics experiments on different Stromboli lavas: Effects on crystal morphologies and phases composition. *Journal of Volcanology and Geothermal Research*, 155(3), pp. 179–200. (<https://doi.org/10.1016/j.jvolgeores.2006.03.025>).
- Coombs, M. L., Eichelberger, J. C., & Rutherford, M. J.** (2003). Experimental and textural constraints on mafic enclave formation in volcanic rocks. *Journal of Volcanology and Geothermal Research*, 119(1–4), pp. 125–144. ([https://doi.org/10.1016/S0377-0273\(02\)00309-8](https://doi.org/10.1016/S0377-0273(02)00309-8)).
- Cordonnier, B., Hess, K. U., Lavallee, Y. & Dingwell, D. B.** (2009). Rheological properties of dome lavas: Case study of Unzen volcano. *Earth and Planetary Science Letters*, 279(3), pp. 263–272. (<http://dx.doi.org/10.1016/j.epsl.2009.01.014>)
- Cordonnier, B., Caricchi, L., Pistone, M., Castro, J., Hess, K. U., Gottschaller, S., Manga, M. & Burlini, L.** (2012). The viscous-brittle transition of crystal-bearing silicic melt: Direct observation of magma rupture and healing. *Geology*, 40(7), pp. 611–614. (<https://doi.org/10.1130/G3914.1>).
- Corrigan, G. M.** (1982). Supercooling and the crystallization of plagioclase, olivine, and clinopyroxene from basaltic magmas. *Mineral Mag*, 46, pp. 31–42.
- Costa, A.** (2005). Viscosity of high crystal content melts: dependence on solid fraction. *Geophys Res Lett* 32 (L22308). (<http://dx.doi.org/10.1029/2005GL024303>)
- Costa, A.; Caricchi, L. & Bagdassarov, N.** (2009). A model for the rheology of particle-bearing suspensions and partially molten rocks. *Geochem Geophys Geosyst* 10 (3). (<http://dx.doi.org/10.1029/2008GC002138>)

- Cottrell, E., Gardner, J. E., & Rutherford, M. J.** (1999). Petrologic and experimental evidence for the movement and heating of the pre-eruptive Minoan rhyodacite (Santorini, Greece). *Contributions to Mineralogy and Petrology*, 135(4), pp. 315-331. (<https://doi.org/10.1007/s004100050514>).
- Couch, S., Sparks, R. S. J., & Carroll, M. R.** (2003a). The kinetics of degassing-induced crystallization at Soufriere Hills Volcano, Montserrat. *Journal of Petrology*, 44(8), pp. 1477-1502. (<https://doi.org/10.1093/petrology/44.8.1477>).
- Couch, S.** (2003b). Experimental investigation of crystallization kinetics in a haplogranite system. *American Mineralogist*, 88(10), pp. 1471-1485. (<https://doi.org/10.2138/am-2003-1011>).
- Couette, M.** (1890). *Etudes sur le frottement des liquids* (Doctoral dissertation).
- Dabak, T. & Yucel, O.** (1986). Shear viscosity behavior of highly concentrated suspensions at low and high shear-rates. *Rheologica Acta*, 25(5), pp. 527-533. (<http://dx.doi.org/10.1007/BF01774404>)
- Dames, B.; Morrison, B. R. & Willenbacher, N.** (2001). An empirical model predicting the viscosity of highly concentrated, bimodal dispersions with colloidal interactions. *Rheologica acta*, 40(5), pp. 434-440. (<http://dx.doi.org/10.1007/s003970100171>)
- Darias, R., Pinto, R., & Medina, E.** (2002). Viscosity minimum in bimodal concentrated suspensions under shear. *The European Physical Journal E*, 9(4), 327-334. (<https://doi.org/10.1140/epje/i2002-10066-4>).
- Dealy, J. M. & Wang, J.** (2013). *Melt rheology and its applications in the plastics industry*. Springer Science & Business Media. (<http://dx.doi.org/10.1007/978-94-007-6395-1>)
- De Bruijn, H.** (1942). The viscosity of suspensions of spherical particles.(The fundamental η - c and ϕ relations). *Recueil des Travaux Chimiques des Pays-Bas*, 61(12), pp. 863-874. (<https://doi.org/10.1002/recl.19420611205>).
- Deering, C. D., Cole, J. W., & Vogel, T. A.** (2011). Extraction of crystal-poor rhyolite from a hornblende-bearing intermediate mush: a case study of the caldera-forming Matahina eruption, Okataina volcanic complex. *Contributions to Mineralogy and Petrology*, 161(1), pp. 129-151. (<https://doi.org/10.1007/s00410-010-0524-0>).
- DeHoff, R. T.** (1991). A geometrically general theory of diffusion controlled coarsening. *Acta Metallurgica et Materialia*, 39(10), pp. 2349-2360. ([https://doi.org/10.1016/0956-7151\(91\)90016-T](https://doi.org/10.1016/0956-7151(91)90016-T)).
- Del Gaudio, P., Ventura, G. & Taddeucci, J.** (2013). The effect of particle size on the rheology of liquid-solid mixtures with application to lava flows: Results from analogue experiments. *Geochemistry, Geophysics, Geosystems* 14, pp. 2661–2669. (<http://dx.doi.org/10.1002/ggge.20172>)
- Del Gaudio, P.** (2014). Rheology of bimodal crystals suspensions: Results from analogue experiments and implications for magma ascent. *Geochemistry, Geophysics, Geosystems*, 15, pp. 284–291. (<http://dx.doi.org/10.1002/2013GC005078>)
- De Maisonneuve, C. B., Bachmann, O., & Burgisser, A.** (2009). Characterization of juvenile pyroclasts from the Kos Plateau Tuff (Aegean Arc): insights into the eruptive dynamics of a large rhyolitic eruption. *Bulletin of volcanology*, 71(6), pp. 643. (<https://doi.org/10.1007/s00445-008-0250-x>).
- Desmond, K. W. & Weeks, E. R.** (2013). Influence of particle size distribution on random close packing of spheres. *Physical Review E*, 90(2), 022204. (<http://dx.doi.org/10.1103/PhysRevE.90.022204>)
- Deubelbeiss, Y., Kaus, B. J., Connolly, J. A. & Caricchi, L.** (2011). Potential causes for the non-Newtonian rheology of crystal-bearing magmas. *Geochemistry, Geophysics, Geosystems*, 12(5). (<http://dx.doi.org/10.1029/2010GC003485>)
- Deubener, J., & Brückner, R.** (1997). Influence of nucleation and crystallisation on the rheological properties of lithium disilicate melt. *Journal of Non-Crystalline Solids*, 209(1-2), pp. 96-111. ([https://doi.org/10.1016/S0022-3093\(96\)00554-6](https://doi.org/10.1016/S0022-3093(96)00554-6)).
- D'Haene, P., & Mewis, J.** (1994). Rheological characterization of bimodal colloidal dispersions. *Rheologica acta*, 33(3), pp. 165-174. (<https://doi.org/10.1007/BF00437301>).
- Dingwell, D. B.** (1996). Volcanic Dilemma--Flow or Blow?. *Science*, 273(5278), pp. 1054-1055. (<https://doi.org/10.1126/science.273.5278.1054>).

- Dingwell, D. B., Hess, K. U., & Romano, C. (1998). Extremely fluid behavior of hydrous peralkaline rhyolites. *Earth and planetary science letters*, 158(1-2), pp. 31-38. ([https://doi.org/10.1016/S0012-821X\(98\)00046-6](https://doi.org/10.1016/S0012-821X(98)00046-6)).
- Dingwell, D. B. (2006). Transport properties of magmas: diffusion and rheology. *Elements*, 2(5), pp. 281-286. (<https://doi.org/10.2113/gselements.2.5.281>).
- Donev, A., I. Cisse, D. Sachs, E. A. Variano, F. H. Stillinger, R. Connelly, S. Torquato & P. M. Chaikin (2004), Improving the density of jammed disordered packings using ellipsoids, *Science*, 303, pp. 990–993. (<http://dx.doi.org/10.1126/science.1093010>)
- Druitt, T. H., Edwards, L., Mellors, R. M., Pyle, D. M., Sparks, R. S. J., Lanphere, M. & Barreirio, B. (1999). Santorini volcano. *Geological Society Memoir*, 19.
- DYNVOLC database (2017). (<http://dx.doi.org/10.25519/DYNVOLC-Database>)
- Eichelberger, J. C., Carrigan, C. R., Westrich, H. R., & Price, R. H. (1986). Non-explosive silicic volcanism. *Nature*, 323(6089), pp. 598. (<https://doi.org/10.1038/323598a0>).
- Eichelberger, J. C. (1995). Silicic volcanism: ascent of viscous magmas from crustal reservoirs. *Annual Review of Earth and Planetary Sciences*, 23(1), pp. 41-63. (<https://doi.org/10.1146/annurev.ea.23.050195.000353>).
- Einarsson, T. (1949). The flowing lava: studies of its main physical and chemical characteristics. *Soc. Sci. Islandica* 4, pp. 1–70.
- Einarsson, T. (1966). Studies of temperature, viscosity, density and some types of materials produced in the Surtsey eruption. *Surtsey Res. Prog. Report* 2, pp. 163–179.
- Einstein, A. (1906). Eine neue Bestimmung der Moleküldimensionen. *Annalen der Physik*, 324(2), pp. 289-306. (<https://doi.org/10.1002/andp.19063240204>).
- Einstein, A. (1911). Berichtigung zu meiner Arbeit: „Eine neue Bestimmung der Moleküldimensionen. *Annalen der Physik*, 339(3), pp. 591-592. (<https://doi.org/10.1002/andp.19113390313>).
- Evans, K. E. & Gibson, A. G. (1986). Prediction of the maximum packing fraction achievable in randomly oriented short-fibre composites. *Composites Science and Technology*, 25(2), pp. 149-162. ([http://dx.doi.org/10.1016/0266-3538\(86\)90040-0](http://dx.doi.org/10.1016/0266-3538(86)90040-0))
- Faroughi, S. A. & Huber, C. (2014). Crowding-based rheological model for suspensions of rigid bimodal-sized particles with interfering size ratios. *Physical Review E*, 90(5), 052303. (<http://dx.doi.org/10.1103/PhysRevE.90.052303>)
- Farr, R. S. & Groot, R. D. (2009). Close packing density of polydisperse hard spheres. *The Journal of chemical physics*, 131(24), 244104. (<http://dx.doi.org/10.1063/1.3276799>)
- Farris, R. J. (1968). Prediction of the viscosity of multimodal suspensions from unimodal viscosity data. *Trans Soc Rheol* 12 (2), pp. 281–301. (<http://dx.doi.org/10.1122/1.549109>)
- Fenn, P. M. (1977). The nucleation and growth of alkali feldspars from hydrous melts. *The Canadian Mineralogist*, 15(2), pp. 135-161.
- Fernandez, N., Mani, R., Rinaldi, D., Kadau, D., Mosquet, M., Lombois-Burger, H. & Isa, L. (2013). Microscopic mechanism for shear thickening of non-Brownian suspensions. *Physical review letters*, 111(10), 108301. (<https://doi.org/10.1103/PhysRevLett.111.108301>).
- Folk, R. L. & Ward, W. C. (1957). Brazos River bar: a study in the significance of grain size parameters. *Journal of Sedimentary Petrology* 27, pp.3–26. (<http://dx.doi.org/10.1306/74D70646-2B21-11D7-8648000102C1865D>)
- Forien, M., Arbaret, L., Burgisser, A., & Champallier, R. (2011). Experimental constrains on shear-induced crystal breakage in magmas. *Journal of Geophysical Research: Solid Earth*, 116(B8). (<https://doi.org/10.1029/2010JB008026>).
- Frankel, N. A. & Acrivos, A. (1970). The constitutive equation for a dilute emulsion. *Journal of Fluid Mechanics*, 44(01), pp. 65-78. (<http://dx.doi.org/10.1017/S0022112070001696>)
- Friedman, G. M. & Johnson, K. G. (1982). *Exercises in Sedimentology*. Wiley: New York.
- Funk, J. E., & Dinger, D. R. (1993). PPC, pt. 3. Effects of particle physics on forming rheology. *Ceramic Industry*, 140(4), pp. 63-70.
- Gallegos, C. & Franco, J. M. (1999). Rheology of food, cosmetics and pharmaceuticals. *Current opinion in colloid & interface science*, (4), pp. 288-293. ([http://dx.doi.org/10.1016/S1359-0294\(99\)00003-5](http://dx.doi.org/10.1016/S1359-0294(99)00003-5))
- Gan, M., N. Gopinathan, X. Jia, & R. A. Williams (2004), Predicting packing characteristics of particles of arbitrary shapes, *Kona*, 22, pp. 82–93. (<http://doi.org/10.14356/kona.200401>)

- Gardner, J. E., Hilton, M., & Carroll, M. R.** (1999). Experimental constraints on degassing of magma: isothermal bubble growth during continuous decompression from high pressure. *Earth and Planetary Science Letters*, 168(1-2), pp. 201-218. ([https://doi.org/10.1016/S0012-821X\(99\)00051-5](https://doi.org/10.1016/S0012-821X(99)00051-5)).
- Gardner, J. E.** (2007). Heterogeneous bubble nucleation in highly viscous silicate melts during instantaneous decompression from high pressure. *Chemical Geology*, 236(1-2), pp. 1-12. (<https://doi.org/10.1016/j.chemgeo.2006.08.006>).
- Gauthier, F.** (1973). Mount Etna and the 1971 eruption-Field and laboratory studies of the rheology of Mount Etna lava. *Phil. Trans. R. Soc. Lond. A*, 274(1238), pp. 83-98. (<https://doi.org/10.1098/rsta.1973.0028>).
- Gay, E. C., Nelson, P. A. & Armstrong, W. P.** (1969). Flow properties of suspensions with high solids concentration. *AIChE J.* 15, pp. 815–822. (<http://dx.doi.org/10.1002/aic.690150606>)
- Geschwind, C. H., & Rutherford, M. J.** (1992). Cummingtonite and the evolution of the Mount St. Helens (Washington) magma system: An experimental study. *Geology*, 20(11), pp. 1011-1014. ([https://doi.org/10.1130/0091-7613\(1992\)020%3C1011:CATEOT%3E2.3.CO;2](https://doi.org/10.1130/0091-7613(1992)020%3C1011:CATEOT%3E2.3.CO;2)).
- Geschwind, C. H., & Rutherford, M. J.** (1995). Crystallization of microlites during magma ascent: the fluid mechanics of 1980–1986 eruptions at Mount St Helens. *Bulletin of Volcanology*, 57(5), pp. 356-370. (<https://doi.org/10.1007/BF00301293>).
- Gill, R.** (2010). *Igneous rocks and processes: a practical guide*. John Wiley & Sons.
- Giordano, D. & Dingwell, D. B.** (2003). Non-Arrhenian multicomponent melt viscosity: a model. *Earth and Planetary Science Letters*, 208, pp. 337–349. ([http://dx.doi.org/10.1016/S0012-821X\(03\)00042-6](http://dx.doi.org/10.1016/S0012-821X(03)00042-6))
- Giordano, D., Romano, C., Dingwell, D. B., Poe, B., & Behrens, H.** (2004). The combined effects of water and fluorine on the viscosity of silicic magmas. *Geochimica et Cosmochimica Acta*, 68(24), pp. 5159-5168. (<https://doi.org/10.1016/j.gca.2004.08.012>).
- Giordano, D., Romano, C., Papale, P., & Dingwell, D. B.** (2004). The viscosity of trachytes, and comparison with basalts, phonolites, and rhyolites. *Chemical Geology*, 213(1-3), 49-61. (<https://doi.org/10.1016/j.chemgeo.2004.08.032>).
- Giordano, D., Mangiacapra, A., Potuzak, M., Russell, J. K., Romano, C., Dingwell, D. B., & Di Muro, A.** (2006). An expanded non-Arrhenian model for silicate melt viscosity: A treatment for metaluminous, peraluminous and peralkaline liquids. *Chemical Geology*, 229(1-3), pp. 42-56. (<https://doi.org/10.1016/j.chemgeo.2006.01.007>).
- Giordano, D.; Russell, J. K. & Dingwell, D. B.** (2008). Viscosity of magmatic liquids: a model. *Earth and Planetary Science Letters*, 271(1), pp. 123-134. (<http://dx.doi.org/10.1016/j.epsl.2008.03.038>)
- Giordano, D., Ardia, P., Romano, C., Dingwell, D. B., Di Muro, A., Schmidt, M. W., Mangiacapra, A. & Hess, K. U.** (2009). The rheological evolution of alkaline Vesuvius magmas and comparison with alkaline series from the Phlegrean Fields, Etna, Stromboli and Teide. *Geochimica et Cosmochimica Acta*, 73(21), pp. 6613-6630. (<https://doi.org/10.1016/j.gca.2009.07.033>).
- Goldstein, J. I., Newbury, D. E., Joy, D. C., Lyman, C. E., Echlin, P., Lifshin, E., Sawyer, L., Michael, J. R.** (1992). *Scanning Electron Microscopy and X-Ray Microanalysis*. New York: Plenum Press. 2nd Edition.
- Gondret, P., & Petit, L.** (1997). Dynamic viscosity of macroscopic suspensions of bimodal sized solid spheres. *Journal of rheology*, 41(6), pp. 1261-1274. (<https://doi.org/10.1122/1.550850>).
- Gonnermann, H. M., & Manga, M.** (2007). The fluid mechanics inside a volcano. *Annu. Rev. Fluid Mech.*, 39, pp. 321-356. (<https://doi.org/10.1146/annurev.fluid.39.050905.110207>).
- Gornitz, V.** (1981). Skeletal crystals. In *Mineralogy* pp. 469-473. Springer, Boston, MA. (https://doi.org/10.1007/0-387-30720-6_130).
- Gu, Y., Ozel, A. & Sundaresan, S.** (2016). Rheology of granular materials with size distributions across dense-flow regimes. *Powder Technology*, 295, pp. 322-329. (<http://dx.doi.org/10.1016/j.powtec.2016.03.035>)

- Gurioli, L., Harris, A. J. L., Houghton, B. F., Polacci, M., & Ripepe, M.** (2008). Textural and geophysical characterization of explosive basaltic activity at Villarrica volcano. *Journal of Geophysical Research: Solid Earth*, 113(B8). (<http://dx.doi.org/10.1029/2007JB005328>)
- Gurioli, L., Colo, L., Bollasina, A. J., Harris, A. J., Whittington, A. & Ripepe, M.** (2014). Dynamics of Strombolian explosions: Inferences from field and laboratory studies of erupted bombs from Stromboli volcano. *Journal of Geophysical Research: Solid Earth*, 119(1), pp. 319-345. (<http://dx.doi.org/10.1002/2013JB010355>)
- Guth, E., & Gold, O.** (1938). Viscosity and electroviscous effect of the AgI sol. II. Influence of the concentration of AgI and of electrolyte on the viscosity. *Phys. Rev.*, 53, 322.
- Hahn, C., Nöbel, S., Maisch, R., Rösingh, W., Weiss, J. & Hinrichs, J.** (2015). Adjusting rheological properties of concentrated microgel suspensions by particle size distribution. *Food Hydrocolloids*, 49, pp. 183-191. (<http://dx.doi.org/10.1016/j.foodhyd.2015.03.020>)
- Hale, A. J., & Wadge, G.** (2008). The transition from endogenous to exogenous growth of lava domes with the development of shear bands. *Journal of Volcanology and Geothermal Research*, 171(3-4), pp. 237-257. (<https://doi.org/10.1016/j.jvolgeores.2007.12.016>).
- Hamed, S. B & Belhadri, M.** (2009). Rheological properties of biopolymers drilling fluids. *Journal of Petroleum Science and Engineering*, 67(3), pp. 84-90. (<http://dx.doi.org/10.1016/j.petrol.2009.04.001>)
- Hammer, J. E.; Cashman, K. V.; Hoblitt, R. P. & Newman, S.** (1999). Degassing and microlite crystallization during pre-climactic events of the 1991 eruption of Mt. Pinatubo, Philippines. *Bull Volcanol* 60, pp. 355-380. (<http://dx.doi.org/10.1007/s004450050238>)
- Hammer, J. E., Cashman, K. V. & Voight, B.** (2000). Magmatic processes revealed by textural and compositional trends in Merapi dome lavas. *J Volcanol Geotherm Res* 100, pp. 165-192. ([http://dx.doi.org/10.1016/S0377-0273\(00\)00136-0](http://dx.doi.org/10.1016/S0377-0273(00)00136-0))
- Hammer, J. E., Rutherford, M. J. & Hildreth, W.** (2002). Magma storage prior to the 1912 eruption at Novarupta, Alaska. *Contrib Mineral Petrol* 144, pp. 144–162. (<http://dx.doi.org/10.1007/s00410-002-0393-2>)
- Hammer, J. E. & Rutherford, M. J.** (2002). An experimental study of the kinetics of decompression-induced crystallization in silicic melt. *J Geophys Res* 107. (<http://dx.doi.org/10.1029/2001JB000281>)
- Hammer, J. E.** (2008). Experimental studies of the kinetics and energetics of magma crystallization. *Reviews in mineralogy and geochemistry*, 69(1), pp. 9-59. (<https://doi.org/10.2138/rmg.2008.69.2>).
- Happel, J.** (1957). Viscosity of suspensions of uniform spheres. *Journal of applied physics*, 28(11), pp. 1288-1292. (<https://doi.org/10.1063/1.1722635>).
- Harris, A. J., & Allen, J. S.** (2008). One-, two- and three-phase viscosity treatments for basaltic lava flows. *Journal of Geophysical Research: Solid Earth*, 113(B9). (<https://doi.org/10.1029/2007JB005035>)
- Harris, A. J., Favalli, M., Wright, R., & Garbeil, H.** (2011). Hazard assessment at Mount Etna using a hybrid lava flow inundation model and satellite-based land classification. *Natural Hazards*, 58(3), pp. 1001-1027. (<https://doi.org/10.1007/s11069-010-9709-0>)
- Hasan, S. W., Ghannam, M. T. & Esmail, N.** (2010). Heavy crude oil viscosity reduction and rheology for pipeline transportation. *Fuel*, 89(5), pp. 1095-1100. (<http://dx.doi.org/10.1016/j.fuel.2009.12.021>)
- He, D., & Ekere, N. N.** (2001). Viscosity of concentrated noncolloidal bidisperse suspensions. *Rheologica acta*, 40(6), pp. 591-598. (<https://doi.org/10.1007/s003970100187>).
- Heiken, G., Wohletz, K., & Eichelberger, J.** (1988). Fracture fillings and intrusive pyroclasts, Inyo Domes, California. *Journal of Geophysical Research: Solid Earth*, 93(B5), pp. 4335-4350. (<https://doi.org/10.1029/JB093iB05p04335>).
- Herschel, W. H. & Bulkley, R.** (1926). Measurement of consistency as applied to rubber-benzene solutions. *Am. Soc. Test Proc* Vol. 26, No. 2, pp. 621-633.
- Hess, K. U. & Dingwell, D. B.** (1996). Viscosities of hydrous leucogranitic melts: A non-Arrhenian model. *American Mineralogist* 81, pp. 1297–1300. (<http://dx.doi.org/10.2138/am-1996-9-1031>)
- Higgins, M. D.** (1994). Determination of crystal morphology and size from bulk measurements on thin sections: numerical modelling. *American Mineralogist*, 79, pp. 113-119.

- Higgins, M. D.** (1998). Origin of anorthosite by textural coarsening: quantitative measurements of a natural sequence of textural development. *Journal of Petrology*, 39(7), pp. 1307-1323. (<https://doi.org/10.1093/etroj/39.7.1307>).
- Higgins, M. D.** (2000). Measurement of crystal size distributions. *American Mineralogist*, 85(9), pp. 1105-1116. (<https://dx.doi.org/10.2138/am-2000-8-901>)
- Higgins, M. D.** (2002a). Closure in crystal size distributions (CSD), verification of CSD calculations, and the significance of CSD fans. *American Mineralogist*, 87(1), pp. 171-175. (<https://doi.org/10.2138/am-2002-0118>).
- Higgins, M. D.** (2002b). A crystal size-distribution study of the Kiglapait layered mafic intrusion, Labrador, Canada: evidence for textural coarsening. *Contributions to mineralogy and petrology*, 144(3), pp. 314-330. (<https://doi.org/10.1007/s00410-002-0399-9>).
- Higgins, M. D., & Roberge, J.** (2003). Crystal size distribution of plagioclase and amphibole from Soufriere Hills Volcano, Montserrat: evidence for dynamic crystallization–textural coarsening cycles. *Journal of Petrology*, 44(8), pp. 1401-1411. (<https://doi.org/10.1093/petrology/44.8.1401>).
- Higgins, M. D.** (2006a). *Quantitative textural measurements in igneous and metamorphic petrology*. Cambridge University Press.
- Higgins, M. D.** (2006b). Verification of ideal semi-logarithmic, lognormal or fractal crystal size distributions from 2D datasets. *Journal of Volcanology and Geothermal Research*, 154(1-2), pp. 8-16. (<https://doi.org/10.1016/j.jvolgeores.2005.09.015>).
- Higgins, M. D., & Roberge, J.** (2007). Three magmatic components in the 1973 eruption of Eldfell volcano, Iceland: Evidence from plagioclase crystal size distribution (CSD) and geochemistry. *Journal of Volcanology and Geothermal Research*, 161(3), pp. 247-260. (<https://doi.org/10.1016/j.jvolgeores.2006.12.002>).
- Higgins, M. D., & Chandrasekharam, D.** (2007). Nature of sub-volcanic magma chambers, Deccan Province, India: evidence from quantitative textural analysis of plagioclase megacrysts in the Giant Plagioclase Basalts. *Journal of Petrology*, 48(5), pp. 885-900. (<https://doi.org/10.1093/petrology/egm005>).
- Hildreth, W.** (2004). Volcanological perspectives on Long Valley, Mammoth Mountain and Mono Craters: several contiguous but discrete systems. *Journal of Volcanology and Geothermal Research*, 136, pp. 69-198. (<https://doi.org/10.1016/j.jvolgeores.2004.05.019>).
- Hildreth, W., & Wilson, C. J.** (2007). Compositional zoning of the Bishop Tuff. *Journal of Petrology*, 48(5), pp. 951-999. (<https://doi.org/10.1093/petrology/egm007>).
- Hinch, E. J., & Leal, L. G.** (1973). Time-dependent shear flows of a suspension of particles with weak Brownian rotations. *Journal of Fluid Mechanics*, 57(4), pp. 753-767. (<https://doi.org/10.1017/S0022112073001990>).
- Hoffman, R. L.** (1974). Discontinuous and dilatant viscosity behavior in concentrated suspensions. II. Theory and experimental tests. *Journal of Colloid and Interface Science*, 46(3), pp. 491-506. ([https://doi.org/10.1016/0021-9797\(74\)90059-9](https://doi.org/10.1016/0021-9797(74)90059-9)).
- Hoffman, R. L.** (1992). Factors affecting the viscosity of unimodal and multimodal colloidal dispersions. *Journal of Rheology*, 36(5), pp. 947-965. (<https://doi.org/10.1122/1.550324>).
- Hort, M., & Spohn, T.** (1991). Numerical simulation of the crystallization of multicomponent melts in thin dikes or sills: 2. Effects of heterocatalytic nucleation and composition. *Journal of Geophysical Research: Solid Earth*, 96(B1), pp. 485-499. (<https://doi.org/10.1029/90JB01896>).
- Hui, H., & Zhang, Y.** (2007). Toward a general viscosity equation for natural anhydrous and hydrous silicate melts. *Geochimica et Cosmochimica Acta*, 71(2), pp. 403-416. (<https://doi.org/10.1016/j.gca.2006.09.003>).
- Hunter, R. H.** (1987). Textural equilibrium in layered igneous rocks. In *Origins of igneous layering* (pp. 473-503). Springer, Dordrecht. (https://doi.org/10.1007/978-94-017-2509-5_15).
- Hunter, R. H.** (1996). Texture development in cumulate rocks. In *Developments in Petrology* (Vol. 15, pp. 77-101). Elsevier.
- Huppert, H. E., Stephen, R., & Sparks, R. S. J.** (1988). The fluid dynamics of crustal melting by injection of basaltic sills. *Earth and Environmental Science Transactions of The Royal Society of Edinburgh*, 79(2-3), pp. 237-243. (<https://doi.org/10.1017/S0263593300014243>).

- Hurwitz, S., & Navon, O.** (1994). Bubble nucleation in rhyolitic melts: Experiments at high pressure, temperature, and water content. *Earth and Planetary Science Letters*, 122(3-4), pp. 267-280. ([https://doi.org/10.1016/0012-821X\(94\)90001-9](https://doi.org/10.1016/0012-821X(94)90001-9)).
- Inman, D. L.** (1952). Measures for describing the size distribution of sediments. *Journal of Sedimentary Petrology* 22: pp. 125–145.
- Ishibashi, H. & Sato, H.** (2007). Viscosity measurements of subliquidus magmas: Alkali olivine basalt from the Higashi-Matsuura district, Southwest Japan. *J of Volcanology and Geothermal Research*, 160, pp. 223-238. (<http://dx.doi.org/10.1016/j.jvolgeores.2006.10.001>)
- Ishibashi, H.** (2009). Non-Newtonian behaviour of plagioclase-bearing basaltic magma: subliquidus viscosity measurement of the 1707 basalt of Fuji volcano, Japan. *J Volcanol Geotherm Res* 181, pp. 78–88. (<http://dx.doi.org/10.1016/j.jvolgeores.2009.01.004>)
- Ivanov, Y., Van de Ven, T. G. M., & Mason, S. G.** (1982). Damped oscillations in the viscosity of suspensions of rigid rods. I. Monomodal suspensions. *Journal of Rheology*, 26(2), pp. 213-230. (<https://doi.org/10.1122/1.549664>).
- Jaupart, C., & Allègre, C. J.** (1991). Gas content, eruption rate and instabilities of eruption regime in silicic volcanoes. *Earth and Planetary Science Letters*, 102(3-4), pp. 413-429. ([https://doi.org/10.1016/0012-821X\(91\)90032-D](https://doi.org/10.1016/0012-821X(91)90032-D)).
- Jeffrey, D. J., & Acrivos, A.** (1976). The rheological properties of suspensions of rigid particles. *AIChE Journal*, 22(3), pp. 417-432. (<https://doi.org/10.1002/aic.690220303>).
- Jerram, D. A., & Higgins, M. D.** (2007). 3D analysis of rock textures: quantifying igneous microstructures. *Elements*, 3(4), 239-245. (<https://doi.org/10.2113/gselements.3.4.239>)
- Jerram, D. A., Mock, A., Davis, G. R., Field, M., & Brown, R. J.** (2009). 3D crystal size distributions: A case study on quantifying olivine populations in kimberlites. *Lithos*, 112, 223-235. (<https://doi.org/10.1016/j.lithos.2009.05.042>)
- Kameda, M., Kuribara, H., & Ichihara, M.** (2008). Dominant time scale for brittle fragmentation of vesicular magma by decompression. *Geophysical Research Letters*, 35(14). (<https://doi.org/10.1029/2008GL034530>).
- Kansal, A. R., Torquato, S., & Stillinger, F. H.** (2002). Diversity of order and densities in jammed hard-particle packings. *Physical Review E*, 66(4), 041109. (<http://dx.doi.org/10.1103/PhysRevE.66.041109>)
- Kitano, T., Kataoka, T. & Shirota, T.** (1981). An empirical equation of the relative viscosity of polymer melts filled with various inorganic fillers. *Rheologica Acta*, 20(2), pp. 207-209. (<http://dx.doi.org/10.1007/BF01513064>)
- Klug, C., & Cashman, K. V.** (1996). Permeability development in vesiculating magmas: implications for fragmentation. *Bulletin of Volcanology*, 58(2-3), pp. 87-100. (<https://doi.org/10.1007/s004450050128>).
- Kohlstedt, D. L., & Holtzman, B. K.** (2009). Shearing melt out of the Earth: An experimentalist's perspective on the influence of deformation on melt extraction. *Annual Review of Earth and Planetary Sciences*, 37, pp. 561-593. (<https://doi.org/10.1146/annurev.earth.031208.100104>).
- Kolzenburg, S., Giordano, D., Cimarelli, C., & Dingwell, D. B.** (2016). In situ thermal characterization of cooling/crystallizing lavas during rheology measurements and implications for lava flow emplacement. *Geochimica et Cosmochimica Acta*, 195, pp. 244-258. (<https://doi.org/10.1016/j.gca.2016.09.022>).
- Krieger, I. M. & Dougherty, T. J.** (1959). A mechanism for non-Newtonian flow in suspensions of rigid spheres. *Trans. Soc. Rheol.* 3, pp. 137–152. (<http://dx.doi.org/10.1122/1.548848>)
- Krumbein, W. C.** (1938). Size frequency distribution of sediments and the normal phi curve. *Journal of Sedimentary Petrology* 8: pp. 84–90. (<http://dx.doi.org/10.1306/D4269008-2B26-11D7-8648000102C1865D>)
- Krumbein, W.C. & Pettijohn, F. J.** (1938). *Manual of Sedimentary Petrography*. Appleton-Century-Crofts: New York.
- Kurita, R., & Weeks, E. R.** (2011). Incompressibility of polydisperse random-close-packed colloidal particles. *Physical Rev E*, 84, 030401. (<https://doi.org/10.1103/PhysRevE.84.030401>).

- Kurita, R., Ruffner, D. B., & Weeks, E. R.** (2012). Measuring the size of individual particles from three-dimensional imaging experiments. *Nature communications*, 3, pp. 1127. (<https://doi.org/10.1038/ncomms2114>).
- Kurita, R.** (2015). Experimental study of the relationship between local particle-size distributions and local ordering in random close packing. *Physical Review E*, 92(6), 062305. (<https://doi.org/10.1103/PhysRevE.92.062305>).
- Latutrie, B., Harris, A., Médard, E., & Gurioli, L.** (2017). Eruption and emplacement dynamics of a thick trachytic lava flow of the Sancy volcano (France). *Bulletin of Volcanology*, 79(1), 4. (<https://doi.org/10.1007/s00445-016-1084-6>).
- Larsen, J. F., & Gardner, J. E.** (2004). Experimental study of water degassing from phonolite melts: implications for volatile oversaturation during magmatic ascent. *Journal of Volcanology and Geothermal Research*, 134(1-2), pp. 109-124. (<https://doi.org/10.1016/j.jvolgeores.2004.01.004>).
- Larson, R. G.** (1999). The structure and rheology of complex fluids (topics in chemical engineering). *Oxford University Press, New York• Oxford*, 86, pp. 108.
- Lautze, N. C., & Houghton, B. F.** (2005). Physical mingling of magma and complex eruption dynamics in the shallow conduit at Stromboli volcano, Italy. *Geology*, 33(5), pp. 425-428. (<https://doi.org/10.1130/G21325.1>).
- Lavallée, Y., Hess, K. U., Cordonnier, B. & Dingwell, D. B.** (2007). Non-Newtonian rheological law for highly crystalline dome lavas. *Geology*, 35(9), pp. 843-846. (<http://dx.doi.org/10.1130/G23594A.1>)
- Lavallée, Y., Meredith, P. G., Dingwell, D. B., Hess, K. U., Wassermann, J., Cordonnier, B., Gerik, A. & Kruhl, J. H.** (2008). Seismogenic lavas and explosive eruption forecasting. *Nature*, 453(7194), pp. 507. (<https://doi.org/10.1038/nature06980>).
- Lee, D. L.** (1970). Packing of Spheres and its Effect on the Viscosity of Suspension. *J. Paint Technol.*, 42, pp. 579-584.
- Lejeune, A. M. & Richet, P.** (1995). Rheology of crystal-bearing silicate melts: An experimental study at high viscosities. *Journal of Geophysical Research: Solid Earth*, 100(B3), pp. 4215-4229. (<http://dx.doi.org/10.1029/94JB02985>)
- Lejeune, A. M., Bottinga, Y., Trull, T. W., & Richet, P.** (1999). Rheology of bubble-bearing magmas. *Earth and Planetary Science Letters*, 166(1-2), pp. 71-84. ([https://doi.org/10.1016/S0012-821X\(98\)00278-7](https://doi.org/10.1016/S0012-821X(98)00278-7)).
- Le Meins, J. F., Moldenaers, P. & Mewis, J.** (2002). Suspensions in polymer melts. 1. Effect of particle size on the shear flow behavior. *Industrial & Engineering Chemistry Research*, 41(25), pp. 6297-6304. (<http://dx.doi.org/10.1021/ie020117r>)
- Leshner, C. E., Cashman, K. V., & Mayfield, J. D.** (1999). Kinetic controls on crystallization of Tertiary North Atlantic basalt and implications for the emplacement and cooling history of lava at Site 989, Southeast Greenland rifted margin. *Proceedings of the Ocean Drilling Program: Scientific Results*, 163, pp. 135-148.
- Liddle, S. M.** (2014). Polydispersity effects on colloidal phase transitions and kinetic arrest. (Doctoral dissertation).
- Lindsay, J. M., Schmitt, A. K., Trumbull, R. B., De Silva, S. L., Siebel, W., & Emmermann, R.** (2001). Magmatic evolution of the La Pacana caldera system, Central Andes, Chile: Compositional variation of two cogenetic, large-volume felsic ignimbrites. *Journal of Petrology*, 42(3), pp. 459-486. (<https://doi.org/10.1093/petrology/42.3.459>).
- Lipman, P. W.** (1984). The roots of ash flow calderas in western North America: windows into the tops of granitic batholiths. *Journal of Geophysical Research: Solid Earth*, 89(B10), pp. 8801-8841. (<https://doi.org/10.1029/JB089iB10p08801>).
- Lipman, P., Dungan, M., & Bachmann, O.** (1997). Comagmatic granophyric granite in the Fish Canyon Tuff, Colorado: Implications for magma-chamber processes during a large ash-flow eruption. *Geology*, 25(10), pp. 915-918. ([https://doi.org/10.1130/0091-7613\(1997\)025%3C0915:CGGITF%3E2.3.CO;2](https://doi.org/10.1130/0091-7613(1997)025%3C0915:CGGITF%3E2.3.CO;2)).
- Lipman, P. W.** (2007). Incremental assembly and prolonged consolidation of Cordilleran magma chambers: Evidence from the Southern Rocky Mountain volcanic field. *Geosphere*, 3(1), pp. 42-70. (<https://doi.org/10.1130/GES00061.1>).

- Liu, D. M.** (2000). Particle packing and rheological property of highly-concentrated ceramic suspensions: ϕ_m determination and viscosity prediction. *Journal of materials science*, 35(21), pp. 5503-5507. (<http://dx.doi.org/10.1023/A:1004885432221>)
- Liu, S. & Masliyah, J. H.** (1996). Rheology of suspensions. *Advances in Chemistry Series*, (251). (<http://dx.doi.org/10.1021/ba-1996-0251.ch003>)
- Liu, S., & Ha, Z.** (2002). Prediction of random packing limit for multimodal particle mixtures. *Powder technology*, 126(3), pp. 283-296. ([https://doi.org/10.1016/S0032-5910\(02\)00075-X](https://doi.org/10.1016/S0032-5910(02)00075-X)).
- Llewellyn, E. W., Mader, H. M. & Wilson, S. D. R.** (2002). The constitutive equation and flow dynamics of bubbly magmas. *Geophysical research letters*, 29(24). (<http://dx.doi.org/10.1029/2002GL015697>)
- Llewellyn, E. W., & Manga, M.** (2005). Bubble suspension rheology and implications for conduit flow. *Journal of Volcanology and Geothermal Research*, 143(1-3), pp. 205-217. (<https://doi.org/10.1016/j.jvolgeores.2004.09.018>).
- Lofgren, G.** (1974). An experimental study of plagioclase crystal morphology; isothermal crystallization. *American journal of Science*, 274(3), pp. 243-273. (<https://doi.org/10.2475/ajs.274.3.243>).
- Lubachevsky, B. D. & Stillinger, F. H.** (1990). Geometric properties of random disk packings. *Journal of statistical Physics*, 60(5-6), pp. 561-583. (<http://dx.doi.org/10.1007/BF01025983>)
- Luckham, P. F. & Ukeje, M. A.** (1999). Effect of particle size distribution on the rheology of dispersed systems. *Journal of colloid and interface science*, 220(2), pp. 347-356. (<http://dx.doi.org/10.1006/jcis.1999.6515>)
- Luhr, J. F.** (2001). Glass inclusions and melt volatile contents at Paricutin Volcano, Mexico. *Contributions to Mineralogy and Petrology*, 142(3), pp. 261-283. (<https://doi.org/10.1007/s004100100293>).
- Lyakhovskiy, V., Hurwitz, S., & Navon, O.** (1996). Bubble growth in rhyolitic melts: experimental and numerical investigation. *Bulletin of Volcanology*, 58(1), pp. 19-32. (<https://doi.org/10.1007/s004450050122>).
- Mader, H. M., Llewellyn, E. W. & Mueller, S. P.** (2013). The Rheology of Two-Phase Magmas : A Review and Analysis. *J Volcanol Geotherm Res* 257, pp. 135-158. (<http://dx.doi.org/10.1016/j.jvolgeores.2013.02.014>)
- Manga, M., Castro, J. M., Cashman, K. V., & Loewenberg, M.** (1998). Rheology of bubble-bearing magmas. *Journal of Volcanology and Geothermal Research*, 87(1), 15-28. ([https://doi.org/10.1016/S0377-0273\(98\)00091-2](https://doi.org/10.1016/S0377-0273(98)00091-2))
- Mangan, M., & Sisson, T.** (2000). Delayed, disequilibrium degassing in rhyolite magma: decompression experiments and implications for explosive volcanism. *Earth and Planetary Science Letters*, 183(3-4), pp. 441-455. ([https://doi.org/10.1016/S0012-821X\(00\)00299-5](https://doi.org/10.1016/S0012-821X(00)00299-5)).
- Mangan, M. T., Sisson, T. W., & Hankins, W. B.** (2004). Decompression experiments identify kinetic controls on explosive silicic eruptions. *Geophysical Research Letters*, 31(8). (<https://doi.org/10.1029/2004GL019509>).
- Manley, R. S. J., & Mason, S. G.** (1955). Particle motions in sheared suspensions III.: Further observations on collisions of spheres. *Canadian Journal of Chemistry*, 33(5), pp. 763-773. (<https://doi.org/10.1139/v55-094>).
- Maron, S. H. & Pierce, P. E.** (1956). Application of Ree–Eyring generalized flow theory to suspensions of spherical particles. *J Coll Sci* 11, pp. 80–95. ([http://dx.doi.org/10.1016/0095-8522\(56\)90023-X](http://dx.doi.org/10.1016/0095-8522(56)90023-X))
- Marsh, B. D.** (1981). On the crystallinity, probability of occurrence, and rheology of lava and magma. *Contributions to Mineralogy and Petrology*, 78(1), pp. 85-98. (<http://dx.doi.org/10.1007/BF00371146>)
- Marsh, B. D.** (1988a). Crystal capture, sorting, and retention in convecting magma. *Geol Soc Am Bull* 100 (11), pp. 1720–1737. ([http://dx.doi.org/10.1130/0016-7606\(1988\)100%3C1720:CCSARI%3E2.3.CO;2](http://dx.doi.org/10.1130/0016-7606(1988)100%3C1720:CCSARI%3E2.3.CO;2))
- Marsh, B. D.** (1988b). Crystal size distribution (CSD). in rocks and the kinetics and dynamics of crystallization; I, Theory. *Contrib Min Petrol* 99, pp. 277–291. (<http://dx.doi.org/10.1007/BF00375362>)

- Marsh, B. D.** (1998). On the interpretation of crystal size distributions in magmatic systems. *J Petrol* 39, pp. 553–599. (<http://dx.doi.org/10.1093/etroj/39.4.553>)
- Martel, C., Bourdier, J.-L., Pichavant, M. & Traineau, H.** (2000). Textures, water content and degassing of silicic andesites from recent plinian and dome-forming eruptions at Mount Pelee volcano (Martinique, Lesser Antilles arc). *J Volcanol Geotherm Res* 96, pp. 191–206. ([http://dx.doi.org/10.1016/S0377-0273\(99\)00147-X](http://dx.doi.org/10.1016/S0377-0273(99)00147-X))
- Martel, C., & Schmidt, B. C.** (2003). Decompression experiments as an insight into ascent rates of silicic magmas. *Contributions to Mineralogy and Petrology*, 144(4), pp. 397–415. (<https://doi.org/10.1007/s00410-002-0404-3>).
- Martel, C.** (2012). Eruption dynamics inferred from microlite crystallization experiments: application to Plinian and dome-forming eruptions of Mt. Pelée (Martinique, Lesser Antilles). *Journal of Petrology*, 53(4), pp. 699–725. (<https://doi.org/10.1093/etrology/egr076>).
- Marxer, H., Bellucci, P., & Nowak, M.** (2015). Degassing of H₂O in a phonolitic melt: A closer look at decompression experiments. *Journal of Volcanology and Geothermal Research*, 297, pp. 109–124. (<https://doi.org/10.1016/j.jvolgeores.2014.11.017>).
- Massol, H., & Jaupart, C.** (2009). Dynamics of magma flow near the vent: Implications for dome eruptions. *Earth and Planetary Science Letters*, 279(3–4), pp. 185–196. (<https://doi.org/10.1016/j.epsl.2008.12.041>).
- Mastin, L. G.** (2002). Insights into volcanic conduit flow from an open source numerical model. *Geochem. Geophys. Geosyst.*, 3(7), pp. 1–18. (<http://dx.doi.org/10.1029/2001GC000192>)
- Maughan, L. L., Christiansen, E. H., Best, M. G., Gromme, C. S., Deino, A. L., & Tingey, D. G.** (2002). The Oligocene Lund Tuff, Great Basin, USA: a very large volume monotonous intermediate. *Journal of Volcanology and Geothermal Research*, 113(1), pp. 129–157. ([https://doi.org/10.1016/S0377-0273\(01\)00256-6](https://doi.org/10.1016/S0377-0273(01)00256-6)).
- McBirney, A. R. & Murase, T.** (1984). Rheological properties of magmas. *Ann. Review of Earth and Planetary Sciences*, 12, 337. (<http://dx.doi.org/10.1146/annurev.ea.12.050184.002005>)
- McCammom, R. B.** (1962). Efficiencies of percentile measures for describing the mean size and sorting of sedimentary particles. *Journal of Geology* 70: pp. 453–465. (<http://dx.doi.org/10.1086/626836>)
- McKay, R. B.** (1993). Crystal morphology of organic pigments and rheology of dispersions in ink and paint media. *Progress in organic coatings*, 22(1–4), pp. 211–229. ([http://dx.doi.org/10.1016/0033-0655\(93\)80025-6](http://dx.doi.org/10.1016/0033-0655(93)80025-6))
- McKenzie, D.** (1985). The extraction of magma from the crust and mantle. *Earth and Planetary Science Letters*, 74(1), pp. 81–91. ([https://doi.org/10.1016/0012-821X\(85\)90168-2](https://doi.org/10.1016/0012-821X(85)90168-2)).
- Mecklenburgh, J. & Rutter, E. H.** (2003). On the rheology of partially molten synthetic granite. *Journal of Structural Geology*, 25(10), pp. 1575–1585. ([http://dx.doi.org/10.1016/S0191-8141\(03\)00014-2](http://dx.doi.org/10.1016/S0191-8141(03)00014-2))
- Melnik, O. & Sparks, R. S. J.** (2005). Controls on conduit magma flow dynamics during lava dome building eruptions. *J Geophys Res* 110 (B02209). (<http://dx.doi.org/10.1029/2004JB003183>)
- Mendoza, C. I., & Santamaria-Holek, I.** (2009). The rheology of hard sphere suspensions at arbitrary volume fractions: An improved differential viscosity model. *The Journal of chemical physics*, 130(4), 044904. (<https://doi.org/10.1063/1.3063120>).
- Metrich, N., Bertagnini, A. & Di Muro, A.** (2010). Conditions of Magma Storage, Degassing and Ascent at Stromboli: New Insights into the Volcano Plumbing System with Inferences on the Eruptive Dynamics. *J Petrol* 51, pp. 603–626. (<http://dx.doi.org/10.1093/etrology/egr083>)
- Metzner, A. B.** (1985). Rheology of suspensions in polymeric liquids. *Journal of rheology*, 29(6), pp. 739–775. (<https://doi.org/10.1122/1.549808>).
- Mezger, T.** (2006). Das Rheologie-Handbuch: Für Anwender von Rotations- und Oszillations-Rheometern. 2. Edition. Hannover, Vincentz Network.
- Milewski, J. V.** (1973). A study of the packing of milled fibreglass and glass beads. *Composites*, 4(6), pp. 258–265. ([http://dx.doi.org/10.1016/0010-4361\(73\)90392-3](http://dx.doi.org/10.1016/0010-4361(73)90392-3))

- Misiti, V., Vetere, F., Freda, C., Scarlato, P., Behrens, H., Mangiacapra, A., & Dingwell, D. B. (2011). A general viscosity model of Campi Flegrei (Italy) melts. *Chemical Geology*, 290(1-2), pp. 50-59. (<https://doi.org/10.1016/j.chemgeo.2011.08.010>).
- Mock, A., Jerram, D. A., & Breiterkreuz, C. (2003). Using quantitative textural analysis to understand the emplacement of shallow-level rhyolitic laccoliths—a case study from the Halle Volcanic Complex, Germany. *Journal of Petrology*, 44(5), pp. 833-849. (<https://doi.org/10.1093/petrology/44.5.833>).
- Mock, A. & Jerram, D. A. (2005). Crystal size distributions (CSD) in three dimensions: insights from the 3D reconstruction of a highly porphyritic rhyolite. *J Petrol* 46, pp. 1525-1541. (<http://dx.doi.org/10.1093/petrology/egi024>)
- Moitra, P., & Gonnermann, H. M. (2015). Effects of crystal shape and size-modality on magma rheology. *Geochemistry, Geophysics, Geosystems*, 16(1). pp. 1-26. (<https://doi.org/10.1002/2014GC005554>).
- Mollard, E., Martel, C., & Bourdier, J. L. (2012). Decompression-induced crystallization in hydrated silica-rich melts: empirical models of experimental plagioclase nucleation and growth kinetics. *Journal of Petrology*, 53(8), pp. 1743-1766. (<https://doi.org/10.1093/petrology/egs031>).
- Moore, G. & Carmichael, I. S. E. (1998). The hydrous phase equilibria (to 3 kbar) of an andesite and basaltic andesite from western Mexico: constraints on water content and conditions of phenocryst growth. *Contrib Mineral Petrol* 130, pp. 304-319. (<https://dx.doi.org/10.1007/s004100050367>)
- Moore, G., Vennemann, T., & Carmichael, I. S. E. (1998). An empirical model for the solubility of H₂O in magmas to 3 kilobars. *American Mineralogist*, 83(1-2), pp. 36-42. (<https://doi.org/10.2138/am-1998-1-203>).
- Morgan, D. J., & Jerram, D. A. (2006). On estimating crystal shape for crystal size distribution analysis. *Journal of Volcanology and Geothermal Research*, 154(1), 1-7. (<https://doi.org/10.1016/j.jvolgeores.2005.09.016>)
- Morgan, D. J., Jerram, D. A., Chertkoff, D. G., Davidson, J. P., Pearson, D. G., Kronz, A., & Nowell, G. M. (2007). Combining CSD and isotopic microanalysis: magma supply and mixing processes at Stromboli Volcano, Aeolian Islands, Italy. *Earth and Planetary Science Letters*, 260(3-4), pp. 419-431. (<https://doi.org/10.1016/j.epsl.2007.05.037>).
- Mourtada-Bonnefoi, C. C., & Laporte, D. (1999). Experimental study of homogeneous bubble nucleation in rhyolitic magmas. *Geophysical Research Letters*, 26(23), pp. 3505-3508. (<https://doi.org/10.1029/1999GL008368>).
- Moynihan, C. T., Lee, S. K., Tatsumisago, M., & Minami, T. (1996). Estimation of activation energies for structural relaxation and viscous flow from DTA and DSC experiments. *Thermochimica acta*, 280, pp. 153-162. ([https://doi.org/10.1016/0040-6031\(95\)02781-5](https://doi.org/10.1016/0040-6031(95)02781-5)).
- Mueller, H. J., Stroncik, N., Naumann, R., Lathe, C., Spiwek, M., Wehber, M., Schilling, F. R. & Lauterjung, J. (2010). High-pressure falling sphere viscosimetry of basaltic and dacitic rocks in conjunction with synchrotron radiation. In *Journal of Physics: Conference Series* (Vol. 215, No. 1, p. 012028). IOP Publishing. (<https://doi.org/10.1088/1742-6596/215/1/012028>).
- Mueller, S. P., Llewellyn, E. W. & Mader, H. M. (2010). The rheology of suspensions of solid particles. *Proc R Soc A* 466, pp. 1201–1228. (<https://dx.doi.org/10.1098/rspa.2009.0445>)
- Mueller, S. P., Llewellyn, E. W. & Mader, H. M. (2011). The effect of particle shape on suspension viscosity and implications for magmatic flows. *Geophys Res Lett* 38, L13316. (<https://dx.doi.org/10.1029/2011GL047167>)
- Muncill, G. E., & Lasaga, A. C. (1988). Crystal-growth kinetics of plagioclase in igneous systems: Isothermal H₂O-saturated experiments and extension of a growth model to complex silicate melts. *American Mineralogist;(USA)*, pp. 73.
- Murase, T., McBirney, A. R., & Melson, W. G. (1985). Viscosity of the dome of Mount St. Helens. *Journal of volcanology and geothermal research*, 24(1-2), pp. 193-204. ([https://doi.org/10.1016/0377-0273\(85\)90033-2](https://doi.org/10.1016/0377-0273(85)90033-2)).

- Mwasame, P. M., Wagner, N. J., & Beris, A. N.** (2016). Modeling the effects of polydispersity on the viscosity of noncolloidal hard sphere suspensions. *Journal of Rheology*, 60(2), pp. 225-240. (<https://dx.doi.org/10.1122/1.4938048>)
- Mysen, B. O., Virgo, D., & Seifert, F. A.** (1982). The structure of silicate melts: implications for chemical and physical properties of natural magma. *Reviews of Geophysics*, 20(3), pp. 353-383. (<https://doi.org/10.1029/RG020i003p00353>).
- Mysen, B. O., Virgo, D., & Seifert, F. A.** (1984). Redox equilibria of iron in alkaline earth silicate melts; relationships between melt structure, oxygen fugacity, temperature and properties of iron-bearing silicate liquids. *American Mineralogist*, 69(9-10), pp. 834-847.
- Mysen, B. O., & Richet, P.** (2005). *Silicate glasses and melts: properties and structure* (Vol. 10). Elsevier.
- Neuville, D. R.** (2006). Viscosity, structure and mixing in (Ca, Na) silicate melts. *Chemical Geology*, 229(1-3), pp. 28-41. (<https://doi.org/10.1016/j.chemgeo.2006.01.008>).
- Newman, S., Epstein, S., & Stolper, E.** (1988). Water, carbon dioxide, and hydrogen isotopes in glasses from the ca. 1340 AD eruption of the Mono Craters, California: constraints on degassing phenomena and initial volatile content. *Journal of Volcanology and Geothermal Research*, 35(1-2), pp. 75-96. ([https://doi.org/10.1016/0377-0273\(88\)90007-8](https://doi.org/10.1016/0377-0273(88)90007-8)).
- Nicholis, M. G., & Rutherford, M. J.** (2004). Experimental constraints on magma ascent rate for the Crater Flat volcanic zone hawaiite. *Geology*, 32(6), pp. 489-492. (<https://doi.org/10.1130/G20324.1>).
- Okagawa, A., Cox, R. G., & Mason, S. G.** (1973). The kinetics of flowing dispersions. VI. Transient orientation and rheological phenomena of rods and discs in shear flow. *Journal of Colloid and Interface Science*, 45(2), pp. 303-329. ([https://doi.org/10.1016/0021-9797\(73\)90271-3](https://doi.org/10.1016/0021-9797(73)90271-3)).
- Okumura, S., Nakamura, M., & Tsuchiyama, A.** (2006). Shear-induced bubble coalescence in rhyolitic melts with low vesicularity. *Geophysical Research Letters*, 33(20). (<https://doi.org/10.1029/2006GL027347>).
- Okumura, S., Nakamura, M., Tsuchiyama, A., Nakano, T., & Uesugi, K.** (2008). Evolution of bubble microstructure in sheared rhyolite: Formation of a channel-like bubble network. *Journal of Geophysical Research: Solid Earth*, 113(B7). (<https://doi.org/10.1029/2007JB005362>).
- Okumura, S., Nakamura, M., Takeuchi, S., Tsuchiyama, A., Nakano, T., & Uesugi, K.** (2009). Magma deformation may induce non-explosive volcanism via degassing through bubble networks. *Earth and Planetary Science Letters*, 281(3-4), pp. 267-274. (<https://doi.org/10.1016/j.epsl.2009.02.036>).
- Okumura, S., Nakamura, M., Nakano, T., Uesugi, K., & Tsuchiyama, A.** (2010). Shear deformation experiments on vesicular rhyolite: Implications for brittle fracturing, degassing, and compaction of magmas in volcanic conduits. *Journal of Geophysical Research: Solid Earth*, 115(B6). (<https://doi.org/10.1029/2009JB006904>).
- Olhero, S. M. & Ferreira, J. M. F.** (2004). Influence of particle size distribution on rheology and particle packing of silica-based suspensions. *Powder Technology*, 139(1), pp. 69-75. (<http://dx.doi.org/10.1016/j.powtec.2003.10.004>)
- Otto, G. H.** (1939). A modified logarithmic probability graph for the interpretation of mechanical analyses of sediments. *Journal of Sedimentary Petrology* 9: pp. 62-75.
- Pabst, W.** (2004). Fundamental considerations on suspension rheology. *CERAMICS SILIKATY.*, 48(1), pp. 6-13.
- Pabst, W., Gregorová, E. & Berthold, C.** (2006). Particle shape and suspension rheology of short-fiber systems. *Journal of the European Ceramic Society*, 26(1), pp. 149-160. (<http://dx.doi.org/10.1016/j.jeurceramsoc.2004.10.016>)
- Pabst, W., & Gregorová, E.** (2013). Elastic properties of silica polymorphs - a review. *Ceramics-Silikaty*, 57(3), pp. 167-184.
- Panov, V.K., Slezin, Y.B. & Storcheus, A.V.** (1988). Mechanical properties of lava extruded in the 1983 Predskazanny eruption (Klyuchevskoi volcano). *J. Volcanol. Seismol.* pp. 25-37.
- Paonita, A., & Martelli, M.** (2006). Magma dynamics at mid-ocean ridges by noble gas kinetic fractionation: assessment of magmatic ascent rates. *Earth and Planetary Science Letters*, 241(1-2), pp. 138-158. (<https://doi.org/10.1016/j.epsl.2005.10.018>).

- Papale, P., Neri, A., & Macedonio, G.** (1998). The role of magma composition and water content in explosive eruptions: 1. Conduit ascent dynamics. *Journal of Volcanology and Geothermal Research*, 87, pp. 75-93. ([https://doi.org/10.1016/S0377-0273\(98\)00101-2](https://doi.org/10.1016/S0377-0273(98)00101-2)).
- Papale, P.** (1999). Strain-induced magma fragmentation in explosive eruptions. *Nature*, 397(6718), pp. 425-428. (<https://doi.org/10.1038/17109>).
- Papale, P., Moretti, R., & Barbato, D.** (2006). The compositional dependence of the saturation surface of H₂O+ CO₂ fluids in silicate melts. *Chemical Geology*, 229(1-3), pp. 78-95. (<https://doi.org/10.1016/j.chemgeo.2006.01.013>).
- Parkhouse, J. G., & Kelly, A.** (1995). The random packing of fibres in three dimensions. *Proceedings of the Royal Society of London A: Mathematical, Physical and Engineering Sciences* 451, No. 1943, pp. 737-746. (<http://dx.doi.org/10.1098/rspa.1995.0152>)
- Paterson, M. S.** (2001). A granular flow theory for the deformation of partially molten rock. *Tectonophysics*, 335(1-2), pp. 51-61. ([https://doi.org/10.1016/S0040-1951\(01\)00045-2](https://doi.org/10.1016/S0040-1951(01)00045-2)).
- Petford, N.** (2003). Rheology of granitic magmas during ascent and emplacement. *Annual Review of Earth and Planetary Sciences*, 31(1), pp. 399-427. (<http://dx.doi.org/10.1146/annurev.earth.31.100901.141352>)
- Phan, S. E., Russel, W. B., Zhu, J. & Chaikin, P. M.** (1998). Effects of polydispersity on hard sphere crystals. *The Journal of chemical physics*, 108(23), pp. 9789-9795. (<http://dx.doi.org/10.1063/1.476453>)
- Phan-Thien, N., & Pham, D. C.** (1997). Differential multiphase models for polydispersed suspensions and particulate solids. *Journal of Non-Newtonian Fluid Mechanics*, 72(2-3), pp. 305-318. ([https://doi.org/10.1016/S0377-0257\(97\)90002-1](https://doi.org/10.1016/S0377-0257(97)90002-1)).
- Pichavant, M., & Macdonald, R.** (2007). Crystallization of primitive basaltic magmas at crustal pressures and genesis of the calc-alkaline igneous suite: experimental evidence from St Vincent, Lesser Antilles arc. *Contributions to Mineralogy and Petrology*, 154(5), pp. 535-558. (<https://doi.org/10.1007/s00410-007-0208-6>).
- Pichavant, M., Di Carlo, I., Le Gac, Y., Rotolo, S. G. & Scaillet, B.** (2009). Experimental constraints on the deep magma feeding system at Stromboli Volcano, Italy. *J Petrol* 50, pp. 601-624. (<http://dx.doi.org/10.1093/petrology/egp014>)
- Pichavant, M., Di Carlo, I., Rotolo, S. G., Scaillet, B., Burgisser, A., Le Gall, N., & Martel, C.** (2013). Generation of CO₂-rich melts during basalt magma ascent and degassing. *Contributions to Mineralogy and Petrology*, 166(2), pp. 545-561. (<https://doi.org/10.1007/s00410-013-0890-5>).
- Pinkerton, H. & Sparks, R.S.J.** (1978). Field measurements of the rheology of lava. *Nature* 276(5686), pp. 383-385.
- Pinkerton, H. & Stevenson, R. J.** (1992). Methods of determining the rheological properties of magmas at sub-liquidus temperatures. *J Volcanol Geotherm Res* 53, pp. 47-66. ([http://dx.doi.org/10.1016/0377-0273\(92\)90073-M](http://dx.doi.org/10.1016/0377-0273(92)90073-M))
- Pinkerton, H., & Norton, G.** (1995). Rheological properties of basaltic lavas at sub-liquidus temperatures: laboratory and field measurements on lavas from Mount Etna. *Journal of Volcanology and Geothermal Research*, 68(4), pp. 307-323. ([https://doi.org/10.1016/0377-0273\(95\)00018-7](https://doi.org/10.1016/0377-0273(95)00018-7)).
- Pistolesi, M., Delle Donne, D., Pioli, L., Rosi, M., & Ripepe, M.** (2011). The 15 March 2007 explosive crisis at Stromboli volcano, Italy: assessing physical parameters through a multidisciplinary approach. *Journal of Geophysical Research: Solid Earth*, 116(B12). (<https://doi.org/10.1029/2011JB008527>)
- Pistone, M., Caricchi, L., Ulmer, P., Burlini, L., Ardia, P., Reusser, E., Marone, F. & Arbaret, L.** (2012). Deformation experiments of bubble-and crystal-bearing magmas: Rheological and microstructural analysis. *Journal of Geophysical Research: Solid Earth*, 117(B5). (<http://dx.doi.org/10.1029/2011JB008986>)
- Pistone, M., Blundy, J. D., & Brooker, R. A.** (2016). Textural and chemical consequences of interaction between hydrous mafic and felsic magmas: an experimental study. *Contributions to Mineralogy and Petrology*, 171(1), pp. 8. (<https://doi.org/10.1007/s00410-015-1218-4>).
- Poe, B. T., Romano, C., Liebske, C., Rubie, D. C., Terasaki, H., Suzuki, A., & Funakoshi, K.** (2006). High-temperature viscosity measurements of hydrous albite liquid using in-situ

- falling-sphere viscometry at 2.5 GPa. *Chemical Geology*, 229(1-3), pp. 2-9. (<https://doi.org/10.1016/j.chemgeo.2006.01.010>).
- Pond, M. J., Errington, J. R., & Truskett, T. M.** (2011). Implications of the effective one-component analysis of pair correlations in colloidal fluids with polydispersity. *The Journal of chemical physics*, 135(12), 124513. (<https://doi.org/10.1063/1.3643118>).
- Poon, W. C., Weeks, E. R., & Royall, C. P.** (2012). On measuring colloidal volume fractions. *Soft Matter*, 8(1), pp. 21-30. (<https://doi.org/10.1039/C1SM06083J>).
- Powell, R. L.** (1991). Rheology of suspensions of rodlike particles. *Journal of statistical physics*, 62(5-6), pp. 1073-1094. (<https://doi.org/10.1007/BF01128178>).
- Probstein, R. F., Sengun, M. Z. & Tseng, T.-C.** (1994). Bimodal model of concentrated suspension viscosity for distributed particle size. *J Rheol* 38(4), pp. 811-829. (<http://dx.doi.org/10.1122/1.550594>)
- Pupier, E., Duchene, S., & Toplis, M. J.** (2008). Experimental quantification of plagioclase crystal size distribution during cooling of a basaltic liquid. *Contributions to Mineralogy and Petrology*, 155(5), pp. 555-570. (<https://doi.org/10.1007/s00410-007-0258-9>).
- Pusey, P. N.** (1987). The effect of polydispersity on the crystallization of hard spherical colloids. *Journal de physique*, 48(5), pp. 709-712. (<http://dx.doi.org/10.1051/jphys:01987004805070900>)
- Quemada, D.** (1978). Rheology of concentrated disperse systems II. A model for non-newtonian shear viscosity in steady flows. *Rheologica Acta*, 17(6), pp. 632-642. (<http://dx.doi.org/10.1007/BF01522036>)
- Rahli, O., L. Tadrist, & R. Blanc** (1999). Experimental analysis of the porosity of randomly packed rigid fibres, *C. R. Acad. Sci.* 327, pp. 725–729. ([https://doi.org/10.1016/S1287-4620\(99\)80127-6](https://doi.org/10.1016/S1287-4620(99)80127-6))
- Randolph, A. D., & Larson, M. A.** (1971). *Theory of Particulate Processes* (Academic Press, New York, 1988).
- Rannou, E. & Caroff, M.** (2010). Crystal Size Distribution in Magmatic Rocks: Proposition of a Synthetic Theoretical Model. *J Petrol* 51 (5), pp. 1087-1098. (<http://dx.doi.org/10.1093/petrology/egq012>)
- Ree, T., & Eyring, H.** (1955a). Theory of non-Newtonian flow. I. Solid plastic system. *Journal of Applied Physics*, 26(7), pp. 793-800. (<https://doi.org/10.1063/1.1722098>).
- Ree, T., & Eyring, H.** (1955b). Theory of non-Newtonian flow. II. Solution system of high polymers. *Journal of applied physics*, 26(7), pp. 800-809. (<https://doi.org/10.1063/1.1722099>).
- Reed, S.J.B.** (1996). *Electron Microprobe Analysis and Scanning Electron Microscopy in geology*. Cambridge University Press.
- Reid, M. R.** (2008). How long does it take to supersize an eruption?. *Elements*, 4(1), pp. 23-28. (<https://doi.org/10.2113/GSELEMENTS.4.1.23>).
- Resmini, R. G.** (2007). Modeling of crystal size distributions (CSDs) in sills. *Journal of Volcanology and Geothermal Research*, 161(1-2), pp. 118-130. (<https://doi.org/10.1016/j.jvolgeores.2006.06.023>).
- Riker, J. M., Cashman, K. V., Rust, A. C. & Blundy, J. D.** (2015). Experimental Constraints on Plagioclase Crystallization during H₂O- and H₂O–CO₂-Saturated Magma Decompression. *Journal of Petrology*. (<http://dx.doi.org/10.1093/petrology/egv059>)
- Rintoul, M. D. & Torquato, S.** (1996). Computer simulations of dense hard-sphere systems. *The Journal of chemical physics*, 105(20), pp. 9258-9265. (<http://dx.doi.org/10.1063/1.473004>)
- Rintoul, M. D. & Torquato, S.** (1997). Erratum:“Computer simulations of dense hard-sphere systems”[*J. Chem. Phys.* 105, 9258 (1996)]. *The Journal of Chemical Physics*, 107(7), pp. 2698-2698.
- Robert, B., Harris, A., Gurioli, L., Médard, E., Sehlke, A., & Whittington, A.** (2014). Textural and rheological evolution of basalt flowing down a lava channel. *Bulletin of Volcanology*, 76(6), pp. 824. (<https://doi.org/10.1007/s00445-014-0824-8>)
- Rollinson, H.** (1993). *Using geochemical data: evaluation, presentation, interpretation*. Edinburgh Gate, Harlow: Pearson Education Limited.
- Roman, D. C., Cashman, K. V., Gardner, C. A., Wallace, P. J., & Donovan, J. J.** (2006). Storage and interaction of compositionally heterogeneous magmas from the 1986 eruption

- of Augustine Volcano, Alaska. *Bulletin of Volcanology*, 68(3), pp. 240-254. (<https://doi.org/10.1007/s00445-005-0003-z>).
- Roscoe, R.** (1952). The viscosity of suspensions of rigid spheres. *British Journal of Applied Physics*, 3(8), pp. 267. (<https://doi.org/10.1088/0508-3443/3/8/306>).
- Roscoe, R.** (1967). On the rheology of a suspension of viscoelastic spheres in a viscous liquid. *Journal of Fluid Mechanics*, 28(2), pp. 273-293. (<https://doi.org/10.1017/S002211206700206X>).
- Rowland, H. D., Sun, A. C., Schunk, P. R., & King, W. P.** (2005). Impact of polymer film thickness and cavity size on polymer flow during embossing: toward process design rules for nanoimprint lithography. *Journal of Micromechanics and Microengineering*, 15(12), pp. 2414. (<https://doi.org/10.1088/0960-1317/15/12/025>).
- Russell, J. K., Giordano, D., Dingwell, D. B., & Hess, K. U.** (2002). Modelling the non-Arrhenian rheology of silicate melts: Numerical considerations. *European Journal of Mineralogy*, 14(2), pp. 417-427. (<https://doi.org/10.1127/0935-1221/2002/0014-0417>).
- Rust, A. C., & Manga, M.** (2002a). Effects of bubble deformation on the viscosity of dilute suspensions. *Journal of non-newtonian fluid mechanics*, 104(1), pp. 53-63. ([https://doi.org/10.1016/S0377-0257\(02\)00013-7](https://doi.org/10.1016/S0377-0257(02)00013-7)).
- Rust, A. C., & Manga, M.** (2002b). Bubble shapes and orientations in low Re simple shear flow. *Journal of Colloid and Interface Science*, 249(2), pp. 476-480. (<https://doi.org/10.1006/jcis.2002.8292>).
- Rust, A. C., & Cashman, K. V.** (2011). Permeability controls on expansion and size distributions of pyroclasts. *Journal of Geophysical Research: Solid Earth*, 116(B11). (<https://doi.org/10.1029/2011JB008494>).
- Rutgers, I. R.** (1962a). Relative viscosity of suspensions of rigid spheres in Newtonian liquids. *Rheologica Acta*, 2(3), pp. 202-210. (<http://dx.doi.org/10.1007/BF01983952>).
- Rutgers, I. R.** (1962b). Relative viscosity and concentration. *Rheologica Acta*, 2(4), 305-348. (<https://doi.org/10.1007/BF01976051>).
- Rutherford, M. J., & Hill, P. M.** (1993). Magma ascent rates from amphibole breakdown: an experimental study applied to the 1980–1986 Mount St. Helens eruptions. *Journal of Geophysical Research: Solid Earth*, 98(B11), pp. 19667-19685. (<https://doi.org/10.1029/93JB01613>).
- Rutherford, M. J., Gardner, J. E., & Sigurdsson, H.** (2000). Rates of magma ascent. *Encyclopedia of Volcanoes*, pp. 207-217.
- Rutherford, M. J.** (2008). Magma ascent rates. *Reviews in Mineralogy and Geochemistry*, 69(1), pp. 241-271. (<https://doi.org/10.2138/rmg.2008.69.7>).
- Rutter, E. H., & Neumann, D. H. K.** (1995). Experimental deformation of partially molten Westerly granite under fluid-absent conditions, with implications for the extraction of granitic magmas. *Journal of Geophysical Research: Solid Earth*, 100(B8), pp. 15697-15715. (<https://doi.org/10.1029/94JB03388>).
- Rutter, E. H., Brodie, K. H., & Irving, D. H.** (2006). Flow of synthetic, wet, partially molten “granite” under undrained conditions: an experimental study. *Journal of Geophysical Research: Solid Earth*, 111(B6). (<https://doi.org/10.1029/2005JB004257>).
- Ryerson, F. J., Weed, H. C., & Piwinski, A. J.** (1988). Rheology of subliquidus magmas: 1. Picritic compositions. *Journal of Geophysical Research: Solid Earth*, 93(B4), pp. 3421-3436. (<https://doi.org/10.1029/JB093iB04p03421>).
- Saar, M. O., Manga, M., Cashman, K. V. & Fremouw, S.** (2001). Numerical models of the onset of yield strength in crystal-melt suspension. *Earth Planet Sci Lett* 187, pp. 367–379. ([http://dx.doi.org/10.1016/S0012-821X\(01\)00289-8](http://dx.doi.org/10.1016/S0012-821X(01)00289-8))
- Sahagian, D. L., & Proussevitch, A. A.** (1998). 3D particle size distributions from 2D observations: stereology for natural applications. *Journal of Volcanology and Geothermal Research*, 84(3), 173-196. ([https://doi.org/10.1016/S0377-0273\(98\)00043-2](https://doi.org/10.1016/S0377-0273(98)00043-2))
- Saitô, N.** (1950). Concentration dependence of the viscosity of high polymer solutions. I. *Journal of the Physical Society of Japan*, 5(1), pp. 4-8. (<https://doi.org/10.1143/JPSJ.5.4>).
- Scandone, R., Cashman, K. V., & Malone, S. D.** (2007). Magma supply, magma ascent and the style of volcanic eruptions. *Earth and Planetary Science Letters*, 253(3-4), pp. 513-529. (<https://doi.org/10.1016/j.epsl.2006.11.016>).

- Schaertl, W. & Sillescu, H.** (1994). Brownian dynamics of polydisperse colloidal hard spheres: Equilibrium structures and random close packings. *Journal of Statistical Physics*, 77(5-6), pp. 1007-1025. (<http://dx.doi.org/10.1007/BF02183148>)
- Schöpe, H. J., Bryant, G., & van Megen, W.** (2007). Effect of polydispersity on the crystallization kinetics of suspensions of colloidal hard spheres when approaching the glass transition. *The Journal of chemical physics*, 127(8), 084505. (<https://doi.org/10.1063/1.2760207>).
- Searle, G. F. C.** (1912). A simple viscometer for very viscous liquids. In *Proc. Cambridge Philos. Soc.*
- Seelos, K. & Sirocko, F.** (2005). RADIUS—rapid particle analysis of digital images by ultra-high-resolution scanning of thin sections. *Sedimentology*, 52(3), pp. 669-681. (<http://dx.doi.org/10.1111/j.1365-3091.2005.00715.x>)
- Servais, C., Jones, R. & Roberts, I.** (2002). The influence of particle size distribution on the processing of food. *Journal of food engineering*, 51(3), pp. 201-208. ([http://dx.doi.org/10.1016/S0260-8774\(01\)00056-5](http://dx.doi.org/10.1016/S0260-8774(01)00056-5))
- Shaw, H. R., Wright, T. L., Peck, D. L., & Okamura, R.** (1968). The viscosity of basaltic magma; an analysis of field measurements in Makaopuhi lava lake, Hawaii. *American Journal of Science*, 266(4), pp. 225-264. (<https://doi.org/10.2475/ajs.266.4.225>).
- Shaw, H. R.** (1972). Viscosities of magmatic silicate liquids; an empirical method of prediction. *American Journal of Science*, 272(9), pp. 870-893. (<https://doi.org/10.2475/ajs.272.9.870>).
- Shea, T., Houghton, B. F., Gurioli, L., Cashman, K. V., Hammer, J. E., & Hobden, B. J.** (2010). Textural studies of vesicles in volcanic rocks: an integrated methodology. *Journal of Volcanology and Geothermal Research*, 190(3-4), pp. 271-289. (<https://doi.org/10.1016/j.jvolgeores.2009.12.003>).
- Shea, T., & Hammer, J. E.** (2013). Kinetics of cooling-and decompression-induced crystallization in hydrous mafic-intermediate magmas. *Journal of Volcanology and Geothermal research*, 260, pp. 127-145. (<https://doi.org/10.1016/j.jvolgeores.2013.04.018>).
- Shewan, H. M. & Stokes, J. R.** (2015). Analytically predicting the viscosity of hard sphere suspensions from the particle size distribution. *Journal of Non-Newtonian Fluid Mechanics*, 222, pp.72-81. (<http://dx.doi.org/10.1016/j.jnnfm.2014.09.002>)
- Sierou, A., & Brady, J. F.** (2002). Rheology and microstructure in concentrated noncolloidal suspensions. *Journal of Rheology*, 46(5), pp. 1031-1056. (<https://doi.org/10.1122/1.1501925>).
- Silver, L. A., Ihinger, P. D., & Stolper, E.** (1990). The influence of bulk composition on the speciation of water in silicate glasses. *Contributions to Mineralogy and Petrology*, 104(2), pp. 142-162. (<https://doi.org/10.1007/BF00306439>).
- Simakin, A. G., & Bindeman, I. N.** (2008). Evolution of crystal sizes in the series of dissolution and precipitation events in open magma systems. *Journal of Volcanology and Geothermal Research*, 177(4), pp. 997-1010. (<https://doi.org/10.1016/j.jvolgeores.2008.07.012>).
- Simmons, J. H.** (1998). What is so exciting about non-linear viscous flow in glass, molecular dynamics simulations of brittle fracture and semiconductor–glass quantum composites? *Journal of non-crystalline solids*, 239(1-3), pp. 1-15. ([https://doi.org/10.1016/S0022-3093\(98\)00741-8](https://doi.org/10.1016/S0022-3093(98)00741-8)).
- Smith, J. V.** (1997). Shear thickening dilatancy in crystal-rich flows. *Journal of Volcanology and Geothermal Research*, 79(1-2), pp. 1-8. ([https://doi.org/10.1016/S0377-0273\(97\)00020-6](https://doi.org/10.1016/S0377-0273(97)00020-6)).
- Soldati, A., Sehlke, A., Chigna, G. et al.** (2016) Field and experimental constraints on the rheology of arc basaltic lavas: the January 2014 Eruption of Pacaya (Guatemala). *Bull Volcanol* 78: 43. (<https://doi.org/10.1007/s00445-016-1031-6>)
- Sparks, R. S. J.** (1978). The dynamics of bubble formation and growth in magmas: a review and analysis. *Journal of Volcanology and Geothermal Research*, 3(1-2), pp. 1-37. ([https://doi.org/10.1016/0377-0273\(78\)90002-1](https://doi.org/10.1016/0377-0273(78)90002-1)).
- Sparks, R. S. J., & Aspinall, W. P.** (2004). Volcanic activity: frontiers and challenges in forecasting, prediction and risk assessment. *The State of the Planet: Frontiers and Challenges in Geophysics*, 150, pp. 359-371. (<https://doi.org/10.1029/150GM28>).

- Sparks, R. S. J., Baker, L., Brown, R. J., Field, M., Schumacher, J., Stripp, G., & Walters, A.** (2006). Dynamical constraints on kimberlite volcanism. *Journal of Volcanology and Geothermal Research*, 155(1-2), pp. 18-48. (<https://doi.org/10.1016/j.jvolgeores.2006.02.010>).
- Spera, F. J.** (2000). Physical properties of magma. *Encyclopedia of volcanoes*, pp. 171-190.
- Stasiuk, M. V., Barclay, J., Carroll, M. R., Jaupart, C., Ratté, J. C., Sparks, R. S. J., & Tait, S. R.** (1996). Degassing during magma ascent in the Mule Creek vent (USA). *Bulletin of Volcanology*, 58(2-3), pp. 117-130. (<https://doi.org/10.1007/s004450050130>).
- Stein, D. J., & Spera, F. J.** (1992). Rheology and microstructure of magmatic emulsions: theory and experiments. *Journal of Volcanology and Geothermal Research*, 49(1-2), pp. 157-174. ([https://doi.org/10.1016/0377-0273\(92\)90011-2](https://doi.org/10.1016/0377-0273(92)90011-2)).
- Stein, D. J., & Spera, F. J.** (2002). Shear viscosity of rhyolite-vapor emulsions at magmatic temperatures by concentric cylinder rheometry. *Journal of Volcanology and Geothermal Research*, 113(1-2), pp. 243-258. ([https://doi.org/10.1016/S0377-0273\(01\)00260-8](https://doi.org/10.1016/S0377-0273(01)00260-8)).
- Stevenson, R. J., Dingwell, D. B., Webb, S. L., & Sharp, T. G.** (1996). Viscosity of microlite bearing rhyolitic obsidians: an experimental study. *Bulletin of Volcanology*, 58(4), pp. 298-309. (<https://doi.org/10.1007/s004450050141>).
- Stickel, J. J. & Powell, R. L.** (2005). Fluid mechanics and rheology of dense suspensions. *Annu. Rev. Fluid Mech.*, 37, pp. 129-149. (<http://dx.doi.org/10.1146/annurev.fluid.36.050802.122132>).
- Strivens, T. A.** (1999). The rheology of paints. *Woodhead Publishers*, pp. 551-574. (<http://dx.doi.org/10.1533/9781855737006.575>).
- Subbanna, M., & Kapur, P. C.** (2002). Role of powder size, packing, solid loading and dispersion in colloidal processing of ceramics. *Ceramics international*, 28(4), pp. 401-405. ([https://doi.org/10.1016/S0272-8842\(01\)00108-0](https://doi.org/10.1016/S0272-8842(01)00108-0)).
- Sudduth, R. D.** (1993a). A generalized model to predict the viscosity of solutions with suspended particles. I. *Journal of Applied Polymer Science*, 48(1), pp. 25-36. (<http://dx.doi.org/10.1002/app.1993.070480104>).
- Sudduth, R. D.** (1993b). A new method to predict the maximum packing fraction and the viscosity of solutions with a size distribution of suspended particles. II. *Journal of applied polymer science*, 48(1), pp. 37-55. (<http://dx.doi.org/10.1002/app.1993.070480105>).
- Sudduth, R. D.** (1993c). A generalized model to predict the viscosity of solutions with suspended particles. III. Effects of particle interaction and particle size distribution. *Journal of appl. polymer science* 50(1), pp. 123-147. (<http://dx.doi.org/10.1002/app.1993.070500115>).
- Suzuki, Y., Gardner, J. E., & Larsen, J. F.** (2007). Experimental constraints on syneruptive magma ascent related to the phreatomagmatic phase of the 2000 AD eruption of Usu volcano, Japan. *Bulletin of Volcanology*, 69(4), pp. 423-444. (<https://doi.org/10.1007/s00445-006-0084-3>).
- Swanson, S. E.** (1977). Relation of nucleation and crystal-growth rate to the development of granitic textures. *American Mineralogist*, 62(9-10), pp. 966-978.
- Szramek, L., Gardner, J. E., & Larsen, J.** (2006). Degassing and microlite crystallization of basaltic andesite magma erupting at Arenal Volcano, Costa Rica. *Journal of Volcanology and Geothermal Research*, 157(1), pp. 182-201. (<https://doi.org/10.1016/j.jvolgeores.2006.03.039>).
- Thomas, D. G.** (1965). Transport characteristics of suspension: VIII. A note on the viscosity of Newtonian suspensions of uniform spherical particles. *Journal of Colloid Science*, 20(3), pp. 267-277. ([https://doi.org/10.1016/0095-8522\(65\)90016-4](https://doi.org/10.1016/0095-8522(65)90016-4)).
- Toramaru, A.** (1989). Vesiculation process and bubble size distributions in ascending magmas with constant velocities. *Journal of Geophysical Research: Solid Earth*, 94(B12), pp. 17523-17542. (<https://doi.org/10.1029/JB094iB12p17523>).
- Torquato, S., Truskett, T. M. & Debenedetti, P. G.** (2000). Is random close packing of spheres well defined?. *Physical review letters*, 84(10), pp. 2064-2067. (<http://dx.doi.org/10.1103/PhysRevLett.84.2064>).
- Torquato, S., & Stillinger, F. H.** (2010). Jammed hard-particle packings: From Kepler to Bernal and beyond. *Reviews of modern physics*, 82(3), 2633. (<https://doi.org/10.1103/RevModPhys.82.2633>).

- Torquato, S.** (2013). *Random heterogeneous materials: microstructure and macroscopic properties* (Vol. 16). Springer Science & Business Media. (<http://dx.doi.org/10.1115/1.1483342>)
- Trask, P. D.** (1932). *Origin and Environment of Source Sediments of Petroleum*. Gulf Publishing Company: Houston
- Truby, J. M., Mueller, S. P., Llewellyn, E. W. & Mader, H. M.** (2015). The rheology of three-phase suspensions at low bubble capillary number. *Proc. R. Soc. A*, Vol. 471, No. 2173, p. 20140557. (<http://dx.doi.org/10.1098/rspa.2014.0557>)
- Tuffen, H., Dingwell, D. B., & Pinkerton, H.** (2003). Repeated fracture and healing of silicic magma generate flow banding and earthquakes?. *Geology*, 31(12), pp. 1089-1092. (<https://doi.org/10.1130/G19777.1>)
- Turner, S., George, R., Jerram, D. A., Carpenter, N., & Hawkesworth, C.** (2003). Case studies of plagioclase growth and residence times in island arc lavas from Tonga and the Lesser Antilles, and a model to reconcile discordant age information. *Earth and Planetary Science Letters*, 214(1), pp. 279-294. ([https://doi.org/10.1016/S0012-821X\(03\)00376-5](https://doi.org/10.1016/S0012-821X(03)00376-5))
- Ubbelohde, A. R.** (1965). Melting and Crystal Structure—Some Current Problems. *Angewandte Chemie International Edition in English*, 4(7), pp. 587-591. (<https://doi.org/10.1002/anie.196505871>)
- Umstätter, H.** (1954). Einführung in die Viskosimetrie (Berlin 1952); K. Edelmann, *Faserforsch. u. Textiltechnik*5, pp. 59.
- Vand, V.** (1948). Viscosity of solutions and suspensions. I. Theory. *The Journal of Physical Chemistry*, 52(2), pp. 277-299. (<https://doi.org/10.1021/j150458a001>)
- Vernon, R. H. & Clarke, G. L.** (2008): Principles of Metamorphic Petrology. Cambridge University Press
- Vetere, F., Behrens, H., Holtz, F., & Neuville, D. R.** (2006). Viscosity of andesitic melts - new experimental data and a revised calculation model. *Chemical Geology*, 228(4), pp. 233-245. (<https://doi.org/10.1016/j.chemgeo.2005.10.009>)
- Vetere, F., Behrens, H., Holtz, F., Vilardo, G. & Ventura, G.** (2010). Viscosity of crystal-bearing melts and its implication for magma ascent. *Journal of mineralogical and petrological sciences*, 105(3), pp. 151-163. (<http://dx.doi.org/10.2465/jmps.090402>)
- Vetere, F., Holtz, F., Behrens, H., Botcharnikov, R. E., & Fanara, S.** (2014). The effect of alkalis and polymerization on the solubility of H₂O and CO₂ in alkali-rich silicate melts. *Contributions to Mineralogy and Petrology*, 167(5), pp. 1014. (<https://doi.org/10.1007/s00410-014-1014-6>)
- Vigneresse, J. L., Barbey, P., & Cuney, M.** (1996). Rheological transitions during partial melting and crystallization with application to felsic magma segregation and transfer. *Journal of Petrology*, 37(6), pp. 1579-1600. (<https://doi.org/10.1093/petrology/37.6.1579>)
- Vona, A., Romano, C., Dingwell, D. B. & Giordano, D.** (2011). The rheology of crystal-bearing basaltic magmas from Stromboli and Etna. *Geochim Cosmochim Acta* 75, pp. 3214–3236. (<http://dx.doi.org/10.1016/j.gca.2011.03.031>)
- Voorhees, P. W.** (1992). Ostwald ripening of two-phase mixtures. *Annual Review of Materials Science*, 22(1), pp. 197-215. (<https://doi.org/10.1146/annurev.ms.22.080192.001213>)
- Wackenhut, M., McNamara, S. & Herrmann, H.** (2005). Shearing behaviour of polydisperse media. *Eur Phys J E* 17, pp. 237-246. (<http://dx.doi.org/10.1140/epje/i2004-10144-7>)
- Wadsworth, F. B., Vasseur, J., Llewellyn, E. W., & Dingwell, D. B.** (2017). Sintering of polydisperse viscous droplets. *Physical Review E*, 95(3), 033114. (<http://dx.doi.org/10.1103/PhysRevE.95.033114>)
- Walker, D., Powell, M. A., Lofgren, G. E., & Hays, J. F.** (1978). Dynamic crystallization of a eucrite basalt. In Lunar and Planetary Science Conference Proceedings (Vol. 9, pp. 1369-1391).
- Walker, B. A., Klemetti, E. W., Grunder, A. L., Dilles, J. H., Tepley, F. J., & Giles, D.** (2013). Crystal reaming during the assembly, maturation, and waning of an eleven-million-year crustal magma cycle: thermobarometry of the Aucanquilcha Volcanic Cluster. *Contributions to Mineralogy and Petrology*, 165(4), pp. 663-682. (<https://doi.org/10.1007/s00410-012-0829-2>)

- Wallace, P. J., Anderson, A. T. & Davis, A. M.** (2002). Quantification of pre-eruptive exsolved gas contents in silicic magmas. *Nature* 377, pp. 612-616. (<http://dx.doi.org/10.1038/377612a0>)
- Wallace, P. J.** (2002). Volatiles in submarine basaltic glasses from the Northern Kerguelen Plateau (ODP Site 1140): Implications for source region compositions, magmatic processes, and plateau subsidence. *Journal of Petrology*, 43(7), pp. 1311-1326. (<https://doi.org/10.1093/petrology/43.7.1311>).
- Webb, S. L. & Dingwell, D. B.** (1990a). The onset of Non-Newtonian rheology of silicate melts—a fiber elongation study. *Phys Chem Min* 17 (2), pp. 125–132. (<http://dx.doi.org/10.1007/BF00199663>)
- Webb, S. L., & Dingwell, D. B.** (1990b). Non-Newtonian rheology of igneous melts at high stresses and strain rates: Experimental results for rhyolite, andesite, basalt, and nephelinite. *Journal of Geophysical Research: Solid Earth*, 95(B10), pp. 15695-15701. (<https://doi.org/10.1029/JB095iB10p15695>).
- Whittington, A. G., Hellwig, B. M., Behrens, H., Joachim, B., Stechern, A., & Vetere, F.** (2009). The viscosity of hydrous dacitic liquids: implications for the rheology of evolving silicic magmas. *Bulletin of Volcanology*, 71(2), pp. 185-199. (<https://doi.org/10.1007/s00445-008-0217-y>).
- Wickham, S. M.** (1987). The segregation and emplacement of granitic magmas. *Journal of the Geological Society*, 144(2), pp. 281-297. (<https://doi.org/10.1144/gsjgs.144.2.0281>).
- Wik, H. B. & Wik, O.** (1993). Rheology of pharmaceuticals. *Industrial aspects of pharmaceuticals*, pp. 42-54.
- Wildemuth, C. R., & Williams, M. C.** (1984). Viscosity of suspensions modeled with a shear-dependent maximum packing fraction. *Rheologica acta*, 23(6), pp. 627-635. (<https://doi.org/10.1007/BF01438803>).
- Wildemuth, C. R., & Williams, M. C.** (1985). A new interpretation of viscosity and yield stress in dense slurries: coal and other irregular particles. *Rheologica Acta*, 24(1), pp. 75-91. (<https://doi.org/10.1007/BF01329266>).
- Willenbacher, N., & Georgieva, K.** (2013). Rheology of disperse systems. *Product design and engineering: Formulation of gels and pastes*, pp. 7-49. (<https://doi.org/10.1002/9783527654741.ch1>).
- Williams, S. R., & A. P. Philipse** (2003), Random packings of spheres and spherocylinders simulated by mechanical contraction. *Physical Review E*, 67, 051301. (<https://doi.org/10.1103/PhysRevE.67.051301>)
- Wilson, L.** (1980). Relationships between pressure, volatile content and ejecta velocity in three types of volcanic explosion. *Journal of Volcanology and Geothermal Research*, 8(2-4), pp. 297-313. ([https://doi.org/10.1016/0377-0273\(80\)90110-9](https://doi.org/10.1016/0377-0273(80)90110-9)).
- Woods, A. W., & Koyaguchi, T.** (1994). Transitions between explosive and effusive eruptions of silicic magmas. *Nature*, 370(6491), pp. 641. (<https://doi.org/10.1038/370641a0>).
- Yilmazer, U., & Kalyon, D. M.** (1989). Slip effects in capillary and parallel disk torsional flows of highly filled suspensions. *Journal of Rheology*, 33(8), pp. 1197-1212. (<https://doi.org/10.1122/1.550049>).
- Yu, A. B., Bridgwater, J., & Burbidge, A.** (1997). On the modelling of the packing of fine particles. *Powder technology*, 92(3), pp. 185-194. ([https://doi.org/10.1016/S0032-5910\(97\)03219-1](https://doi.org/10.1016/S0032-5910(97)03219-1)).
- Yue, Y., & Brückner, R.** (1994). A new description and interpretation of the flow behavior of glass forming melts. *Journal of non-crystalline solids*, 180(1), pp. 66-79. ([https://doi.org/10.1016/0022-3093\(94\)90398-0](https://doi.org/10.1016/0022-3093(94)90398-0)).
- Zarraga, I. E., Hill, D. A., & Leighton Jr, D. T.** (2000). The characterization of the total stress of concentrated suspensions of noncolloidal spheres in Newtonian fluids. *Journal of Rheology*, 44(2), pp. 185-220. (<https://doi.org/10.1122/1.551083>).
- Zheng, J., Johnson, P. F., & Reed, J. S.** (1990). Improved equation of the continuous particle size distribution for dense packing. *Journal of the American Ceramic Society*, 73(5), pp. 1392-1398. (<https://doi.org/10.1111/j.1151-2916.1990.tb05210.x>).

- Zhou, J. Z. Q., Uhlherr, P. H., & Luo, F. T.** (1995). Yield stress and maximum packing fraction of concentrated suspensions. *Rheologica acta*, *34*(6), pp. 544-561. (<https://doi.org/10.1007/BF00712315>).
- Zieg, M. J., & Marsh, B. D.** (2002). Crystal size distributions and scaling laws in the quantification of igneous textures. *Journal of Petrology*, *43*(1), pp. 85-101. (<https://doi.org/10.1093/petrology/43.1.85>).
- Zimova, M., & Webb, S.** (2006). The effect of chlorine on the viscosity of Na₂O-Fe₂O₃-Al₂O₃-SiO₂ melts. *American Mineralogist*, *91*(2-3), pp. 344-352. (<https://doi.org/10.2138/am.2006.1799>).

Acknowledgements

Appendices

The following supplementary data can be found on the attached DVD:

PDF version of the thesis

Rheological data

Data and images of HP/HT-experiments

Curriculum vitae